Molecular studies of the replication mechanisms of coronavirus

Wang, Jibin

2007

Wang, J. B. (2007). Molecular studies of the replication mechanisms of coronavirus. Doctoral thesis, Nanyang Technological University, Singapore.

https://hdl.handle.net/10356/6574

https://doi.org/10.32657/10356/6574

Nanyang Technological University

MOLECULAR STUDIES OF THE REPLICATION MECHANISMS OF CORONAVIRUS

WANG JIBIN

SCHOOL OF BIOLOGICAL SCIENCES

NANYANG TECHNOLOGICAL UNIVERSITY

2007

Molecular Studies of the Replication Mechanisms of Coronavirus

Wang Jibin

School of Biological Sciences

A thesis submitted to the Nanyang Technological University

in fulfillment of the requirement for the degree of

Doctor of Philosophy

2007

Acknowledgments

Before I began to write the acknowledgments, I searched fast for my past five years in my memory. I realized that how much help and encouragement I had received during my Ph.D. program. Now, I would like to write down their names in my dissertation and remember them in my science journey.

I would like to express my deepest appreciation to my supervisor, Liu Ding Xiang, for his excellent scientific and technical guidance. His expert advice and encouragement has been invaluable. I want to thank professor, James P. Tam, my co-supervisor, for taking us in and allowing us to focus on our jobs after our supervisor shifted to Institute of Molecular and Cell Biology (IMCB).

I would also like to acknowledge all the members of Dr Wen Zi Long laboratory in IMCB for their endless help. I am especially thankful to Dr Huang Mei for her patience and kindness.

I am deeply indebted to all the members of our group. I am honored to have spent time with such intelligent and talented persons. Thanks for being there with me and accompanying me to get through some rough points. Thanks also to all the members of my supervisor lab in IMCB, for their huge support for our NTU lab.

Lastly, I would like to acknowledge the tremendous support and encouragement of my parents and husband, Mom, Dad, Lianghua, without whom I could not have achieved my goal.

Table of Contents

Abstract

Coronavirus M protein is an essential component of virions and plays pivotal roles in virion assembly, budding and maturation. The M protein is integrated into the viral envelope with three transmembrane domains flanked by a short amino-terminal ectodomain and a large carboxy-terminal endodomain. To understand the cellular factors that may be involved in virion assembly, budding and maturation processes, the M protein from coronavirus infectious bronchitis virus (IBV) was used as a bait in a yeast two-hybrid screen, resulting in the identification of β-Actin as a potentially interacting partner. This interaction was subsequent confirmed by coimmunoprecipitation and immunofluorescence in mammalian cells, and mutation of amino acids A159 and K160 in the M protein abolished the interaction. Introduction of the A159-K160 mutation into an infectious IBV clone system blocked the infectivity of the clone, although viral RNA replication and subgenomic mRNA transcription appeared to be normal. More interestingly, disruption of actin filaments with cell-permeable agent cytochalasin D inhibited virion assembly and budding, but not release of the virus particles. This study reveals an essential function of actin in the replication cycle of a coronavirus.

IBV belongs to group 3 of Coronavirus, which possesses a 27.6 kb positive-stranded RNA genome. This kind of enveloped virus replication is mediated by two virus-encoded proteases: a papain-like protease and a 3C-like protease. The 3CLpro, a 33-kDa protein in IBV-infected cells, is the main viral protease, responsible for the processing of the replicase proteins necessary for RNA synthesis. The highly strict substrate specificity of 3CLpro is very

important to all coronaviruses because of the accurate need for functional proteins to be released from the polyprotein one by one. It cleaves the bulk of the polyprotein at Q-S (G, A and N) dipeptide bonds. The Q residue in P1 position of 3CLpro cleavage site is more conserved than other positions. This conserved residue was hence replaced separately with four amino acids (A, E, N and R). RNA replication analysis showed that the mutant virus could be easily detected only when the substitution did not affect 3CLpro cleavage of polyproteins. Additionally, more N residue mutants at the P1 position could be cleaved by IBV 3CLpro than the E residue mutants. These data show that IBV 3CLpro favorably tolerates N substitution more than E substitution in the P1 position. Furthermore, it also demonstrates that the Q residue in P1 position is very important for virus replication.

List of abbreviations

aa……..…amino acids

A…….alanine

ACE2……..angiotensinconverting enzyme 2

APN…….. ……canine aminopeptidase N

Arg……arginine

BCoV……...bovine coronavirus

bp…….base pair

CCoV……...canine coronavirus

CEACAM1…….carcinoembryonic antigen-cell adhesion molecule

CECoV…….....canine enteric coronavirus

3CLpro……...……...3C-like protease

CMC…….carboxymethy cellulose

CoV…….coronavirus

CPE…….....cytopathic effect

CRCoV……..canine respiratory coronavirus

C-terminal……...carboxy-terminal

DCoV…… ……duck coronavirus

DMEM…….. ...dulbecco's modified eagle medium

DMVs……double-membraned vesicles

DNaseI…… deoxyribonuclease I

DTT……...dithiothreitol

E ……..Glutamic acid

E protein……..coronavirus envelope protein

EAV……..equine arteritis virus

ER……..endoplasmic reticulum

ERGIC……ER-to-Golgi intermediate compartment

ExoN……...exonuclease

FBS…….. fetal bovine serum

FCoV…….……feline enteric coronavirus

FIPV……...feline infectious peritonitis virus

GCoV…….. goose coronavirus

Q……..glutamine

HCV…….. .....heptatis C virus

HCoV……..human coronavirus

HCoV OC43…….. ……..human coronavirus OC43

HE…….haemagglutinin

HEV……..porcine haemagglutinating encephalomyelitis coronavirus

His……histidine

HIV-1……..…….human immunodeficiency virus type 1

HR…….heptad repeat

HRV14……..human rhinovirus 14

HS……..heparan sulfate

IBV……...infectious bronchitis virus

Kb……kilo-base

kDa……...kilo-dalton

M protein……..membrane protein

MCS……..multiple cloning site

MEM……modified eagle medium

MHV…….mouse heptatis virus

ml…….miniliter

mM……minimolar

MW……molecular weight

N……...…Asparagine

NDV……Newcastle disease virus

N protein……...coronavirus nucleocapsid protein

nsp…….....non-structural protein

nt……nucleotide

µl……microliter

ORFs……..open reading frames

PAGE…….polyacrylamide gel electrophoresis

PBS……...phosphate buffered saline

PEDV…… porcine epidemic diarrhoea coronavirus

PFU……plaque forming unit

PhCoV…….. ……pheasant coronavirus

PiCoV…….....pigeon coronavirus

Pro……...proline

PVDF…….polyvinylidene difluoride

R……..……...…Arginine

RDRP……RNA dependent RNA polymerase

RT-PCR……reverse transcriptase-PCR

S protein……spike protein

SARS ……..severe acute respiratory syndrome

SARS-CoV……..severe acute respiratory syndrome coronavirus

SDS……...sodium dodecyl sulfate

TCoV……...turkey coronavirus

TGEV……...transmissible gastroenteritis virus

TRSs……transcription regulating sequences

Tyr…….tyrosine

UTR.……....untranslated region

VLP……virus-like particle

vTF7-3…….. vaccinia virus-T7

Chapter 1

General introduction

1. 1. Taxonomy

Coranaviruses are a family of enveloped, plus-stranded RNA viruses with helical nucleocapsids and very large genomes (Sawicki and Sawicki, 1990), causing principally respiratory or enteric diseases (Lai and Holmes, 2001). They are currently classified in the family *Coronaviridae*, which is united in the order *Nidovirales* together with three other families: the *Toroviridae*, the *Arteriviridae* (Snijder and Meulenberg, 1998), and the *Roniviridae* (Cowley *et al*., 2000). Coronaviruses have the largest genomes among all the discovered RNA viruses.

Up to now, there are approximately 20 species in the family *Coronaviridae*, classified into 3 groups (Table 1-1). They can infect not only humans but also cattle, pigs, rodents, cats, dogs and birds to cause acute or chronic respiratory, enteric and central nervous systems diseases (Cavanagh, 1986; Weiss and Navas-Martin, 2005).

1.2. History of Coronavirus

Coronavirus was first isolated from chickens in 1937, i.e. avian infectious bronchitis virus (IBV). In 1965, Tyrrell and Bynoe used cultures of human ciliated embryonal trachea to propagate the first human coronavirus (HCoV) in vitro. Because coronaviruses showed high similarity by morphology in negative staining electron microscopy (Almeida and Tyrrell, 1967), they were classified as a new virus family. The unusual morphology with “spikes” is a special

characteristic of coronaviruses, which is also the origin of the name for this family (Almeida *et al*., 1968).

In 2003, a new type of coronavirus was identified as the cause of the emergent disease called severe acute respiratory syndrome (SARS), resulting in more than 8000 patients and 774 deaths in 30 countries (WHO: http://www.who.int/csr/sars/ country/tale2003_09_23/en).

Following the identification of SARS-CoV, two more human respiratory coronaviruses, HCoV-NL63 (van der Hoek *et al*., 2004) and HCoV-HKU1 (Woo *et al*., 2005), were identified. Three distinct bat coronaviruses were also been found (Lau *et al*., 2005; Li *et al*., 2005; Poon *et al*., 2005). Meanwhile, new IBV-like viruses have been discovered that infect geese, pigeons and ducks (Jonassen *et al*., 2005).

Table 1-1. Coronavirus species and groups

Group	Species
Group 1	
Subgroup 1a	Porcine transmissible gastroenteritis virus (TGEV)
	Canine enteric coronavirus (CECoV)
	Feline coronavirus (FCoV)
Subgroup 1b	
	Porcine epidemic diarrhea virus (PEDV)
	Human coronavirus 229E (HCoV-229E) and other species (HCoV-NL63)
	Bat coronavirus (Bat-CoV-61, Bat-CoV-HKU2)
Group 2	
Subgroup 2a	
	Murine hepatitis virus (MHV)
	Human coronavirus OC43 (HCoV-OC43) and other species (HCoV-HKU1)
	Bovine coronavirus (BCoV)
	Canine respiratory coronavirus (CRCoV)
	Porcine hemagglutinating encephalomyelitis virus (HEV)

	Puffinosis coronavirus (PCoV)
Subgroup 2b	
	Severe acute respiratory syndrome coronavirus (SARS-CoV)
	Bat SARS coronavirus (Bat-SARS-CoV)
Group 3	
	Infectious bronchitis virus (IBV)
	Turkey coronavirus (TCoV)
	Pheasant coronavirus (PhCoV)
	Goose coronavirus (GCoV)
	Duck coronavirus (DCoV)
	Pigeon coronavirus (PiCoV)

1.3. Virion morphology

The name "coronavirus," is derived from the "corona"-like or crown-like morphology when observed under electron microscopy. Coronaviruses are spherically shaped particles about 80-120 nm in diameter (Fig. 1-1). They are also moderately pleiomorphic with club-like peplomers (spike proteins) projecting some 17-20 nm from the virion surface (McIntosh, 1974). A short structure under the spikes is also found, but only in a subset of group 2 coronaviruses, known as hemagglutinin-esterase (HE) protein (Guy *et al*., 2000).

Inside the virion, there is a helical nucleocapsid, which shows filamentous structures 9-11 or 11-13 nm in diameter, with a 3-4 nm central canal (Caul *et al*., 1979). It is composed of the single-stranded, positive-sense RNA genome and the nucleocapsid protein. The RNA genome, ranging from approximately 27.3 to 31.3 kb, is the largest genome among all RNA viruses, including those RNA viruses with segmented genomes (Masters, 2006).

a

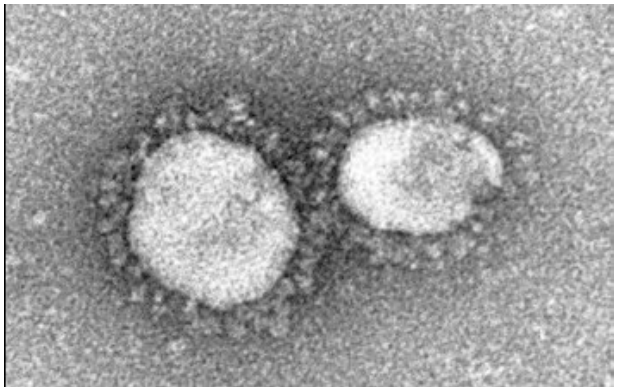

b

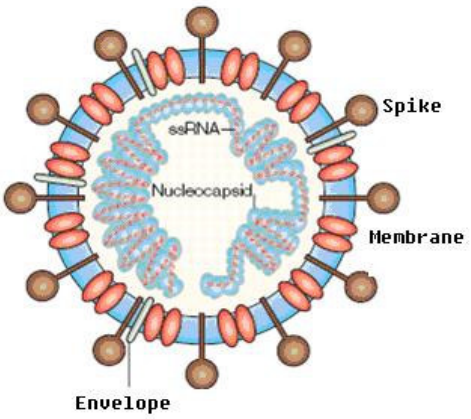

Figure 1-1

(a) Coronavirus in electron microscopy (adapted from Almeida and Tyrrell ,1967).

(b) Schematics of coronavirus viron with minimal structural proteins.

1.4. Genome

Coronaviruses have a single-stranded, positive-sense RNA genome, which ranges from 27.3 kb to 31kb in length. It contains both 5'caps (Lai *et al*., 1981) and 3' poly (A) tails (Wege *et al*., 1978). The RNA genome (5'-end) starts with a leader sequence of 65-98 nucleotides, followed by a 210-530 nulceotide untranslated region (UTR). At the 3'-end of the RNA genome is another UTR of 270 to 500 nucleotides. Almost two-thirds of the entire genome from 5'-end is gene 1, consisting of two overlapping ORFs (1a and 1b), which encodes the necessary viral polymerases. Genes for the four structural proteins are arranged in the order 5'-replicase-S-E-M-N-3', and clustered at the 3' end, comprising less than one-third of the entire length (Fig. 1-2). The locations of other protein genes vary significantly among different coronavirus species.

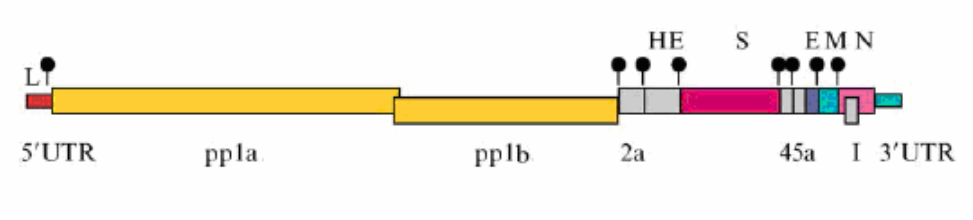

Figure 1-2

Coronavirus genome organization as illustrated by the group 2 virus MHV (Adapted from de Haan and Rottier, 2005).

The single-stranded, positive-sense RNA genome contains a 5'-terminal cap and a 3'-terminal poly(A) tract. The leader sequence (L) in the 5' UTR is indicated. All coronaviruses have their essential genes in the order 5'-pol-S-E-M-N-3'. The gene 1 comprises approximately two-thirds of the genome. The ORF1b is translated by translational read-through by a ribosomal frameshift mechanism. Transcription regulatory sequences (TRSs) located upstream of each gene, which serve as signals for the transcription of the subgenomic (sg) RNAs, are indicated by circles. The genes encoding the structural proteins HE, S, E, M, and N are specified. Gray boxes indicate the accessory, group-specific genes, in the case of group 2 coronaviruses, genes 2a, HE, 4, 5a, and I.

1.5. Structural proteins

Proteins that contribute to the overall structure of all coronaviruses are the spike (S), envelope (E), membrane (M) and nucleocapsid (N) proteins (Table 1-2).

1.5.1. Spike protein (S)

The S protein is the outermost component of coronavirus, responsible for receptor binding, viral and host cell membrane fusion (Fig. 1-3a) (Collins *et al*., 1982). It is a very large, N-exo, C-endo transmembrane protein that builds up into trimers (Delmas and Laude, 1990; Song *et al*., 2004).

The S protein is highly glycosylated: with a size of approximately 128-160 kDa for monomers, 150-200 kDa for glycosylated forms (Holmes et al., 1981). It can be cleaved by a trypsin-like host protease into two polypeptides: S1 and S2, except that of the group 1 coronaviruses and SARS-CoV. From N- to C-terminus, S protein can be divided into three structural domains: a large external domain that contains S1 and S2, a transmembrane domain and a short C-terminal cytoplasmic domain.

S1 sequence is much more variable than S2, which is associated with antigenicity and pathogenicity of the virus (Fazakerley et al., 1992). S2 contains two heptad repeat motifs (HR1 and HR2) that suggest a coiled-coil structure (de Groot et al., 1987; Luo et al., 1998). There is a cleavage site at a higly basic

motif: RRFRR in IBV S protein (Cavanagh et al., 1986), and RRAGR in MHV strain A59 S protein (Luytjes et al., 1987).

Entry of coronavirus into target cells is driven by interactions of the S protein with the cellular receptor. Angiotensin converting enzyme 2 (ACE2), an integral component of the renin angiotensin systmem, was identified as a functional receptor for SARS-CoV (Li et al., 2005). It also mediates cellular entry of the newly discovered human coronavirus (HCoV) NL63 (Hofmann et al., 2006). Meanwhile, the SARS-CoV S protein has been demonstrated to be able to induce apoptosis in Vero E6 cells in a time- and dose-dependent manner (Chow et al., 2005).

a.

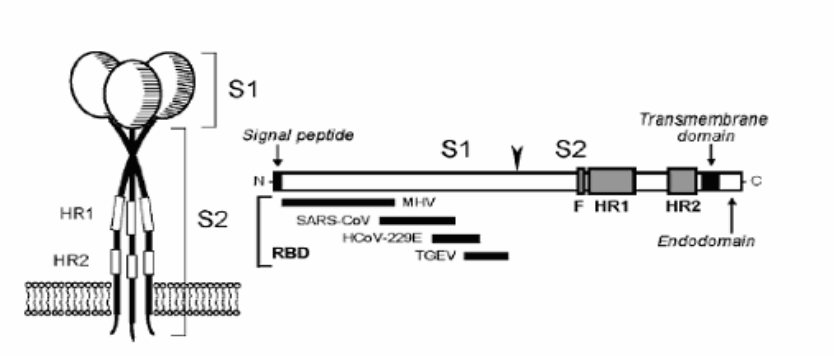

b.

c.

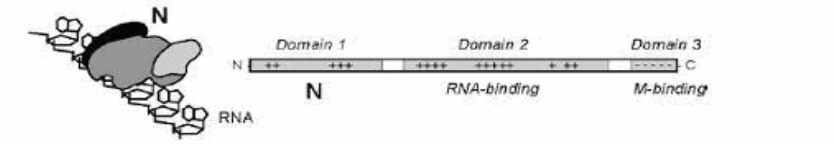

Figure 1-3

The schemes of spike (S), envelope (E), and nucelocapsid (N) proteins of coronviruses. The linear maps of the proteins are at the right part. Models of each protein are at the left part. Tm: transmembrane domain (Adapted from Masters, 2006).

1.5.2. Membrane protein (M)

The M protein is the most abundant component of coronaviruses and ranges in size from 25-30 kDa (221-262 amino acids) (Sturman, 1977). M protein is a triple-spanning membrane protein with a small amino-terminal domain located on the exterior of the virion, or intracellularly, in the lumen of the ER. The amino-terminal 20 or so residues are hydrophilic, exposed at the virion surface, and have a small number of glycosylation sites (Fig. 1-4).

The precise topology of M protein is still not clear. The ectodomain of M protein is followed by three transmembrane domains and then a large carboxy terminus. Generally, the endodomain is situated in the interior of the virion or on the cytoplasmic face of intracellular membranes (Rottier, 1995). However, some M proteins of MHV and TGEV expose their C terminus at the viron surface (Risco et al., 1995; Locker et al., 1992).

In group 2 coronavirus, M protein is O-linked glycosylated except MHV strain 2 (Yamada et al., 2000) and SARS-CoV (Nal et al., 2005). N-linked glycosylation is found in group 1 and 3 coronavirus M proteins (Cavanagh et al., 1988). It is demonstrated that the glycosylated M protein can induce alpha interferon in vitro and influence organ tropism in vivo (Charley and Laude, 1988; de Haan et al., 2003; Laude et al., 1992).

The M protein can interact with each other through three transmembrane domains, which is the driving force for virion envelope formation (de Haan et al., 2000). The C-terminus of M is extremely sensitive to small changes in the

virus-like particles (VLPs) formation (de Haan et al., 1998). However, virus can tolerate more alterations than VLPs because of some extra intermolecule needed in virus replication.

The interaction of M with S was demonstrated by several lines of evidence: complexes of the M and S proteins are observed in BCoV-infected cells (Nguyen and Hogue, 1997); the S protein is retained by the presence of M protein and coimmunoprecipitated with M protein (Opstelten et al., 1995). It is shown that the ectododomain of M protein and the C-terminal 25 residues of the endodomain are not involved in the interaction of M and S proteins (de Haan et al., 1999). Nevertheless, a cysteine-rich, C-terminal region of the endodomain of S protein is found to be important for incorporation of S proteins into VLP (Godeke et al., 2000; Kuo et al., 2000; Bos et al., 1995; Chang et al., 2000; Bosch et al., 2005).

The M protein was integrated with viral cores after treatment with NP-40, which provides evidence for M-N interaction (Risco et al., 1996). Similarly, the nucleocapsid purified from virions is bound by M proteins (Escors et al., 2001). Additionally, the M and N protein interaction region maps to a segment of 16 residues adjacent to the C-terminus of M protein (Escors et al., 2001). Meanwhile, swapping the N protein domain 3 with a heterologous protein allows the incorporation of this foreign protein into virions (Hurst et al., 2005).

The IBV M protein has been found to be crosslinked to E protein (Lim and Liu, 2001). Furthermore, the two proteins could be observed in close physical

proximity in infected and transfected cells (Corse and Machamer, 2003). When the M protein is expressed alone, it is localizes in the Golgi complex (Tooze et al., 1984); when co-expressed with E protein, it localizes to the pre-Golgi compartments, where virus particles bud (Lim and Liu, 2001).

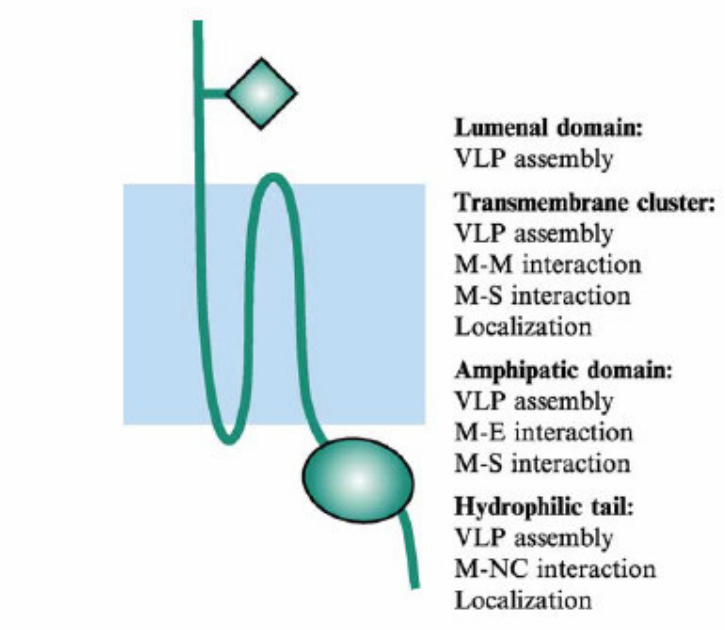

Figure 1-4

The various domains of the MHV M protein and the processes for which they are important. The amphipathic domain of the M protein is represented by an oval structure (Adapted from de Haan and Rottier, 2005).

1.5.3. Envelope protein (E)

The E protein is a small protein, varying from 8.4 to 12 kDa (76-109 amino acids) (Fig. 1-3b). Due to its low quantity, E was discovered as a structural protein much later than other structural proteins (Liu and Inglis, 1991, Godet et al., 1992).

The E protein possesses a short hydrophilic amino terminus (8-12 residues), followed by a large hydrophobic region (21-29 residues), and a hydrophilic carboxy-terminal tail (39-76 residues). The E protein of TGEV is a C-exo, N-endo membrane protein (Godet et al., 1992); however, the orientation is N-exo, C-endo for MHV and IBV E proteins (Corse and Machamer, 2000; Raamsman et al., 2000).

Functionally, it has been reported that co-expression of the E and M protein can produce VLPs, which are of the same size and morphology as the authentic virions (Bos et al., 1996; Vennema et al., 1996; Baudoux et al., 1998; Corse and Machamer, 2000). In addition, the singly expressed E protein can be released in vesicles (Corse and Machamer, 2000; Maeda et al., 2001). The direct interaction of IBV M and E protein via their cytoplasmic domains in pre-Golgi compartments has been reported (Lim and Liu, 2001). However, the recombinant MHV can be recovered with the entire E gene deletion, which indicates that the E protein is not essential for MHV replication in vitro (Kuo and Masters, 2003). Furthermore, the SARS-CoV E protein is characterized by viroporins which modify membrane permeability and help the efficient release

of progeny viruses (Liao *et al.*, 2005).

1.5.4. Nucleocapsid protein (N)

The N protein binds the genomic RNA in a beads-to-a-string fashion to form a helical nucleocapsid (RNP) (Fig. 1-3c). The RNP of coronaviruses varies from 9-11 to 14-16 nm in diameter (Laude and Masters, 1995).

The N protein, ranging from 377 to 455 amino acids (43-50 KDa) in length, has a high (7-10 %) serine content. Three structural domains have been identified on the N protein, which are separated by two highly variable spacer regions (Parker and Masters, 1990).

Domains 1 and 2 are rich in arginines and lysines, which are candidates for RNA binding (Fig. 1-2c). Domain 3 is a negatively charged region because of many more acidic residues. Both sequence-specific and nonspecific sequence of RNA can be bound by the N protein: positive-sense transcription regulating sequence within the leader RNA (Chen *et al.*, 2005; Nelson *et al.*, 2000); regions of the 3' UTR (Zhou *et al.*, 1996); the N gene (Cologna *et al.*, 2000); and the genomic RNA packaging signal (Molenkamp and Spaan, 1997). The N protein can also bind to the 5'- and 3'-end of viral RNA, suggesting that N may be one component of the RNA synthesizing machinery (Compton *et al.*, 1987). Finally, it is reported that N binding to the membrane enables the formation of the RNA replication or transcription complex (Anderson and Wong, 1993).

To assemble nucleocapsids, IBV N protein forms a dimer, which is

composed of two globular domains that are resistant to proteolysis. Amino acids 29 to 160 form the N-terminal RNA-binding domain and residues 218 to 329 form its C-terminal dimerization domain (Fan et al., 2005; Tan et al., 2006). In contrast, the carboxyl terminus of SARS-CoV N protein is responsible for its self-association and nucleic acid binding (Luo *et al*., 2006).

The N protein is the most abundant viral protein produced in the infected cells. It is an important multifunctional protein and plays roles in viral packaging, viral core formation, and signal transduction (Hiscox *et al*., 2001; He *et al*., 2003).

The SARS-CoV N protein is reported to associate with several cell signaling pathways, such as AP-1 or Akt pathway (He *et al*., 2003; Surjit *et al*., 2004). It also reorganizes actin in mammalian cells under stressed conditions (Surjit *et al*., 2004).

It has been reported that the SARS-CoV N protein plays a crucial role in viral RNP assembly and replication by interacting with cyclophylin A and human cellular heterogeneous nuclear ribonucleoprotein A1 (Luo *et al*., 2004, 2005). The SARS-CoV N protein can also be sumoylated by human ubiqutin-conjugating enzyme 2 (hUbc9), which promotes homo-oligomerization and plays a role in the N protein-mediated interference of host cell division (Li *et al*., 2005).

1.5.5. Hemagglytinin-Esterase protein (HE)

Only group 2 coronaviruses belonging to the MHV group possess the HE protein. The HE protein is approximately 48 kDa in size, and increases to 65 kDa after glycosylation (Kienzle *et al*., 1990). It forms a second set of small spikes on the coronavirus virion surface. The HE protein can serve as a cofactor for S protein, assisting in the attachment of virus to host cells. HE alone can mediate hemagglutination and hemadsorption, though it has a weaker activity than S protein (Pfleiderer *et al*., 1991).

Additionally, HE also has esterase activity: neuraminate-O-acetylesterase. The role of HE protein in coronavirus infection has been systematically documented: in vitro, MHV loses the expression of HE after several passages (Lissenberg *et al.*, 2005). However, in vivo, the HE protein dramatically enhances virulence, as measured by viral spread and lethality (Kazi *et al*., 2005).

Table 1-2. Properties and functions of coronavirus structural proteins

Nucleocapsid phosphoprotein (N)	Forms nucleocapsid by binding to viral RNA Influences cell cycle
Membrane glycoprotein (M)	Triggers virus particle assembly Interacts with viral nucleocapsid and main structural proteins Induces α-interferon
Envelope protein (E)	Triggers virus particle assembly
Spike glycoprotein (S)	Determines viral cell tropism Induces cell-cell fusion
Hemagglutinin-esterase glycoprotein (HE)	Causes hemagglutination Esterase cleaves acetyl froups from 9-O-acetyl neuraminic acid

1.6. 3C-like protease (3CLpro)

The 3CLpro, the main viral protease, was identified as a 33 kDa protein in IBV-infected cells (Liu and Brown, 1995; Lim *et al.*, 2000; Ng and Liu, 2000), which is responsible for the processing of the C-terminal part of pp1a and pp1ab polyproteins (Ziebuhr *et al.*, 2000).

The coronavirus '3C-like protease' is named after picornavirus 3C protease because they have similar substrate specificities and the identification of cysteine as the principal catalytic residue in the context of a predicted two-β-barrel fold (Gorbalenya *et al.*, 1989).

At present, the 3CLpro is a well-characterized coronavirus protease. It is confirmed that the predicted Q-S dipeptide bonds in the 1b ORF are the targets for the protease activity of 3CLpro of IBV (Liu *et al.*, 1994, 1997, 1998; Ng and Liu, 1998, 2000). Furthermore, the 3CLpro is the only coronavirus protein for which structural information is available (Anand et al., 2002, 2003).

Coronavirus 3CLpros have a three-domain structure, with an active site located in a cleft between the first and second domains (Anand *et al.*, 2002,2003; Barrette-Ng *et al.*, 2002; Yang *et al.*, 2003). Domains I and II (residues 8 to 99 and 100 to 183, respectively) are six-stranded anti-parallel β barrels and together resemble the architecture of chymotrypsin and of picornavirus 3CLpro. The substrate-binding site is located in a cleft between these two domains. A long loop (residues 184 to 199) connects domain II to the C-terminal domain (domain Ⅲ, residues 200 to 300). This latter domain, a globular cluster of five

helices, has been implicated in the proteolytic activity of 3CLpro (Ziebuhr, et al., 1997). For TGEV 3CLpro, residues 8-100 form domain I; residues 101-183 constitute domain II; and residues 200-302 make up domain III (Anand *et al.*, 2002). The interior of the β-barrel of domain I consists of hydrophobic residues. Domain III is composed of five α-helices (Hegyi & Ziebuhr, 2002) and the loops connecting them. The SARS-CoV 3CLpro undergoes major pH-dependent conformational changes, essentially explaining the varying activity of 3CLpro at different pH values (Yang *et al.*, 2003).

The 3CLpro of coronavirus forms a tight dimer in the crystal. In the 3CLpro dimer, the N-terminal amino acid residues are squeezed in between domains II and III of the parent monomer and domain II of the other monomer, where they make a number of very specific interactions that appear tailor-made to bind this segment with high affinity after auto-cleavage. This mechanism would immediately enable the catalytic site to act on other cleavage sites in the polyprotein (Anand *et al*., 2002).

1.7. Accessory proteins

Coronaviruses contain 6-9 ORFs among different species. Through natural or engineered mutants, some accessory genes have been found to be nonessential for viral replication in tissue culture: genes 5a and 5b of IBV (Casais *et al*., 2005; Youn *et al*., 2005); genes 4 and 5a of MHV (de Haan *et al*., 2002); genes 2a and HE of MHV (de Haan *et al*., 2002; Schwarz *et al*., 1990).

Furthermore, some accessory proteins are not important in infecting the natural host: gene 4 of MHV (Ontiveros *et al*., 2001) and gene 7b of FIPV (Haijema *et al*., 2003). In contrast, gene 7 of TGEV can greatly improve virus replication in its host (Ortego *et al*., 2003).

SARS-CoV 3a protein localizes at the surface of Golgi apparatus, SARS-CoV-infected cells and SARS-CoV virions (Ito *et al*., 2005). Moreover, SARS-CoV 3a protein forms a potassium-sensitive channel to promote virus release (Lu *et al*., 2006). Additionally, it has been reported that SARS-CoV 7a proteins are viral structural proteins (Huang *et al*., 2006). Interestingly, when the gene 6 of SARS-CoV is inserted into the genome of MHV, the virulence of this attenuated MHV can be enhanced greatly (Pewe *et al*., 2005).

1.8. Viral replication cycle

Coronavirus infections are initiated by the binding of virions to cellular receptors. After entering the cells, they release their genetic material (RNA) into the cytoplasm, where it directs the production of new virus genetic material and virus proteins. These components bud into the endoplasmic reticulum-Golgi intermediate compartment (ERGIC) and assemble into new virions. These progeny virions are transported to other cells in smooth-walled vesicles and eventually released onto the surface of the cell in large numbers (Fig. 1-5).

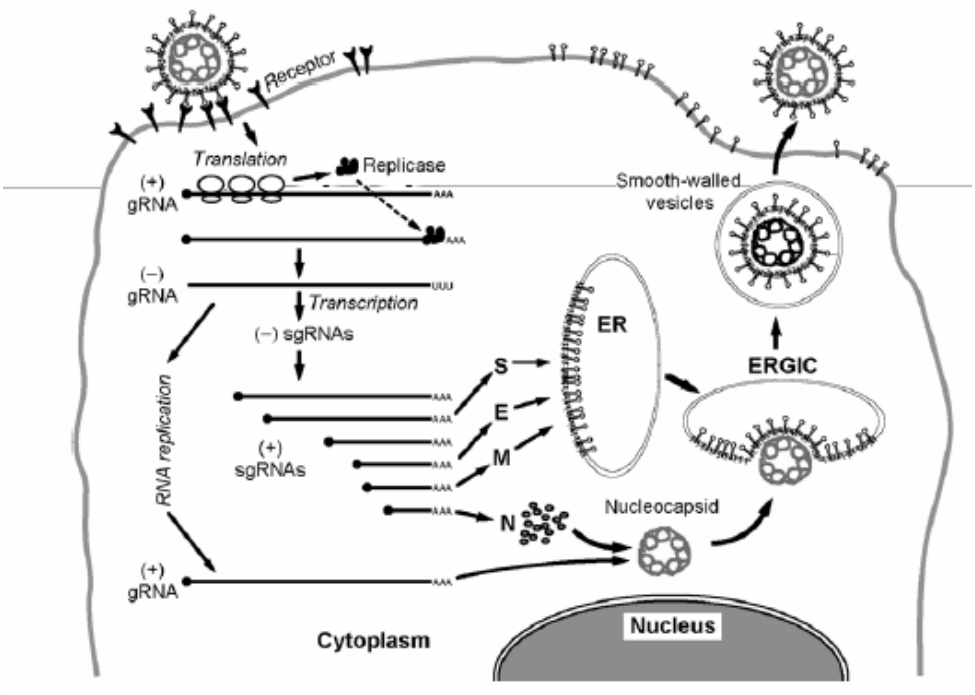

Figure 1-5

Coronavirus life cycle (Adapted from Masters, 2006).

Coronavirus infections are initiated by the binding of virions to cellular receptors. After entering the cells, they release their genetic material (RNA) into the cytoplasm, where it directs the production of new virus genetic material and virus proteins. These components bud into the endoplasmic reticulum-Golgi intermediate compartment (ERGIC) and assemble into new virions. These progeny virions are transported to other cells in smooth-walled vesicles, and are eventually released onto the surface of the cell in large numbers.

1.8.1. Attachment

The first step in viral replication cycle is the binding of virions to the plasma membranes of target cells. The main determinant of viral tropism is the binding of the S protein to a specific receptor glycoprotein on the cell surface. Receptors have been identified for several coronaviruses (Table 1-3). The MHV receptor is a murine biliary glycoprotein belonging to the carcinoembryonic antigen (CEA) family in the immunoglobulin (Ig) superfamily (Nedellec *et al.*, 1994). Aminopeptidase N serves as a receptor for different coronaviruses in serogroup 1: feline infectious peritonitis virus (FIPV) (Tresnan *et al.*, 1996) and feline enteric coronavirus (FCoV). It is also a receptor for canine coronavirus (CCoV) (Benbacer *et al.*, 1997), porcine transmissible gastroenteritis virus (TGEV) (Delmas *et al.*, 1992), and human coronaviruses 229E (HCoV-229E) (Yeager *et al.*, 1992). In addition, it serves as a receptor for infectious bronchitis virus (IBV, Arkansas 99 serotype) in serogroup 3 (Christine *et al.*, 2006).

Aminopeptidase N is a broad specificity aminopeptidase, which plays a role in the final digestion of peptides, generated from hydrolysis of proteins, by gastric and pancreatic proteases. It may be involved in the metabolism of regulatory peptides of diverse cell types (Lachance *et al.*, 1998).

Li *et al.* reported that angiotensin-converting enzyme 2 (ACE-2) is the receptor critical for mediating SARS-CoV entry into host cells (Li *et al.*, 2003). ACE-2 is a recently described type I transmembrane metallocarboxypeptidase with homology to ACE, an enzyme long-known to be a key player in the

renin-angiotensin system (RAS) and a target for the treatment of hypertension (Riordan *et al.*, 2003). Although its roles continue to be elucidated, ACE-2 appears to be involved in cardiac function and may act as a negative regulator of RAS (Crackower *et al.*, 2002).

1.8.2. Penetration and uncoating

After binding to its specific receptor through a major conformational change in the S molecule (Sturman *et al.*, 1990), the virus enters the cell. This process involves the fusion of the viral envelope with either the plasma membrane, such as in the case of MHV (Sturman *et al.*, 1990; Weismiller *et al.*, 1990) or the endosomal membranes, such as in HCoV-229E and SARS-CoV (Normura *et al.*, 2004; Hofmann *et al.*, 2004; Simmons *et al.*, 2004). Current experimental evidence indicates that different coronaviruses can enter cells either by pH-independent endocytosis (Gallagher *et al.*, 1991; Nash and Buchmeier, 1997) or by acidic pH-dependent fusion at the plasma membrane.

Table 1-3. Coronavirus receptors

Group	Virus species	Receptor
1	TGEV	Porcine aminopeptidase N (pAPN)
	FIPV	Feline aminopeptidase N (fAPN)
	CCoV	Canine aminopeptidase N (cAPN)
	HCoV-229E	Human aminopeptidase N (hAPN)
	HCoV-NL63	Angiotensin-converting enzyme 2 (ACE2)
2	MHV	Murine carcinoembryonic antigen-related adhesion molecules 1 and 2 (mCEACAM1 , mCEACAM2)
	BCoV	9-O-acetyl sialic acid
	SARS-CoV	Angiotensin-converting enzyme 2 (ACE2), CD209L (L-SIGN)
3	IBV	Sialic acid

1.8.3. RNA synthesis

The coronavirus genomic RNA is approximately 30,000 nucleotides, which encodes structural and non-structural proteins of the virus. Some of these non-structural proteins have a critical role in viral RNA synthesis, such as papain-like protease and 3C-like protease. RNA synthesis includes two parts: RNA replication and RNA transcription. Replication is defined as the process whereby genome-sized RNA, which also functions as mRNA, is produced. Transcription is a process whereby subgenome-sized mRNAs are produced.

Initially, the 5'- two-thirds of the positive-sense genome is translated to produce replicase polyproteins, which then produce a full-length negative-sense strand (Lai and Cavanagh, 1997). This negative strand is used as a template to produce a nested set of subgenomic mRNA through a discontinuous transcription method (Sawicki *et al.*, 1990).

All of the subgenomic mRNAs have an identical 5' non-translated leader sequence of 70-100 nucleotides and coincident 3' polyadenylated ends (Baric and Yount, 2000; Sethna *et al.*, 1989, 1991). Each mRNA is monocistronic, the genes at the 5'-end being translated from the longest mRNA and so on. Between each of the genes there is a repeated intergenic sequence, called transcription-regulating sequence (TRS), which interacts with the transcriptase and cellular factors to attach the leader sequence onto the start of each ORF (Thiel *et al.*, 2003; van der Most *et al.*, 1995) (Fig. 1-6).

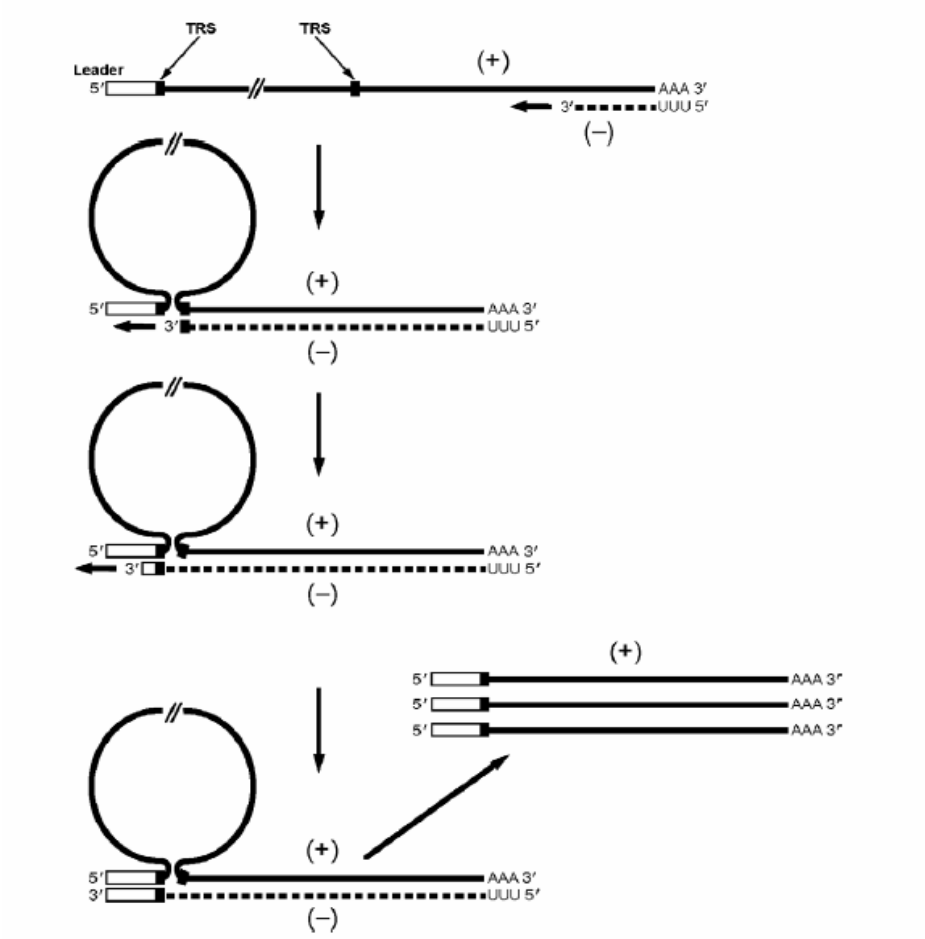

Figure 1-6

Model for discontinuous negative-strand transcription (Adapted from, Masters, 2006).

Negative-strand sgRNAs are initiated at the 3' end of the genomic mRNA template. A complex of the (+)gRNA and the (-)sgRNA then serves as the template for synthesis of multiple (+)sgRNAs.

In the discontinuous transcription model (Fig.1-6), the viral polymerase begins transcription from the 3' end of a genomic template, which can switch templates at an internal TRS and resumes synthesis at the homologue TRS sequence at the 3' end of the genomic leader RNA. The nascent negative-strand subgenomic RNAs, associated with positive-strand genomic RNA, then serve as the template for synthesis of multiple copies of the corresponding positive-strand subgenomic RNAs (Sethna *et al.*, 1989).

Minus strand RNA synthesis begins from the 3'-end of a genomic RNA with the help of a functional membrane-bound replication-transcription complex (RTC). The elongation of nascent minus strand RNA either stops at the first body TRS, or relocates at other TRS motif by complementarity and then continues to complete its synthesis. The newly synthesized minus strand RNA is extended by copying the 5'-end of a genome, and later, it will serve as a template for mRNA synthesis (Pasternak *et al.* 2006; Sawicki *et al.* 2005).

The plus strand RNAs produced by coronaviruses are 50-100 fold more than their minus-strand templates. Coronavirus RNA synthesis can be detectable at 2-3 hours post-infection. Throughout the infection, the various kinds of plus stands are synthesized constantly in a fixed molar ratio to each other (Sawicki *et al.* 2005). The minus strand RNAs are produced shortly after the formation of RTCs. Their synthesis rate reaches a peak at 5-6 hours post-infection, and declines but does not cease. The amount of mRNA synthesis is determined at the level of minus-strand synthesis (Sawicki *et al.* 1986).

1.8.4. Assembly and release of virions

The first step is the formation of nucleocapsids. It is demonstrated that an MHV packaging signal was present within the 61 nucleotides, which are located on MHV genomic RNA 1,381 to 1,441 nucleotides upstream of the 3' end of gene 1. (Fosmire et al., 1992, Molenkamp and Spaan, 1997).

Once the nucleocapsid is formed, it interacts with the M protein at the membranes of the ER or the Golgi complex (Sturman *et al.*, 1980). Virus budding is first detected at a specialized membrane structure called the budding compartment, located between the ER and the Golgi, near the sites of accumulation of the M proteins (Dubois-Dalcq *et al.*, 1982; Tooze *et al.*, 1984; Tooze and Tooze, 1985; Klumperman *et al.*, 1994).

Virus budding is most likely triggered by the interaction of E protein with the M protein locating on the membrane (Bos *et al.*, 1996). Although the E protein is a minor component of the virion, the E protein is essential for the initiation of virus assembly and budding (Vennema *et al.*, 1996). The S and HE proteins are incorporated into virions through their interactions with M protein (Opstelten *et al.*, 1995). They form an S-M-HE ternary complex before the glycoproteins undergo trimming of their sugar chains (Opstelten *et al.*, 1995).

After budding, virus particles may undergo further morphologic changes within the Golgi, resulting in the appearance of mature virus particles with a compact, electron-dense internal core, as they reach the secretory vesicles (Risco, *et al.*, 1998; Salanueva, *et al.*, 1999). Eventually the virions

were released into extracellular space through vesicles transport or exocytosis (Griffiths and Rottier, 1992).

1.8.5. Coronavirus genetics

1.8.5.1. Virus mutants

Coronaiviruses mutate at a high frequency because of the absence of proof-reading function of RNA polymerase (Steinhauer *et al.*, 1986). Temperature-sensitive (ts) MHV mutants have been grouped into seven classes, five of which are RNA synthesis negative at the non-permissive temperature. All of these mutations have been mapped within gene 1 (Baric *et al.*, 1990). Several RNA-positive mutants can replicate viral RNA at the non-permissive temperature but alter cytopathic effects or no infectious virions are produced (Leibowitz *et al.*, 1982). These kinds of mutation are located in N or S genes (Koetzner *et al.*, 1992; Masters *et al.*, 1994; Peng *et al.*, 1995).

Another kind of viral mutants was obtained by treating viruses with neutralizing monoclonal antibody, and selecting mutant viruses resistant to neutralization (Cavanagh *et al.*, 1995). These mutant viruses were presumed to have defects in the S gene, which have similar growth properties to their parental strains (Wang *et al.*, 1992).

Deletion mutants also occur frequently. PRCoV comes from TGEV, which has a large deletion within the S protein (Bae *et al.*, 1991). Moreover, FIPV is

most likely derived from FECoV due to a deletion in S gene (Vennema *et al.*, 1998).

1.8.5.2. RNA recombination

Although non-segmented genomes of RNA viruses undergo low recombination frequencies, coronaviruses have high recombination frequencies, calculated to be 25 % (Baric *et al.*, 1990). MHV, TGEV and IBV have been demonstrated to have RNA recombination both in tissue culture and in experimental and natural animal infections (Ballesteros *et al.*, 1997; Keck *et al.*, 1988; Kottier *et al.*, 1995).

RNA recombination plays an important role in both the natural evolution of coronaviruses and the evolution of different coronavirus species (Cavanagh D, 1992; Jia *et al.*, 1995; Masters *et al.*, 1994).

1.8.5.3. Defective-interfering RNA (DI RNA)

The DI-RNAs are small RNA molecules derived from a parental virus genome when coronaviruses are passaged at a high multiplicity of infection (Makino *et al.*, 1984). Their formation in infected cells can strongly influence virus life cycle (replication, accumulation or symptoms). There are three types of DI RNAs in coronaviruses. All of them contain both the 5' and 3' ends of the viral genome, which include the cis-acting signals for RNA replication (Makino

et al., 1988). The biologic significance of DI RNAs is less well established because DI RNAs have not been detected during natural coronavirus infections.

1.9. Replicase complex

The replicase complex carries out the viral RNA replication and transcription. The proteins in it are encoded by the first gene of coronavirus. The first gene has two ORFs, which are expressed by a programmed ribosomal frameshift. That is, the latter ORF is in the –1 frame relative to the former ORF.

1.9.1. Ribosomal frameshifting

Coronaivrus ribosomal frameshifting was first demonstrated in IBV (Brierley *et al.*, 1989). The rate of ribosomal frameshifting incidence is 25-30%. IBV ribosomal frameshifting depends on two genomic RNA elements: a heptanucleotide "slippery sequence" (UUUAAAC) and a downstream, hairpin-type pseudoknot (Brierley *et al.*, 1989). Moreover, the spacing between the two elements is very important.

1.9.2. Replicase proteins

Only recently, the replicase cleavage maps have been completed for each coronavirus group (Bonilla *et al.*, 1997; Lim and Liu, 1998). The final products of pp1a and pp1ab are 15-16 nonstructural proteins, named nsp1-nsp16 (Fig. 1-7). The nsp1 of MHV plays a role in cell cycle arrest to set up a favorable

cellular environment for viral replication (Chen and Makino, 2004; Chen *et al.*, 2004).

Nsp2 is different among coronaviruses. Recombinant virus can be recovered from the nsp2 deletion genome of MHV, but it shows delayed viral growth kinetics (Graham *et al.*, 2005).

Nsp3 is Papain-like protease (PLP). Most coronaviruses have two papain-like proteases (PL1pro and PL2pro). However, IBV and SARS-CoV just have a single PLpro. Furthermore, nsp3 in some coronaviruses have a functional domain: ADP-ribose-1"-monophosphatase activity, which plays a role in tRNA processing (Putics *et al.*, 2005). There is a special "SARS-unique" domain in nsp3 of SARS-CoV (Snijder *et al.*, 2003).

Nsp5 is 3CLpro, also called main protease. This protein can form a dimer and each monomer has a three-domain structure, with an active site in a cleft surrounded by the first and second domains (Anand *et al.*, 2003; Yang *et al.*, 2003).

Transmembrane domains in nsp3, nsp4 and nsp6 lead the replicase complex to the intracellular membranes and remodel the membrane to form double-membrane compartments. Viral RNA synthesis is carried out in these compartments (Bi *et al.*, 1999; Gosert *et al.*, 2002; Prentice *et al.*, 2004).

The solved 3-D structures of nsp7 and nsp8 of SARS-CoV showed that eight monomers of each protein form a hollow cylindrical structure, which encircles an RNA template to be processed by RNA polymerase (Peti *et al.*,

2005; Zhai *et al.*, 2005). Furthermore, the nsp9 of SARS-CoV, binding RNA nonspecifically, can form a dimer to interact with nsp8 (Egloff *et al.*, 2004; Sutton *et al.*, 1991). The nsp7-nsp10 localize in discrete perinuclear and cytoplasmic foci in infected cells, in a membrane-associated complex that also includes nsp2 (Bost *et al.*, 2000).

Nsp12 is RNA-dependent RNA polymerase (RdRp), a membrane associated protein. It has the fingers, palm and thumb domains similar to reverse transcriptases. It is reported that RdRp interacts with 3Cpro, nsp8 and nsp9 (Brockway *et al.*, 2003).

Nsp13 is a helicase for unwinding the RNA with 5'-3' polarity. In addition, the nsp13 has RNA-dependent NTPase and dNTPase activities, which provide the energy for its translocation along RNA templates. Moreover, nsp13 is a RNA 5'-triphophatase to initiate the RNA capping (Ivanov and Ziebuhr, 2004; Ivanov *et al.*, 2004; Seybert *et al.*, 2000).

Nsp14 is an exonuclease, designated ExoN, involved in an RNA processing step integral to RNA transcription (Snijder *et al.*, 2003). Nsp15 is an endoribonuclease, called EendoU, hydrolyzing both single- and double-stranded RNA upstream of uridylate residues (Bhardwaj *et al.*, 2004; Ivanov *et al.*, 2004).The nsp16 has 2'-O-methyltransferse activity involved in RNA capping (von Grotthuss *et al.*, 2003).

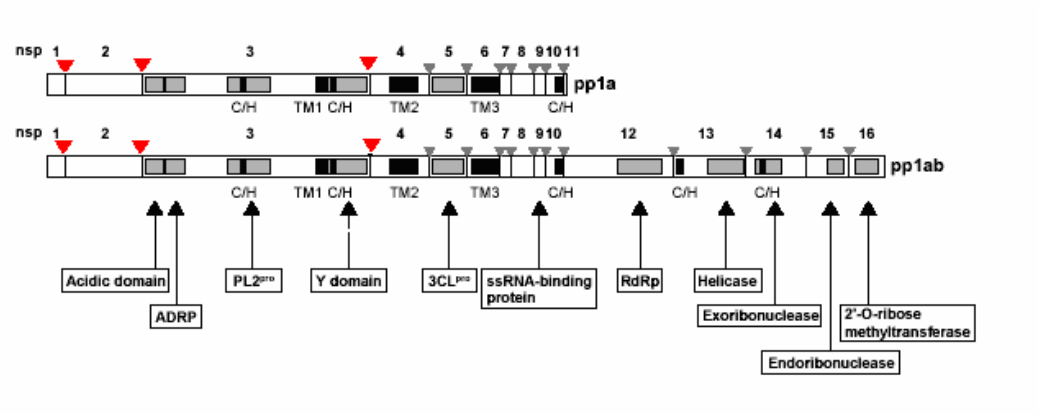

Figure 1-7

Protein products of the replicase gene (Adapted from Ziebuhr, 2004).

Cleavage sites and processed products of pp1a (nap1-nsp11) and of pp1ab (nsp1-nsp10, nsp12-nsp16) are shown. Predicted and / or experimentally demonstrated activities are indicated. The red arrows represent the cleavage sites of papain-like protease; the gray arrows point to the cleavage sites of 3C-like protease.

1.10. Effects of coronavirus infection on host cells

Extensive morphological and biochemical changes, such as alterations in transcription and translation patterns, cell cycle, cell morphology, cytoskeleton and apoptosis pathways of host cells, occur in coronavirus infected cells. MHV, BCoV, IBV and FIPV induce cell fusion in culture and in infected tissues. Some other coronaviruses, which cannot cause cell fusion, induce rounding-up and lysis of cells (Gallagher *et al.*, 1991; Gombold *et al.*, 1993).

Infection by MHV leads to partial shutoff of host protein translation (Banerjee *et al.*, 2000) that is accompanied by an increase of MHV protein synthesis (Banerjee *et al.*, 2002). Firstly, the induced p38 MAPK by MHV infections increases the phosphorylation of elongation initiation factor (eIF) 4E to enhance translation rates of capped mRNA (Gingras *et al.*, 1999; Mizutani *et al.*, 2004). Secondly, 28S rRNA, an integral component of the 60S ribosome, is cleaved in MHV-infected cells (Banerjee *et al.*, 2000). Furthermore, specific host mRNAs are degraded by MHV and SARS-CoV infections (Kyuwa *et al.*, 1994; Leung *et al.*, 2005). Finally, in late infection of MHV, the Golgi apparatus undergoes fragmentation and rearrangement (Lavi *et al.*, 1996).

MHV, IBV, TGEV and SARS-CoV infections lead to the accumulation of infected cells in the G0/G1 phase, which is induced by MHV nsp1(Chen *et al.*, 2004), SARS-CoV 3b and 7a (Yuan *et al.*,2005; Yuan *et al.*, 2006), and N proteins (Wurm *et al.*, 2001). Moreover, many viral proteins induce apoptosis,

such as MHV E protein (An *et al.*, 1999), SARS-CoV E (Yang *et al.*, 2005) and 7a proteins (Tan *et al.*, 2004).

Several reports have shown that the proinflammatory response, for example, the upregulation of IL-8 expression, is increased after SARS-CoV infection (Cinatl *et al.*, 2004; Tang *et al.*, 2005).

1.11. Vaccines

More knowledge on coronavirus vaccines has been generated recently (Table 1-4). Live attenuated and killed coronavirus vaccines have been evaluated successfully. For IBV, live attenuated vaccine is more effective than killed vaccine (Farsang *et al*, 2002). The killed canine and bovine coronavirus vaccine have been proved to be safe and effective ((Pratelli *et al*, 2003).

Chickens immunized with a DNA plasmid encoding a CTL epitope from IBV are protected from acute viral infection (Wang and Khan, 2000). Antibodies elicited with a synthetic peptide comprising of a B-cell epitope and a T-helper cell determinant can protect mice against an acute fetal MHV infection (Koolen *et al*, 1990).

A DNA vaccine containing the nucleoprotein of the porcine TGEV has been used to vaccinate against gastroenteritis, inducing both humoral and cellular immune responses (Liu *et al*, 2001).

Table 1-4. Coronavirus vaccines

Live attenuated vaccines
PEDV: passaged 90 times in Vero cells
IBV: multiple serotypes, and recombination are problems
Killed vaccines
Canine CoV vaccine
IBV
Vectored vaccines
Adenovector for lactogenic immunity to TGEV spike
Baculovirus for TGEV S or S, M, N partly protects vs enteric challenge
Passive immunization
Neutralizing monoclonal antibody
Antibody dependent enhancement (ADE) with FCoV vaccines

1.12. Infectious bronchitis virus (IBV)

Infectious bronchitis (IB) is an acute, highly contagious respiratory disease occurring in chickens of all ages. It is characterized by coughing, sneezing, and a nasal discharge, which was caused by IBV. The major economic loss in mature chickens is the reduction in egg production and inferior egg quality. In younger birds, there may be a high death rate with a loss in weight gain and feed efficiency (http://www.omafra.gov.on.ca/english/livestock/poultry /facts/inf-75050.htm). In 1937, Beaudette and Hudson grew the virus on the chorioallantoic membrane of 12-day-old embryonated chicken eggs (Bijlenga, *et al.,* 2004).

IBV is in the third group of the order *Nidovirales*, family *Coronaviridae*, and genus *Coronavirus*. It possesses a large, positive-stranded RNA, approximately 27.6 kb, which produces five subgenomic mRNAs after being released into the cells. It has four structural proteins: S, N, M and E proteins. Gene 1, taking up approximately two-thirds of the genome, encodes many proteins that are associated with RNA replication and transcription.

In the case of IBV, interspersed among the genes encoding the structural proteins are two genes encoding four non-structural proteins: 3a, 3b, 5a and 5b (Boursnell *et al.,* 1987; Breslin *et al.,* 1999). These four proteins are not necessary for IBV replication in cell culture, in tracheal organ culture or in chicken embryos. Recombinant IBVs which inactivate these genes can still replicate to the same titers as the parent virus (Casais *et al.,* 2005).

The S protein of other coronaviruses is a determinant of host range and pathogenicity (Haijema *et al.,* 2004). However, the S protein of IBV is possibly, but not necessarily, a determinant of pathogenicity (Casais *et al.,* 2003; Hodgson *et al.,* 2004).

The N protein is a basic, phosphorylated structural protein, which is highly conserved among IBV strains (Williams *et al.,* 1992). The N proteins have multiple functions in the virus life cycle both in terms of interacting with viral RNA and modulating host cell processes (Wurm *et al.,* 2001). It is reported that IBV N proteins can interact specifically with RNA sequences within the 3' non-coding region of genomic RNA (Zhou *et al.,* 1996, 2000).

The major modification of IBV M protein is the co-translationally added aminoterminal N-linked glycans (Setern and Sefton, 1982). In the M protein of IBV, there is an internal membrane insertion sequence (Laude *et al.,* 1987). The M proteins are transported to the Golgi apparatus but not to the plasma membrane (Machamer *et al.,* 1987, 1990).

The E proteins of IBV are translated from the third ORF (a polycistronic mRNA), which has 109 amino acids, corresponding to molecular weights of 12,400 Da (Siddell, 1995). The E proteins are localized both in the perinuclear region and on the cell surface (Godet *et al.,* 1992; Yu *et al.,* 1994). It has also demonstrated that E proteins play an important role in virion assembly (Lai & Cavanagh *et al.,* 1997).

In the past 50 years, many new IBV serotypes or variants have been found,

which arise either as a result of spontaneous mutation or by recombination (Zheng *et al.*, 2005). Rapid and accurate diagnosis of the serotype of IBV is necessary to quickly establish an effective vaccine strategy. Currently, many diagnostic tests exist for differentiating IBV isolates, including monoclonal antibodies, dot blots, DNA probes, rapid plate hemagglutination test, SDS-PAGE polymorphism, direct S1 gene DNA sequencing, RT-PCR with serotype-specific primers, and RT-PCR/RFLP (Callison *et al.*, 2005).

There is no specific treatment for IBV. Modified live or killed vaccines are used for prevention and control (Bijlenga *et al.*, 2004). The vaccination strategy is dependent on the serotype of IBV prevalent within a geographical area because different serotypes do not cross-protect (Huang *et al.*, 2006).

1.13. Actin

Actin is the most abundant protein in a typical eukaryotic cell, accounting for about 15 % in some cell types. It is also one of the most highly conserved proteins, with 80.2 % sequence conservation at the gene level, and 95 % conservation of the primary structure of the protein product (Welch and Mullins, 2002).

1.13.1. History

Actin was first observed by W.D. Halliburton in 1887, who extracted a protein from muscle (Halliburton, 1887). In 1942 Straub developed a novel

technique for extracting substantial amounts of relatively pure actin. He continued to work on actin, and in 1950 reported that actin contains bound ATP (Straub and Feuer, 1950), and that, during polymerisation of the protein into microfilaments, the nucleotide is hydrolysed to ADP and inorganic phosphate, which remain bound in the microfilament. The crystal structure of G-actin was solved in 1990 by Kabsch (Kabsch, *et al.*, 1990). In the same year, a model for F-actin was proposed by Holmes (Holmes, *et. al*., 1990).

1.13.2. Genetics

The actin gene has an approximately 100 nucleotide 5' UTR, a 1200 nucleotide translated region, and a 200 nucleotide 3' UTR with 6 introns in it. Mammals have at least six actins, divided into three classes (alpha, beta and gamma): cardiac alpha-actin and skeletal-alpha actin (expressed in striated muscle), vascular alpha-actin and enteric gamma-actin (expressed in smooth muscle), and cytoplasmic beta- and gamma-actins {http://www.cbil.upenn.edu /MTIR/gammaActin_E-toc.html}. The majority of the isotype heterogeneity is located in the N-terminal 30 amino acids. Although there are small differences in sequence and properties between the isoforms, all actins assemble into microfilaments and are essentially identical in the majority of tests performed in vitro.

1.13.3. Structure

Actin, a 43-kDa globular protein, polymerizes in a helical fashion to form an actin filament or microfilament. Actin monomer consists of a small and a large domain, each divided into two subdomains, designated 1-4. ATP binds, along with Mg^{2++}, within a deep cleft between subdomains 2 and 4 (Fig.1-8) (Carlier, 1991).

In eukaryotic cells, actin forms the cytoskeleton - a three-dimensional network. The actin filaments are dispersed all throughout the entire cell. A thin dense actin-cortex supports the plasma membrane like an underlying shell. A shell of cortical actin also surrounds many membrane organelles (Ott *et al.*, 1996; Wilk *et al.*, 1999). It is reported that actin exists in the nucleus to remodel chromatin, and splice (Rando *et al.*, 2000; Pederson and Aebi, 2002).

1.13.4. Microfilament assembly

Actin exists in two principal forms: globular, monomeric (G) actin and filamentous polymeric (F) actin. G-actin is the individual subunit of actin, while F-actin is composed of G-actin subunits forming the filamentous polymer. The microfilaments are the thinnest component of the cytoskeleton, measuring only 5 nm in diameter (Welch and Mullins, 2002).

Actin filaments are polarized, characterized by a fast growing (plus or barbed) end and a slow growing (minus or pointed) end. Elongation of the filaments at the plus end is about 10 times faster than the minus end. The

process of actin polymerization starts with the association of three G-actin monomers into a trimer (Zigmond, 1993).

Actin is an ATPase. ATP-bound G-actin binds the plus end. When the filament matures, ATP bound in the central cleft of actin is hydrolysed (half time ~2 s) (Pollard and Earnshaw, 2004) and the phosphate is released (half time ~6 min) (Pollard and Earnshaw, 2004), which reduces the binding strength between neighboring units and generally destabilizes the filament. ADP-actin dissociates from the minus end and the increase in ADP-actin stimulates the exchange of bound ADP for ATP, leading to more ATP-actin units. This rapid turnover is important for the cell's movement (Carlier, 1991).

When the polymerization rate at the plus end equals the depolymerization rate at the minus end, the result is a "treadmilling" effect, where the filament moves, in vitro or in vivo, without changing its overall length (Pantaloni, *et al.*, 2001).

1.13.5. Actin-binding protein

In cells, the assembly and disassembly of actin filaments and functional higher-order networks is regulated by a large number of actin-binding proteins (Maciver, 2004; dos Remedios *et al.,* 2003). These proteins are involved in different signaling pathways (Fig. 1-9).

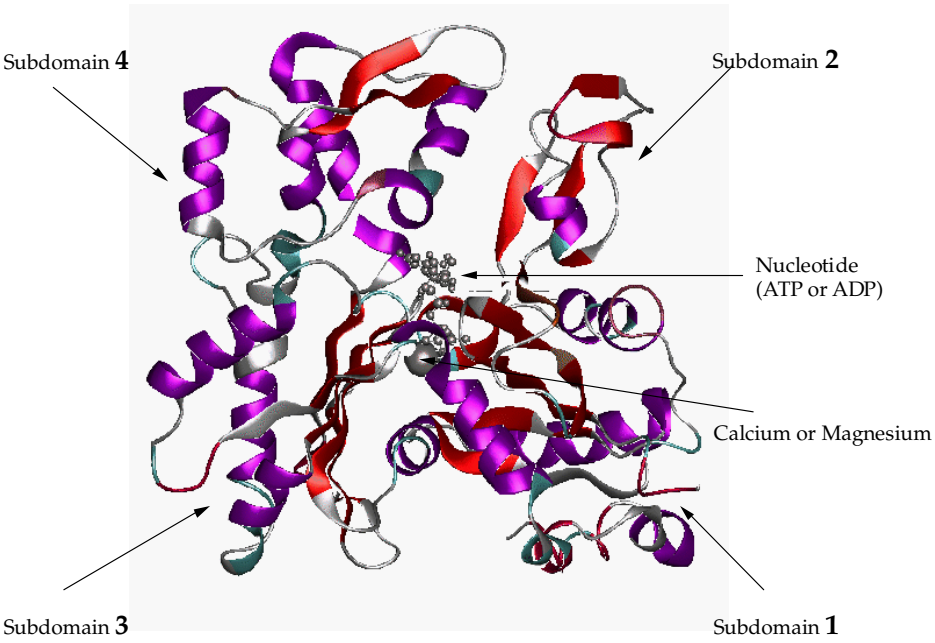

Figure 1-8

Schematic representation of the three-dimensional structure of actin monomer (Adapted from Kabsch, 1990).

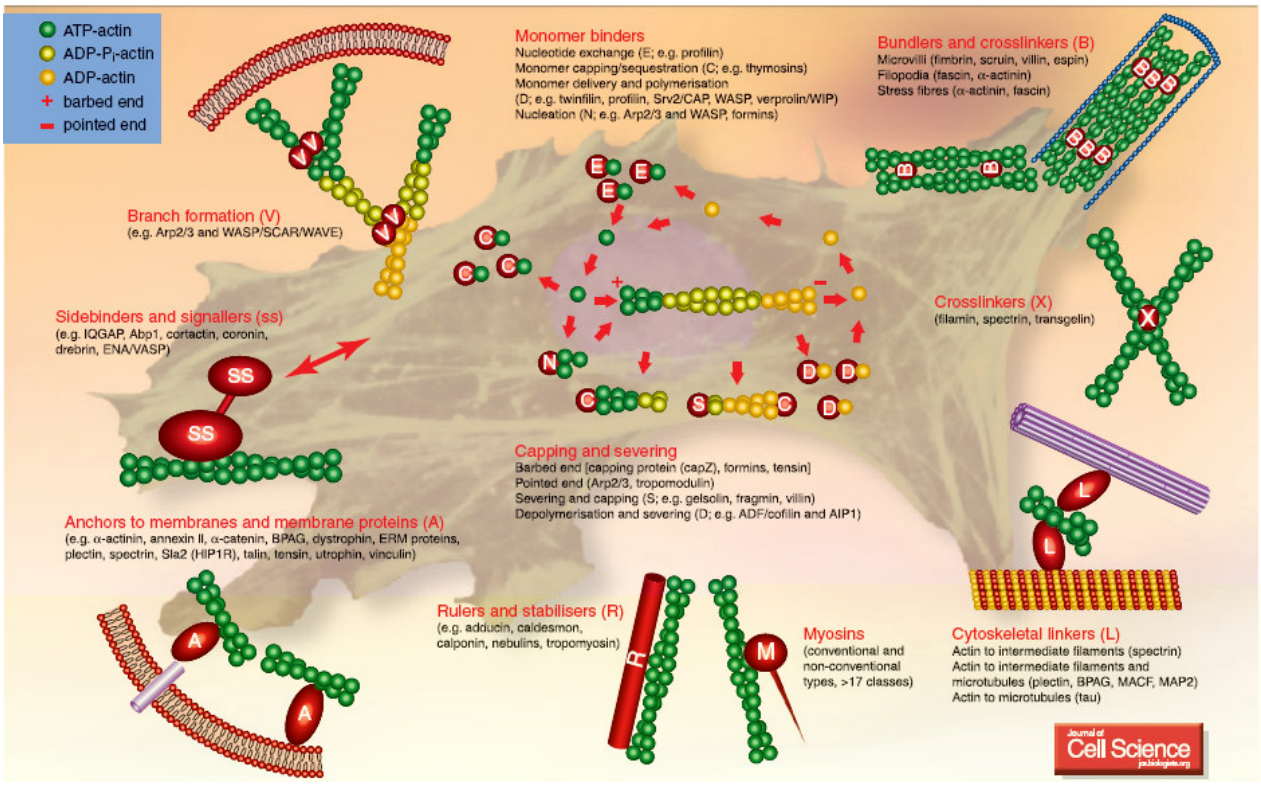

Figure 1-9

Actin-binding proteins (Adapted from Winder and Ayscough, 2005).

The protein cofilin binds to ADP-actin units and promotes their dissociation from the minus end and prevents their reassembly. The protein profilin reverses this effect by stimulating the exchange of bound ADP for ATP. In addition, ATP-actin units bound to profilin will dissociate from cofilin and are then free to polymerize. Another important component in filament production is the Arp2/3 complex, which nucleates new actin filaments while bound to existing filaments, thus creating the branched network (Paavilainen, *et al.*, 2004). All of these three proteins are regulated by cell signaling mechanisms.

Besides affecting actin structures, the actin-binding proteins can also use actin as a scaffold, physical support or track. For example, myosins are actin-dependent molecular motors that produce movement (and force) through the hydrolysis of ATP (Hodge and Cope, 2000). Talin can connect actin to membranes to interconnect different cytoskeletal elements. Plectin can link actin to both microtubules and intermediate filaments (Winder and Ayscough, 2005).

1.13.6. Organization

Actin filaments are assembled in two general types of structures: bundles and networks. Actin-binding proteins dictate the formation of either structure since they cross-link actin filaments. Actin filaments have the appearance of a double-stranded helix. In non-muscle actin bundles, the filaments are held together such that they are parallel to each other by actin-bundling proteins

and/or cationic species. Bundles play a role in many cellular processes such as cell division (cytokinesis) and cell movement (Welch and Mullins, 2002).

1.13.7. Actin in virus replication

HIV, the representative of retroviruses, enters cells primarily by membrane fusion at the plasma membrane (Greene and Peterlin, 2002). It is reported that actin can promote the co-clustering of HIV receptors CD4 and CXCR4 on gp120 binding, followed by HIV fusion with the plasma membrane (Iyengar et al., 1998). Furthermore, the HIV reverse transcription requires intact actin filaments (Bukrinskaya et al., 1998).

Baculoviruses, such as *Autographa Californica* M Nuclear Polyhedrosis Virus (AcMNPV), can rearrange the actin cytoskeleton during different stages of viral replication (Charlton and Volkman, 1993; Lanier and Volkman, 1998). Two AcMNPV proteins can bind to actin directly to induce actin filament assembly (Machesky, et al., 2001).

There are several reports that the host cytoskeleton (actin filaments) is involved in the budding of both enveloped DNA and RNA viruses (Garoff *et al.*, 1998). For example, measles virus has been shown to interact with actin filaments during budding (Bohn, *et al.,* 1986). In this study, actin filaments were observed to protrude into virus particles with their barbed ends and are in close association with the virus nucleocapsids. Other viruses, such as the frog virus 3, retrovirus, West Nile virus, Black creek canal virus and fowlpox virus, have also

been documented to be associated with actin filaments at the site of release (Murti, *et al.,* 1985; Perotti, *et al.,* 1996; Lanier and Volkman, 1998; Ravkov, *et al.,* 1998; Boulanger, *et al.*, 2000, Chu, et al., 2003).

Actin is definitely co-purified with murine mammary tumor virus (MuMTV), not a contaminating population of virus-free vesicles (Damsky *et al.,* 1977). Furthermore, it shows that the extrusion of MuMTV before its release requires an interaction with actin by the viral components, which is a general phenomenon in the release of other enveloped viruses.

1.14. Reverse genetics

The transcription of infectious RNA from a full-length cDNA copy of poliovirus genome was established in 1981, which is the first report for positive-stranded RNA virus reverse genetics (Racaniello and Baltimore, 1981). Recently, this scheme was applied to coronaviruses. The first reverse genetics system for coronavirus is targeted RNA recombination, originally developed in MHV, which results from the high rate of homologous RNA recombination in coronaviruses (Koetzner *et al.*, 1992). The mutation of interest is introduced into a synthetic donor RNA. Subsequently, this mutant RNA is transfected into the infected cells by a recipient parent virus, whose characteristics would be changed after recombination. The limitation of this method is that only the downstream one-third of the genome can be engineered because of selection.

The second method is the assembly of full-length genomic cDNAs by in

vitro ligation of smaller, more stable subcloned cDNAs. The ligated product is transcribed in vitro into infectious RNA (Baric and Sims, 2005). The key point of this method is to use the seamless restriction enzyme in order to ligate all the fragments in a predetermined order without extra nucleotides. This method is used successfully to produce TGEV (Thiel *et al.*, 1997), MHV (Yount *et al.*, 2002), SARS-CoV (Yount *et al.*, 2003) and IBV (Youn *et al.*, 2005).

The third method is to insert the entire coronavirus cDNAs, produced by long-range RT-PCR, into a unique restriction site in the genome of vaccinia virus (Thiel and Siddell, 2005). Infectious RNA is then generated by in vitro transcription from the purified vaccinia virus DNA. This vaccinia virus is used as a huge cloning vector to avoid the instabilities encountered in *E. coli* plasmids.

1.15. Objectives

All eukaryotic organisms, humans included, are continuously attacked by infectious pathogens, including viruses. Interactions between a virus and a cell of the immune system can lead to suppression of the host's immune response and/or suppression of viral replication. The interaction between humans and viruses is linked to both the evolution of the human immune defense system and the evolution of the virus survival strategies. The current evolutionary equilibrium allows the co-existence of humans and viruses. Indeed, viruses are extremely well-adapted to human host cells (http://risoe-staged.

risoe.dk/Research/health_technology/medical_nanotechnology/projects/human_cell_virus.aspx).

After getting into the cells, viruses exploit various kinds of cellular machineries to achieve their successful replication in the cell. The reason is that viruses have limited-length viral genomes because of their small size. For example, coronaviruses make use of cellular ribosomes to express the necessary proteins for RNA synthesis. After being expressed, viral proteins are modified and transported to their exact destinations by cellular ER and Golgi organelles. Furthermore, during budding, viruses use the membrane of the pre-Golgi compartment as their envelopes to wrap the nucleocapsids. Finally, the progeny viruses are transported to the cell membrane via cellular excreted vesicles. Thus, it is very important to conduct research on the relationship between virus and host cells to determine the detailed mechanisms of virus replication.

M protein, a scaffold-like protein, is the most abundant protein in IBV virions. Also, M protein is a very important component for virus. The objectives of this thesis are:

(1) To determine if there are specific host cell proteins which interact with M protein. In this study, the IBV M protein acted as a bait to screen mammalian cells by the yeast two-hybrid system to identify the interaction proteins.

(2) To investigate which region of M protein is responsible for the interaction. Several M mutants were cloned, and their interactions with actin were

investigated through yeast two-hybrid system.

(3) To elucidate the functions of the interaction for virus replication. Actin was disrupted by cytochalasin D in the cells infected with IBV to find out the importance of this interaction.

IBV 3CLpro is the main protease, whose P1 position of 11 cleavage sites was reported to be conserved (i.e. Q residue) in previous studies. 3CLpro cleaves polyproteins to release replication proteins. Other objectives of this thesis are:

(1) To test if the P1 position in the cleavage site is conserved. The Q residue in P1 position was replaced by several amino acids (A, R, N, and E). These mutations were then checked by the cleavage assay of IBV 3CLpro to demonstrate which amino acid could substitute the Q residue at the P1 position.

(2) To confirm these substitutions at the P1 position function consistently both in vivo and in vitro. These mutations were introduced into IBV clones, and these mutant clones were electroporated into Vero cells to recover the mutant viruses.

Chapter 2

Materials and methods

2.1. Materials

2.1.1. Viruses

a. Recombinant Vaccinia Virus (vTF7-3)

The Bacteriophage T7 polymerase gene was inserted into the vaccinia virus genome. This recombinant vaccinia virus can express T7 RNA polymerase in infected cells (Fuerst et al, 1986). The T7 RNA polymerase produced by the recombinant vaccinia virus can express target genes at very high efficiency (Fuerst et al, 1986).

b. Avian Infectious Bronchitis Virus (IBV)

Beaudette strain: the IBV strain Beaudette is an embryo-adapted virus that has extended species tropism in cell culture. The S protein sequence of the Beaudette strain contains a putative heparan sulfate (HS)-binding site compared with other strains, indicating that the Beaudette virus may use HS as a selective receptor. It may explain in part the extended tropism of IBV Beaudette (Madu, *et al.*, 2007).

2.1.2. Cell lines

a. HeLa cells

HeLa cell is an immortal cell line derived from cervical cancer cells taken from Henrietta Lacks, who died from her cancer in 1951 (Masters, 2002; Landecker, 2000; van Valen et al., 1991). HeLa cells were grown at 37 °C in 5 % CO_2 and maintained in Glasgow's modified Eagle's medium supplemented with 10 % fetal calf serum.

b. Vero cells (African Green Monkey kidney cells)

Vero cells were grown at 37 °C in 5 % CO_2 and maintained in Glasgow's modified Eagle's medium supplemented with 10 % fetal calf serum.

c. H1299 cells

H1299 cell line is an adherent epithelial cell line that was derived from a human lung carcinoma. H1299 cells lack endogenous p53. H1299 cells were grown at 37 °C in 5 % CO_2 and maintained in Hyclone's RPMI-1640 medium supplemented with 10 % fetal calf serum.

2.1.3. Bacterial strains

Competent cells of *E coli* strain DH5α: The genotype of *E coli* strain DH5α is *supE*44, Δ*lac*U169 (φ80*lacZ*ΔM15), *hsdR*17, *recA*1, *endA*1, *gyrA*96, *thi*-1, *relA*1. Competent cells of *E coli* strain DH5α represent one of the standard competent cells for molecular biology applications. The DH5α strain has the mutation of φ80*lacZ*ΔM15 and lacks *laq*Iq gene, which allows blue-white color screening of transformants with X-gal (IPTG is not required) (Product information of subcloning competent DH5α from BioDynamics Laboratory Inc.).

2.1.4. Yeast strain

AH109: The genotype of AH109 yeast strain is: MATa, trp1-901, leu2-3, 112, ura3-52, his3-200 gal4Δ, gal80Δ, LYS2::$GAL1_{UAS}$-$GAL1_{TATA}$-HIS3, $GAL2_{UAS}$-$GAL2_{TATA}$-ADE2, URA3::$MEL1_{UAS}$-$MEL1_{TATA}$-lacZ. The AH109 cells were cultured in YPDA media.

2.1.5. Plasmid vectors

a. pKT0

pKT0 originated from pING14 by inserting a T7 RNA polymerase promoter sequence in it (Liu and Inglis, 1991). It encodes ampicillin resistance.

b. pFlag

pFlag was derived from pKT0 by inserting a flag tag (MDWKDDDDK) sequence downstream of the NcoI restriction endonuclease site. It encodes ampicillin resistance.

c. pXJ-40

pXJ-40 was constructed by replacing the SV40 early promoter with the human cytomegalovirus early promoter in pSG5. It encodes ampicillin resistance.

d. pGBKT7

pGBKT7 is a yeast expression vector that is designed to express a fusion protein of the GAL4 DNA-binding domain (DNA-BD; amino acids 1 – 147) and a bait protein. The fusion protein also contains a c-Myc epitope tag. To facilitate *in vitro* transcription/translation, pGBKT7 includes the T7 promoter between the GAL4 DNA-BD and the epitope tag. It encodes kanamycin resistance.

2.1.6. Antibodies

Polyclonal rabbit anti-β-actin antibody	Santa Cruz Biotechnology
Polyclonal rabbit anti-β-tubulin antibody	Santa Cruz Biotechnology
Polyclonal anti-IBVM antibody	raised in Rabbit
Polyclonal anti-IBVN antibody	raised in Rabbit

Polyclonal anti-IBVS antibody	raised in Rabbit
Polyclonal anti-IBVE antibody	raised in Rabbit
Monoclonal mouse anti-Flag antibody	Stratagene Inc.
Polyclonal goat anti-rabbit immunoglobulin HRP	DAKO
Polyclonal rabbit anti-mouse immunoglobulin HRP	DAKO
Polyclonal Swine anti-rabbit immunoglobulin TRITC	DAKO

2.1.7. Commercial Kits

QIAquick PCR Purication Kits	QIAGEN Ltd
QIAquick Gel Extraction Kits	QIAGEN Ltd
QIAprep Miniprep Kits	QIAGEN Ltd
HiSpeed Plasmid Midi Kits	QIAGEN Ltd
ECL Plus Western Blotting Detection System	Amersham. Pharmacia biotech.
Supersignal west pico chemiluminescent substrate	Pierce Biotechnology
Quickchange site-directed mutagenesis kit	Stratagene Inc.
Lipofectamine 2000	Invitrogen life technologies
mMessage mMachine T7	Ambion Inc.

2.1.8. Chemicals

Cytochalasin D	Sigma-Aldrich Co.
Cytomatin Fluorescent Mounting medium	DAKO
Low-Range Rainbow Molecular Weight Markers	Amersham Bioscience
Dulbecco's Modified Eagle's Medium	Hyclone
Alexa fluor 488 phalloidin	Invitrogen life technologies
RPMI-1640	Hyclone

2.1.9. Enzymes

Pfu DNA polymerase	New England Biolabs Inc
T4 ligase	Fermentas Inc.
Restriction Endonuclease	New England Biolabs Inc
Turbo Pfu DNA polymerase	Stratagene Inc.
Proteinase K	New England Biolabs Inc
T7 transcriptase	Ambion Inc.
DspI	New England Biolabs Inc

2.1.10. Buffers

a. Buffers for Western blot

1.5 M Tris-Cl (pH 8.8): Tris (MW 121.1): 36.3 g, add H_2O to 200 ml. Adjust pH to 8.8 with HCl.

0.5 M Tris-Cl (pH 6.8): Tris (MW 121.1): 6.06 g, add H_2O to 100 ml. Adjust pH to 6.8 with HCl.

10 % SDS: SDS: 10 g, add H_2O to 100 ml.

10 % Ammonium Persulphate: Ammonium persulphate: 1 g, add H_2O to 10 ml. Prepare fresh (can be stored at 4 °C for a few days).

2X Sample buffer (with β-ME): 0.5 M Tris-Cl (pH 6.8): 2.5 ml, 10 % SDS: 4 ml, Glycerol: 2 ml, 2-Mercaptoethanol: 1 ml, Bromophenol Blue: 0.1 mg, add H_2O to 10 ml. Divide into 1 ml aliquots and freeze.

5X Running buffer: Tris (MW 121.1): 60 g, Glycine: 288 g; SDS: 10 g, add H_2O to 2 Liter. The pH of the solution does not need to be adjusted.

b. Buffers for Northern blot

1% Formaldehyde gel: 1.52 g agarose, 113 ml H_2O Microwave to melt, add 15.2 ml 10 x MOPS buffer, 24.65 ml formaldehyde, total volume 152 ml.

Running buffer: 1 x MOPS buffer (not DEPC-treated, no formaldehyde)

10 x MOPS: 0.4 M Morpholinopropanesulfonic acid (free acid); 0.1 M Na-acetate-3; 10 mM EDTA; adjust to pH 7.2 with NaOH; store dark in fridge. [**500 ml:** 41.9 g MOPS, 6.8 g NaAc, 10 ml 0.5 M EDTA]

Loading buffer: 1 x MOPS; 18.5 % Formaldehyde; 50 % Formamide; 4 % Ficoll 400; Bromophenolblue; store at -20 °C. [**1 ml:** 100 µl 10 x MOPS, 500 µl Formamide, 185 µl Formaldehyde, 40 mg Ficoll 400, Bromophenol blue, 215 µl H_2O]

Prehybridization-buffer: 5 x SSC; 50 % Formamide; 5 x Denhardt's solution; 1 % SDS; 100 µg/ml heat-denatured sheared non- homologous DNA (Salmon sperm DNA or yeast tRNA). [**100 ml:** 25 ml 20 x SSC, 50 ml Formamide, 5 ml 100 x Denhardt's, 1 g SDS, 1 ml 10 mg/ml DNA]

Hybridization-buffer: Prehybridization buffer with 5 % Dextran sulfate (Na-salt, MW 500,000, 50 % stock-solution) and without non-homologous DNA.

20 x SSC: 3 M NaCl; 0.3 M Na-citrate. [**1 l:** 175.3 g NaCl, 88.2 g NaCitrate]

Strip-solution: 5 mM Tris pH 8; 0.2 mM EDTA; 0.05 % Na-pyrophosphate; 0.1 x Denhardt's solution. [**500 ml:** 2.5 ml 1 M Tris, 200 µl 0.5 M EDTA, 5 ml 5 % NaPP, 1 ml 50 x Denhardt's]

c. Buffers for Yeast

YPD medium: prepare YPD mixture as follows: 20 g/L Difco peptone, 10 g/L Yeast extract, add H_2O to 950 ml. Adjust pH to 6.5 if necessary, and autoclave. Allow medium to cool to ~ 55 °C and then add dextrose (glucose) to 2 % (50 ml of a sterile 40 % stock solution).

1X TE/LiAc Solution: Prepare fresh just prior to transformation using the stock solutions. Combine 1 ml of 10 X TE Buffer with 1 ml of 1 M LiAc (10 X). Bring the total volume to 10 ml using sterile, deionized H_2O.

PEG/LiAc Solution (polyethylene glycol 3350/lithium acetate): Prepare fresh just prior to transformation using the stock solutions provided. To prepare 10 ml of solution: 8 ml of 50 % PEG 3350, 1 ml of 10 X TE Buffer, 1 ml of 1 M LiAc (10 X).

d. Buffers for others

LB/Amp plates: 10 g/L bactotryptone, 5 g/L yeast extract, 10 g/L NaCl, 16 g/L bactoagar. Autoclave and when cooled add ampicillin to 100 ug/ml.

Cell freezing medium: 50 % DMEM, 10 % DMSO and 40 % FBS.

2 x YT medium: 16 g/L bactotryptone, 5 g/L yeast extract, 10 g/L NaCl, Autoclave for 20 minutes at 121 °C.

2.2. Methods

2.2.1. Phenol/chloroform extraction with ethanol precipitation (removes proteins and other contaminants from DNA)

An equal volume of phenol/ chloroform was added to the tube containing DNA solution, and the mix was then centrifuged at 14,000 rpm for 5

minutes after vortexing. The supernatant was removed to a fresh tube and 1/10 volume of Na acetate pH 5.2 and 2.5 volumes of 100 % ethanol were added. The tube was frozen at -20 °C after vortexing. 30 minutes later, the tube was centrifuged for 30 minutes at 14,000 rpm. The supernatant was poured off and the DNA pellet was washed with 1 ml of 70 % ethanol, followed with centrifugation for 15 minutes at 14,000 rpm. The DNA pellet was dried in the vacuum for 10 minutes after pouring off the supernatant. TE buffer was added to resuspend the DNA.

2.2.2. Competent cells

A frozen glycerol stock of the appropriate strain of *E. coli* was thawed, and added to an Erlenmeyer flask containing 50 ml of 2 x TY media. The flask was pre-incubated in a 37 °C water bath for 1 hour without shaking and further incubated for 2-3 hours at 37 °C with shaking at 250 rpm. 40 ml of the cells were transferred to a sterile 50 ml polypropylene centrifuge tube, and collected by centrifugation at 3,000 rpm for 8 minutes at 4 °C. After centrifugation, the supernatant was decanted and the cell pellet was resuspended in one-half volume (20 ml) of cold, sterile 50 mM calcium chloride. The cells were incubated in an ice-water bath for 20 minutes, and centrifuged as before. The cell pellet was gently resuspended in one-tenth volume (4 ml) of cold, sterile 50 mM calcium chloride to yield the final competent cell suspension. The cells were dispensed in 100 ml aliquots and frozen at –80 ^{o}C.

2.2.3. Bacterial transformation

5 ul of DNA was added to 50 ul competent cells, and incubated on ice for 30 minutes. The mix was incubated on ice for 2 minutes after heat shock at 42 °C for 1 - 2 minutes. 1 ml of LB was added to the mix, and incubated at 37°C for 1 hour. The cells were centrifuged at 800 rpm for 5 minutes. The cells were resuspended in the remaining LB after pouring off the supernatant. The entire volume of resuspended cells was plated on LB/(relevant antibiotic) plates.

2.2.4. Agarose gel electrophoresis

1 L of 1 X TAE buffer was prepared from the 50 X stock. 0.5 g of agarose was microwaved in 50 ml of 1 x TAE buffer (1 % gel) for 2 minutes. 2 ul of 10 mg/ml ethidium bromide was added after cooling the agarose to lukewarm, and the comb was placed. The 1 x TAE buffer was added until the gel was solid. Samples were loaded and run at 100 V until the running dye reaches the end of the gel.

2.2.5. Polymerase Chain Reaction (PCR)

1) The following reagents were added to a microfuge tube:

5 ul of reaction buffer

1 ul of 10 uM forward primer

1 ul of 10 uM reverse primer

1 ul of template DNA

5 ul of 2.5 mM dNTP

1 ul of enzyme (Taq or Pfu polymerase)

add water to make up to 50 ul.

2) The PCR cycles were started according the following profiles: denaturation at 94 ° C for 30-90 seconds, annealing at 55 °C (or -5° Tm) for 0.5-2 minutes, extension at 72 °C for 1 minute / kb fragment length. The cycles were repeated 30 times.

2.2.6. DNA Ligations

1. The following reagents were combined in a microcentrifuge tube, and incubated overnight at 4 °C:

DNA fragments	100-1000 ng
cloning vector	2 ul (10 ng/ul)
10 X ligation buffer	1 ul
T4 DNA ligase (NEB 202L)	1 ul (400 U/ul)
sterile ddH_2O	up to 10 ul

2. Control ligation reactions were incubated without insert DNA fragments.

2.2.7. Cell culture

The cells were subcultured when the culture turned yellow. The yellow medium was removed, and the cells were washed twice with PBS using a volume equivalent to half the volume of culture medium. Trypsin/EDTA was pipetted onto the washed cell monolayer. After incubation for 2-10 minutes, the cells were resuspended in a small volume of fresh serum-containing medium to inactivate the trypsin. The required numbers of cells are transferred to a newly labeled flask with medium. The flask was incubated at an appropriate

environment. This process was repeated as required by the growth characteristics of the cell line.

2.2.8. Preparation and resuscitation of frozen cell line stock

Fully confluent cells in 75 cm^2 flasks were detached from the well by trypsin/EDTA. Cells were resuspended in cell-freezing medium and aliquoted into tubes. The tubes were stored at -80 ºC for 2 hours, and then kept at -150 ºC for longer storage.

Cells were collected from liquid nitrogen storage and thawed at room temperature for 1-2 minutes. The ampoule was wiped with a tissue moistened (not excessively) with 70 % alcohol. The cells were transferred into the flask and incubated at the appropriate temperature and appropriate concentration of CO_2 in atmosphere. Cells were examined by phase contrast microscopy after 24 hours and sub-cultured as necessary.

2.2.9. Reverse transcription, RT-PCR, and real-time PCR

Viral RNA was reverse-transcribed to cDNA using SuperScript III (Invitrogen) with modification to the protocol as follows: Random hexamers (300 ng) and total RNA (5 ug) were incubated for 10 minutes at 70 ºC. The remaining reagents were then added according to the manufacturer's recommendation and the reaction was incubated at 55 ºC for 1 hour followed by 20 minutes at 70 ºC to inactivate the RT. For RT-PCR, a forward primer in the leader sequence and a reverse primer were used to generate a product by PCR. Quantitative real time RT-PCR was conducted using Smart Cycler II (Cepheid) with SYBR green (Cepheid) to detect subgenomic cDNA with primers (7.5 pM)

optimized to detect a product spanning the leader sequence to the 5' end of M gene or genomic cDNA with primers (7.5 pM). The cDNA from the RT reaction of each virus was diluted 1:10, and 1 ul was used for each PCR, with a total reaction volume of 25 ul.

2.2.10. Construction and sequencing of an infectious IBV clone

Five fragments spanning the entire IBV genome were amplified by RT-PCR from Vero cells infected with the Vero cell-adapted IBV p65 strain. Briefly, total cellular RNA was extracted from the infected Vero cells with TRI Reagent (Molecular Research Center, Inc.), according to the manufacturer's instructions. Reverse transcription was performed with Expand Reverse Transcriptase (Roche) using reverse primers IBV-5753R, IBV-8694R, IBV-15532R, IBV-20930R, IBV-27608R. Each cDNA fragment was amplified from RT products by PCR using KOD Hot Start DNA polymerase according to the manufacturer's directions (Novagen).

The PCR products were purified from agarose gels and cloned into pCR-XL-TOPO (Invitrogen) or pGEM-T Easy (Promega) vectors, according to the manufacturer's instructions. Subsequently, fragment A was removed from pCR-XL-TOPO by digestion with NheI and EcoRI, and subcloned into pKT0 vector. Two to three independent clones of each fragment were selected and sequenced by automated sequencing using specific primers and the ABI dye termination sequencing method. Sequence comparison, assembly and analysis were performed by BLAST and DNA STAR software.

2.2.11. PCR mutagenesis

This is a highly effective and simple method for generating site directed lesions in plasmids without subcloning based on the work of Fisher and Pei (1997).

1. Amplification of mutant DNA:

DNA template plasmid	5-20 ng
10 X pfu DNA polymerase buffer	5.0 µl
25 uM oligo1	0.5 µl
25 uM oligo 2	0.5 µl
10 mM dNTP	1.0 µl
Pfu DNA polymerase (2.5 units)	1.0 µl
fill with ddH_2O to	50 µl

PCR conditions:

95° for 30 seconds,

18 cycles of : 95 ºC for 30 seconds, 55 ºC for 1 minute, 68 ºC for 1 minute/kb of plasmid length

2. 1µl of Dpn I (10 units) was added to PCR reaction, and incubated at 37 °C for 1 hour to degrade methylated (parental) DNA.

3. The PCR product was transformed into *E. coli*, 6 plasmids were prepared from separate colonies and digested to detect mutants. The lesion was sequenced to confirm the mutations.

2.2.12. In vitro assembly of full-length cDNA clones

Plasmids were digested with either BsmBI (fragment A) or BsaI (fragments B, C, D and E). The digested plasmids were separated on 0.8 %

agarose gels containing crystal violet. Bands corresponding to each of the fragments were cut from the gels and purified with QIAquick gel extraction kit (QIAGEN Inc.).

Fragments A and B, and fragments C, D and E were first ligated with T4 DNA ligase at 4 °C overnight. The two reaction mixtures were then mixed and further ligated at 4 °C overnight. The final ligation products were extracted with phenol/chloroform/isoamyl alcohol (25:24:1), precipitated with ethanol, and detected by electrophoresis on 0.4 % agarose gels.

2.2.13. In vitro transcription and electroporation

Full-length transcripts were generated in vitro using the mMessage mMachine T7 kit (Ambion, Austin, Texas) according to the manufacturer's instructions with certain modifications. Briefly, 30 µl of transcription reaction with a 1:1 ratio of GTP to cap analog was sequentially incubated at 40.5 °C for 25 minutes, 37.5 °C for 50 minutes, 40.5 °C for 25 minutes and 37.5 °C for 20 minutes.

The N transcripts were generated by using a linearized pKTO-IBVN containing the IBV N gene and the 3'-UTR as templates. A 1:2 ratio of GTP to cap analog was used for the transcription of IBV N gene.

2.2.14. Introduction of in vitro synthesized transcripts into Vero cells by electroporation

The in vitro synthesized full-length and N transcripts were treated with DNase I and purified with phenol/chloroform. Vero cells were grown to 90 % confluence, trypsinized, washed twice with cold PBS, and resuspended in PBS.

RNA transcripts were added to 400 µl of Vero cell suspension in an electroporation cuvette, and electroporated with one pulse at 450 V, 50 µF with a Bio-Rad Gene Pulser II electroporator. The transfected Vero cells were cultured overnight in 1 % FBS-containing MEM in a 60 mm dish or a six-well plate and further cultured in MEM without FBS.

2.2.15. Preparation of competent yeast cells

A YPDA agar plate was streaked with a small portion of frozen AH109 yeast stock. The plate was incubated at 30 °C until colonies appeared (~ 3 days). One colony (< 4 weeks old, 2–3 mm in diameter) was inoculated into 3 ml of YPD medium in a sterile, 15-ml centrifuge tube. The tube was incubated at 30 °C with shaking for 8–12 hours.

5 ul of the culture was transferred to a 250-ml flask containing 50 ml of YPD, and incubated at 30 °C with shaking at 230–250 rpm for 16–20 hours. The OD600 should reach 0.15–0.3. If not, incubation was continued until this density was reached, taking care not to overgrow the culture.

The cells were centrifuged at 700 x g for 5 minutes at room temperature, and the cell pellet was resuspended in 100 ml of YPD after discarding the supernatant. The cells were incubated at 30 °C for 3–5 hours (final OD600 = 0.4–0.5), and centrifuged at 700 x g for 5 minutes at room temperature. The cell pellet was resuspended again in 50 ml of sterile, deionized H_2O. The cells were centrifuged at 700 x g for 5 minutes at room temperature.

The cells were resuspended in 3 ml of 1X TE/LiAc solution. The resuspension was split into two 1.5-ml microcentrifuge tubes (1.5 ml per tube), and centrifuged at high speed for 15 seconds. The cells were resuspended again

in 600 ul of 1X TE/LiAc solution (Competent cells should be used for transformation immediately following preparation. However, if necessary, they can be stored at room temperature for a few hours without significantly affecting the competency).

2.2.16. Transformation of Competent Yeast Cells

Directions for both small- and library-scale yeast transformation protocols are provided below. Volumes and quantities for the library-scale protocol are given in brackets.

The required sterile 1.5-ml [15-ml] tubes were set up for the planned transformations. In a sterile, prechilled, 1.5-ml [15-ml] tube, the following were combined: 0.1–1 mg [1–10 mg] plasmid DNA, 5ml [20 ml] herring testes carrier DNA, (denatured at 100 °C for 5 minutes), 50 ml [600 ml] of competent cells, 0.5 ml [2.5 ml] PEG/LiAc Solution. The reagents were mixed thoroughly by vortexing, and shaken at 30 °C for 30 minutes [45 minutes].

20 ml [160 ml] of DMSO was added and mixed. The tube was then placed in a 42 °C water bath for 15 minutes [20 minutes], and mixed gently every 5 minutes [10 minutes]. The cells were centrifuged at high speed in a microcentrifuge for 15 seconds [library-scale reactions were centrifuged at 700 x g for 5 minutes], resuspended in 1 ml [3 ml] of YPD liquid medium**,** and incubated at 30°C with shaking for 90 minutes. The yeast cells were pelleted by centrifugation (For speeds and times, see above).

The cells were resuspended in 1 ml [15 ml] 1 x TE buffer, and spread onto 100-mm [150-mm] plates containing the appropriate SD selection medium. To obtain well-isolated colonies, the mixture was diluted (e.g., 1:10, 1:100, or

1:1000) before spreading.

The plates were incubated (upside down) at 30 °C until colonies appeared (3–6 days). The largest colonies were picked and streaked on the same selection medium. These master plates were sealed with Parafilm and stored at 4 °C (not longer than 1 month).

2.2.17. Cell transfection

H1299 and Vero cells were cultured in RPMI-1640 and complete Dulbecco's modified Eagle's medium (Invitrogen), respectively, supplemented with 10 % new-born calf serum (Sterile) and 1 % penicillin/streptomycin (Invitrogen) and maintained at 37 ºC in humidified 5 % CO_2.

Constructs containing plasmid DNA under the control of a T7 promoter were transiently expressed in mammalian cells using a Vaccinia Virus-T7 system. Briefly, 90 % monolayers of H1299 cells were infected with 10 plaque forming units (PFU)/cell of the vTF-3 which expressed the T7 RNA polymerase gene, for 2 hours at 37 ºC prior to transfection. The plasmid DNA was transfected into vTF-3 infected cells using Lipofectamine 2000 reagent according to the instructions of the manufacturer (Invitrogen).

2.2.18. Coimmunoprecipitaion

HeLa cells were transfected with the appropriate expression vectors. At 16 hours post-transfection, cells were lysed with TNTG lysis buffer (30 mM Tris-HCl pH7.4, 150 mM NaCl, 1 % NP40, and 10 % glycerol) in the presence of 1 X protease inhibitor mixture (Sigma), and the cells were pipetted up and down extensively and then incubated on ice for 30 minutes. The cell extracts

were centrifuged at maximum speed for 10 minutes at 4 ºC. For immunoprecipitation, 10 µl (polyclonal serum) or 10 µg (monoclonal antibody) was added to 1 ml of extract, and incubated with end-over-end mixing for 2 hours at 4 ºC. 50 µl of each cell extract was saved, 50 µl of 2 X SDS-PAGE sample buffer was added, and boiled for 10 minutes. After the 2 hour incubation, the washed Protein A/G Sepharose was added (Santa Cruz Biotech) to the immunoprecipitates and mixed end-over-end for 1 hour at 4 ºC. The immunoprecipitates were washed 3 X with 1 ml of lysis buffer and remaining buffer was carefully removed. 50 µl of 2 X SDS-PAGE sample buffer was added, boiled for 10 minutes, and loaded on a SDS-PAGE gel for analysis.

2.2.19. Indirect immunofluorescence assay

H1299 cells were grown to 60-70 % confluence on 4-well chamber slides (IWAKI), and transfected with plasmids containing the protein gene of interst. At 16 hours post-transfection, the media was aspirated, and the cells were fixed with 4 % paraformaldehyde for 15 minutes at room temperature and permeabilized with 0.2 % Triton X-100. Cells were rehydrated in PBS for 30 minutes, and blocked in buffer comprising PBS with 5 % bovine serum albumin. After blocking, cells were incubated in primary antibody at 1:200 dilution for 1 hour. Cells were then washed in PBS wash buffer three times at 10 minutes/wash. Next, cells were incubated with FITC-conjugated anti-rabbit secondary antibodies (DAKO) in fluorescence dilution buffer at 4 ºC for 1 hour. Cells were then washed three times at 10 minutes/wash in PBS. Cells were mounted and then visualized by confocal immunofluorescence microscopy

using a Zeiss LSM 510 laser scanning confocal microscope at 488 and 543 nm with a final magnification of 40 X with the oil immersion lens.

2.2.20. Sucrose gradient purification of coronavirus

The virus was layered onto 20 % TNE-buffered sucrose solution (TNE buffer: 50 mM Tris-Hcl, pH 7.4, 100 mM NaCl, 1 mM EDTA) and centrifuged at 175,000 g for 3 hours at 4 ºC (cushion). The resulting virus pellets were resuspended in TNE buffer, layered onto 10-50 % linear sucrose gradient prepared with TNE buffer, and centrifuged at 175,000g for 18 hours at 4 ºC. Aliquots of fractions starting from the top of the gradient were analyzed by SDS-PAGE.

2.2.21. IBV growth analysis

All results presented were of experiments performed in triplicate. Error bars represent 1 standard deviation. T75 flasks of cells were infected with IBV at a multiplicity of infection of 1 PFU/cell, and virus was allowed to adsorb at 37 ºC for 1 hour. The inoculum was removed and the cells were washed 3 times with PBS before being overlaid with 10 ml of the appropriate media. The flasks were removed from the incubator at 0, 8, 16, 24 and 32 hours post-infection. Virus was stocked at -80 ºC.

2.2.22. TCID 50 (50 % tissue culture infective doses)

Vero cells were cultured in 96-well plates at 5,000 cells/well in DMEM with 10 % FCS for about 2 days. In a separate 96-well plate, virus was serially diluted ten-fold with cells being resuspended very well before going to the next

dilution. 100 ul of each dilution was transferred to the 96-well plate with Vero cells to make a total of 200 ul per well (leaving columns 1 and 2 without virus as the negative control). The plates were incubated at 37 °C in 5 % CO_2 for approximately 5 days and checked daily. Finally, virus titer was calculated as PFU/ml. The growth curve of the virus was plotted according to the virus titer at each time-point.

2.2.23. Purification and plaque sizes of the recombinant viruses

Serial 10-fold dilutions of media supernatants sampled for IBV growth analyses were made. 200 ul of each dilution was added (each sample was assayed in duplicate) to the monolayer of Vero cells grown in six-well plates and incubated at 37 °C in 5 % CO_2. After 1 hour, the inoculum was removed. The infected cells were washed twice with PBS, and overlaid with 1 % low-melting agarose. After 4 days, single plaques was picked up and propagated in Vero cells.

200 µl of 10-fold serial dilutions of virus was added to Vero cells. 1 hour later, the cells were overlaid with 3.5 ml of DMEM containing 0.5 % carboxymethyl cellulose (CMC) (Purified Agar, SPD) and 1 % FBS after removing the inoculum. Five days later, the plaques were fixed with 4 % formaldehyde (BDH) in PBS for 15 minutes, and visualized by staining the intact cells with 0.1 % toluidine blue (Sigma) for 30 minutes.

2.2.24. Synthesis of DNA probes

PCR fragment covering the IBV genome from 20887 to 27608 nucleotides was cloned into a plasmid. The DIG-labeled DNA probes were

made in vitro using the PCR DIG probe synthesis kit according to the instructions of the manufacturer (Roche).

2.2.25. Western blot analysis

Total proteins extracted from cells were lysed with 2 × SDS loading buffer in the presence of 200 mM DTT plus 10 mM of iodoacetamide and subjected to SDS–PAGE. Proteins were transferred to PVDF membrane (Stratagene) and blocked overnight at 4 ^{o}C in blocking buffer (10 % fat free milk powder in PBST buffer). The membrane was incubated with 1:2000 diluted primary antibodies in blocking buffer for 2 hours at room temperature. After washing three times with PBST, the membrane was incubated with 1:2000 diluted anti-mouse or anti-rabbit IgG antibodies conjugated with horseradish peroxidase (DAKO) in blocking buffer for 1 hour at room temperature. After washing three times with PBST, the polypeptides were detected with a chemiluminescence detection kit (ECL, Amersham Biosciences) according to the manufacturer's instructions.

2.2.26. Northern hybridization

10 ug RNA was loaded on 1 % formaldehyde gel, and the gel was electrophoresed at 60 V for 3 hours. The RNA gel was soaked in 20 X SSC for twice, 15 minutes each time. Capillary blotting apparatus was set up with layers of: (1) Whatman 3MM in contact with the transfer buffer (20 x SSC), (2) the gel, (3) the blotting membrane (Hybond-N^{+} nylon membrane (Amersham pharmacia biotech)), (4) Whatman 3MM, (5) lots of paper towels. Transfer overnight with copious 20 x SSC and several changes of paper towels.

The blot was disassembled and RNA was fixed to the membrane by exposure to UV light, and membranes were prehybridized at 50 °C for 2 hours. The labeled probes were added to the prehybridization mix and hybridized at 50 °C for 16 hours. The membranes were then washed to remove nonspecific hybridizations twice in 2 × SSC, 0.1% SDS at room temperature for 15 minutes, followed by 0.5 × SSC, 1 % SDS at 68 °C for 15 minutes (twice). After blocking, anti-digoxigenin-AP was added in a 1:20000 dilution in blocking buffer. Specific hybridization was then detected by chemiluminescence substrate CDP-star (Roche).

2.2.27. Southern blot

DNA samples mixed with loading dye were loaded onto a 1 % agarose gel which was electrophoresed at 60 V for 4 hours. After that, the gel was carefully transferred into a tray and washed with ddH_2O. Large pieces of DNA would be denatured by depurinating the gel in 0.25 M HCl with shaking for 7 minutes. The gel was rinsed twice with ddH_2O, the DNA was then denatured 2 x 20 minutes with 1.5 M NaCl, 0.5 M NaOH. The DNA was transferred to Hybond N membrane by capillary blotting in 10 x SSC overnight and autocrosslinked to the membrane by UV crosslinking. After probing, the membrane was washed 30 minutes in 200 ml blocking buffer, washed 30 minutes in blocking buffer and antibody (diluted 1:10,000), and washed 2 x15 minutes in 200 ml wash buffer. Finally, 2 ml of CSPD was added to the membrane for 5 minutes, and the film was developed in the dark room.

2.2.28. Plasmid construction

The M gene was cloned by digesting pIBVM with NcoI and EcoRI, and inserting into EcoRI/NcoI digested pGBKT7 to generate pGBKT7-M. The PCR fragment for actin was amplified by using primers 5' CGCGGATCCATGGATGATGATATCGCC GCG-3' and 5'-CCGCTCGAGGAAGCATTTGCGGYGGACGAT-3'. The PCR fragment was digested with BamHI and XhoI, and ligated into BamHI and XhoI digested pXJ-myc to generate pXJ-myc-actin. Other mutant plasmids were cloned by PCR.

The following primers pairs were used for MΔ1:

5'-AACTGCAGTTAGCAAGCCACTGACCCTC-3'

5'-GCGAATTCATGCCCAACGAGACAAATTG-3';

for MΔ2:

5'-TCTTTTGTAGGTTATAAGTGTGAACCAGAC-3'

5'-GTCTGGTTCACACTTATAACCTACAAAAGA-3';.

for MΔ3:

5'-AACTGCAGCCGCTTTGGTCACCAG-3'

5'-GCGAATTCATGCCCAACGAGACAAATTG-3';

for MΔ4:

5'-TGTGAGGGTCCAGACCACTTG-3'

5'-CAAGTGGTCTGGACCCTCACA-3';

for MΔ5:

5'-GGTCAGTGGCTTTGTGAACCAGAC-3'

5'-GTCTGGTTCACAAAGCCACTGACC-3;

for pFlagQ(1):

5'-ATCCACTCGTAAGCTGTATGATGGC-3'

5'-CGGCTGCAGTTATTGAGTTGTAACTTCAAACTC-3';

for pFlagQ(2):

5'-ATCCGCAATTATTAGTGTTAAGGAG-3'

5'-CGGCTGCAGTTAAGTAT CCATATATGCCATAAC-3';

for pFlagQ(4):

5’-ATCCGCTAAATTGAGTGATGTAAAG-3’

5’-CGCTGCAGTTATTGCAAAACAACATCAACCTT-3’;

for pFlagQ(5)

5’-ATCCTCGGTTACTCAAGAATTCTCA-3’

5’-CGCTGCAGTTACTGTAAGACAACAACATTAGA-3’;

for pFlagQ(6):

5’-ATCCGCAGGTGTAGATCAAGCACAT-3’

5’-CGGCTGCAGTTAGTGTGCTCTACAATAGAGACA-3’;

for pFlagQ(7):

5’-ATCCTGTCTCTATTGTAGAGCACAC-3’

5’-CGGCTGCAGTCAGCCGAGCCTCACTGCTAC-3’;

for pFlagQ(9):

5’-ATCCGCAGATTCGCAGCATGCACTG-3’

5’-CGGCTGCAGTTAATCACGTGTTATAAACATGTT;

for pFlagQ(10):

5’-ATCCAGCTTCCGCAATTTGAAAGCT-3’

5’-CGGCTGCAGTTATAAACCTTTCAAAATACGGTT3’;

for pFlagQ(11):

5’-ATCCTTTGTATTGTCGGACAATGGT-3’

5’-CGGCTGCAGTTAATCATTATCGACAAGGAGTGT-3’.

All constructs were confirmed by automated nucleotide sequencing.

Chapter 3

Interaction of IBV M protein with β-Actin promotes virion assembly and budding in cultured cells

3.1. Introduction

Coronavirus is an enveloped virus with a large, positive-stranded RNA genome. IBV belongs to the third group of the coronavirus genus. Coronaviruses are known to assemble and bud at membranes of the intermediate compartment (IC), located between the ER and Golgi complex (Nguyen and Hogue, 1997). The M protein is a type III membrane protein and a key player in coronavirus assembly. Lateral interactions between M proteins are thought to mediate the formation of the virion envelope (Klumperman, *et al.*, 1994). Actin is the most abundant protein in a typical eukaryotic cell, which polymerizes in a helical fashion to form actin filaments (or microfilaments) that form the cytoskeleton, a three-dimensional network inside a eukaryotic cell.

In the present study, actin was identified as a potential interacting protein of the IBV M protein by yeast two-hybrid screening, and the interaction was subsequently confirmed by coimmunoprecipitaion and immunofluorescent staining. Mutations of amino acids A159 and K160 in the M protein abolished the interaction. Introduction of the A159-K160 mutations into an infectious IBV clone system showed that no infectious virus could be recovered, although viral RNA replication and subgenomic mRNA transcription appeared to be normal. Furthermore, disruption of actin filaments with the cell-permeable agent cytochalasin D induced decreased amount of virions in medium by time-course experiment, which showed cytochalasin D inhibited virion assembly and budding, but not release of the virus particles.

3.2. Results

3.2.1. Co-purification of actin with IBV

In a previous study, it was observed that a cellular protein with migration properties on SDS-PAGE similar to actin was consistently co-purified with highly purified IBV particles (Liu and Inglis, 1991). However, as no suitable antibodies against actin were readily available at the time, the identity of this protein was not established. For this purpose, confluent monolayers of Vero cells were infected with IBV at a multiplicity of infection of approximately 2 PFU/cell. The supernatants were collected at 18 hours post-infection and centrifuged at 4,000 rpm for 20 minutes to remove cell debris. The virus particles were spun down by ultracentrifugation through a 2 ml sucrose cushion (20 %), and purified using a 10-50 % sucrose gradient. Following ultracentrifugation, 11 fractions were collected from top to bottom, and the presence of viral proteins was checked by Western blot with anti-M antibodies (1: top, 11: bottom). As can be seen in Fig. 3-1b, the N protein was detected in fractions 7-11 with majority of the protein located in fractions 9-11 (Fig. 3-1, upper panel). Analysis of the same fractions by Western blot with anti-actin antibodies showed that actin appeared in the same fractions as N protein, with the majority of the protein detected in fractions 8-10 (Fig. 3-1b, lower panel). The lysates of Vero cells were loaded onto the sucrose gradient to serve as a control (Fig 3-1a). The actin were found to migrate at the fractions 3-4. These results demonstrate that actin could indeed be co-purified with the virus

particles. However, it is currently uncertain if actin could be incorporated into the virions.

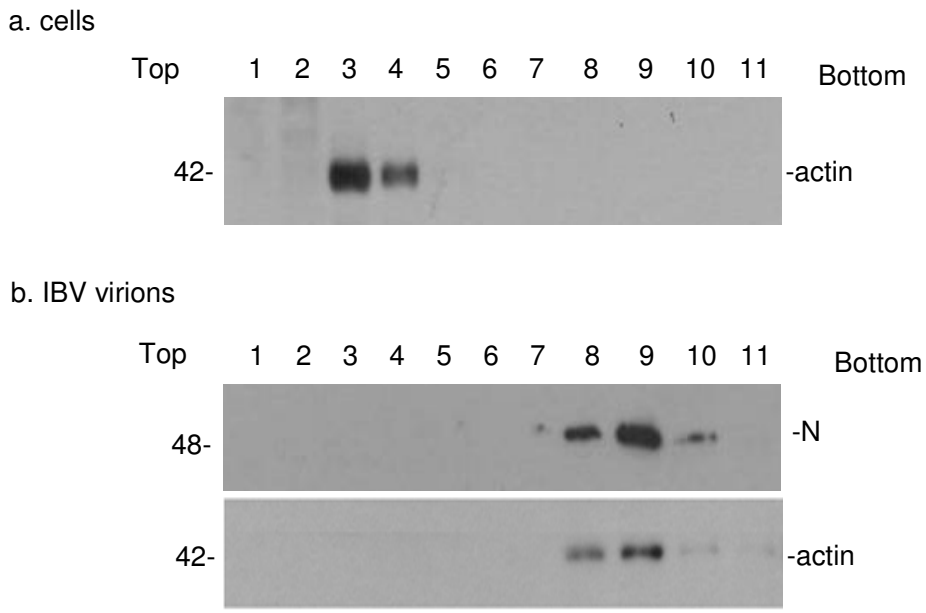

Figure 3-1

Co-Purification of actin with IBV virions. (a) The lysates of Vero cells were loaded onto a linear gradient of 10-50 % sucrose and centrifuged at 175,000 x g for 18 hours. (b) Confluent monolayers of Vero cells were infected with IBV at a multiplicity of infection of approximately 2 PFU/cell. At 18 hours post-infection, the supernatants were collected, centrifuged at 4,000 rpm for 15 minutes to remove cell debris. The virus pellets were obtained by ultra-centrifugation through a 2 ml sucrose cushion (20 %) at 175,000 x g for 3 hours and further purified using a linear gradient of 10-50 % sucrose at 175,000 x g for 18 hours. Eleven fractions from top to bottom were collected and separated by SDS-PAGE. Polypeptides were analyzed by Western blot with anti-M antibodies (upper panel) and anti-actin antibodies (lower panel). Numbers on the left indicate molecular masses in kilodaltons. 1: top fraction; 11: bottom fraction.

3.2.2. Interaction of the IBV M protein with β-actin

Coronavirus M protein is an essential component of the virus particles and plays important roles in virion assembly, budding and maturation. To search for cellular proteins that may interact with the M protein and regulate its functions, the IBV M protein was used as a bait to screen a human bone marrow cDNA library in yeast two-hybrid screening. Eight hundred colonies were initially selected and re-inoculated onto fresh SD/-Trp/-Leu/-His/-Ade plates for the β-gal assay, resulting in the selection of 76 blue colonies with potentially positive interactions. The cDNA fragments were extracted from bacteria transformed with total DNAs extracted from these positive colonies and sequenced. The potentially interesting interactions were further verified by switching the bait and prey constructs, and 13 putative interactions were confirmed. Among them, β-actin was chosen for further studies.

To confirm the interaction by co-immunoprecipitation, the full-length cDNA for β-actin was amplified by RT-PCR from HeLa cells, cloned into an expression vector with a c-Myc tag at its N-terminus (Myc-actin), and co-transfected into HeLa cells with the IBV M. Analysis of cells expressing the Myc-tagged actin either on its own or together with the M protein by Western blot with anti-Myc monoclonal antibody showed the detection of the Myc-tagged actin (Fig. 3-2, lanes 1 and 3). Similarly, analysis of cells expressing the M protein either on its own or together with the Myc-tagged actin by Western blot with anti-M polyclonal antibodies showed the detection of

the full-length glycosylated and unglycosylated forms of the M protein (Fig. 3-2, lanes 5 and 6). The same cell lysates were then subjected to immunoprecipitation with anti-Myc antibody. Western blot analysis of the precipitates with the same anti-Myc antibody showed the detection of the Myc-tagged actin expressed either on its own or together with the M protein (Fig. 3-2, lanes 7 and 9). Western blot analysis of the same precipitates with anti-M antibodies showed the detection of the Myc-tagged actin only in cells co-expressing the two proteins (Fig. 3-2, lane 12). No M protein was detected from the anti-Myc antibody precipitates in cells expressing either the M protein or Myc-actin alone (Fig. 3-2, lanes 10 and 11). These results confirm that the IBV M protein could indeed interact with actin.

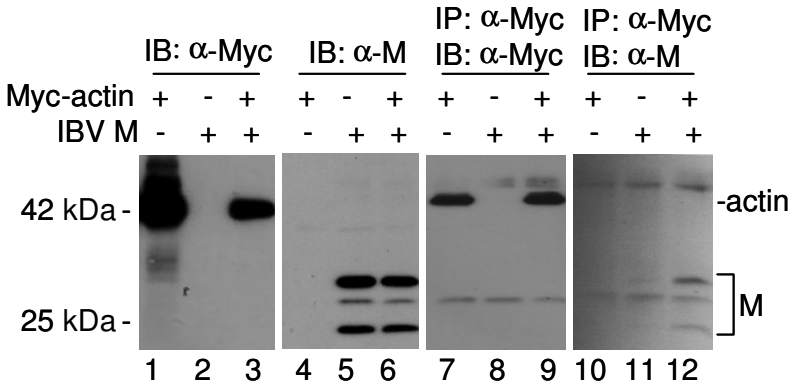

Figure 3-2

Interaction of the IBV M protein with human β-actin. HeLa cells were transfected with the Myc-tagged actin alone (lanes 1, 4, 7 and 10), IBV M alone (lanes 2, 5, 8 and 11) or co-transfected with actin and IBV M (lanes 3, 6, 9 and 12). Cells were harvested at 24 hours post-transfection and lysates prepared. Polypeptides were either analyzed directly by Western blot with anti-Myc (lanes 1-3) and anti-IBV M (lanes 4-6) antibodies, or subjected to immunoprecipitation with anti-Myc antibodies. The precipitates were analyzed by Western blot with anti-Myc (lanes 7-9) anti anti-IBV M (lanes 10–12) antibodies. Numbers on the left indicate molecular masses in kilodaltons. The three bands of M protein represent one un-modified band and two glycolated bands.

3.2.3. Mapping of the interacting region in the M protein

To map the region in the M protein responsible for the interaction with actin by yeast two-hybrid screening, six mutations constructs were made (Fig. 3-3a). MΔ1 contains the amino acid sequence from 1 to 159 (with deletion of amino acids 160 to 225); MΔ2 contains the deletion of amino acids 96-159; MΔ3 contains the amino acid sequence from 1 to 192 (with deletion of amino acids 193 to 225); MΔ4 contains the deletion of amino acids 155-162; and MΔ5 contains the deletion of amino acids 159-160; MAPKE contains A159-P/K160-E mutations (Fig. 3-3a). Introduction of individual mutation constructs into the yeast strain AH109 together with pACT-actin showed growth of wild type construct on SD-Trp/-Leu/-His/-Ade selective plates (Fig. 3-3b). However, none of the mutant constructs could grow on the same plate except MΔ3 (Fig. 3-3b). As MΔ5 and MAPKE contain the minimal mutation of two amino acids, this study maps the actin-binding site on the M protein to the region containing amino acids A159 and K160.

a

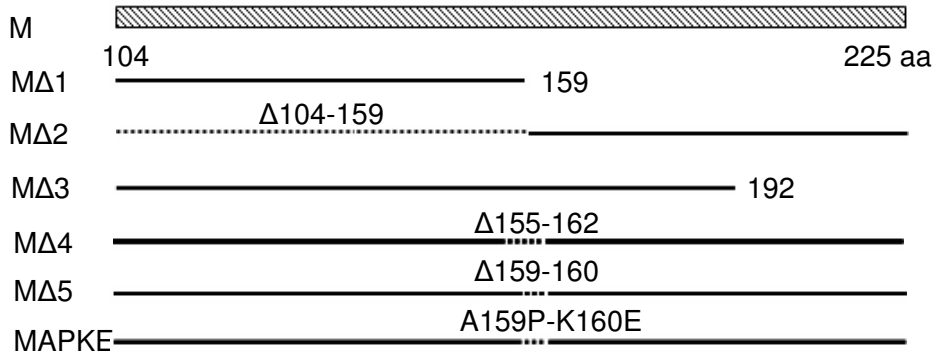

Figure 3-3

Mapping the region in M responsible for interaction with β-actin.

(a) Diagram showing the full-length IBV and six mutation constructs (MΔ1, MΔ2, MΔ3, MΔ4, MΔ5 and MAPKE). The amino acid positions of the mutated region in each constructs are shown. M protein was divided into two parts at the N-terminus. Each part deletion was cloned to check where the interaction region is. It was found that this interaction region covered A159-K160.

b

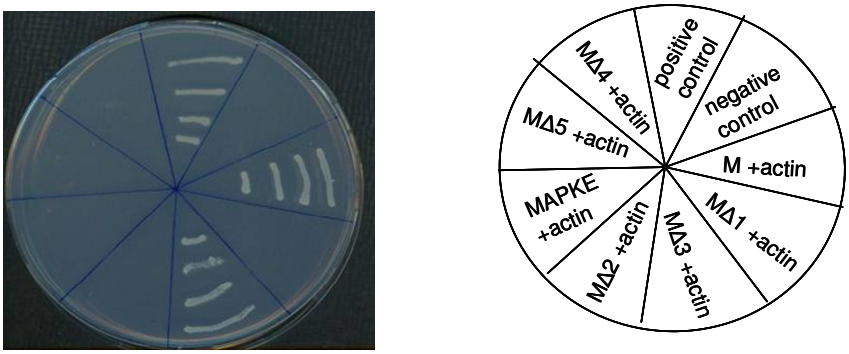

(b) The full-length IBV M and the six mutation constructs, respectively, were transformed into yeast cells with pACT-actin. The growth of the yeast cells on SD-Trp/-Leu/-His/-Ade- plate is shown. Also shown are the positive and negative controls. The negative control is pGBKT-7+pACT-2. The positive control is pGBKT-p53+pACT-T (from the Clontech yeast two hybrid kit).

3.2.4. Colocalizaion of the M protein with actin in cells treated with cytochalasin D

As a type III membrane protein with three transmembrane domains, the IBV M protein is mainly localized to the Golgi apparatus in virus-infected cells and in cells expressing the M protein (Klumperman *et al.*, 1994). Cytochalasin D is a cell-permeable fungal toxin. It can bind to the barbed end of actin filaments and inhibit both the association and dissociation of subunits, resulting in the disruption of actin filaments and inhibition of actin polymerization. To test the subcellular localization of the M protein in cells treated with cytochalasin D, H1299 cells were transfected with M construct and 12.5 μg/ml of cytochalasin D was added to the cells 4 hours post-transfection. Cells were permeabilized with 0.2 % Triton X-100 and stained with anti-M antibodies at 48 hours post-transfection. The same cells were also stained with Alexa Fluor 488 Phalloidin, a specific dye for actin (Molecular Probe). Staining of cells with Alexa Fluor 488 Phalloidin showed a three-dimensional network inside a eukaryotic cell (normal cells). Staining of cells treated with cytochalasin D with Alexa Fluor 488 Phalloidin showed that the regular cell actin filaments were destroyed (Fig. 3-4); with diffuse dots in the cells without the M protein expression. However, when M protein was expressed, actin interacted with M protein, forming a bright “ball” in the cells (Fig. 3-4). Under microscopy, actin and M proteins overlapped well in the cells treated with cytochalasin D and in control cells (treated with DMSO).

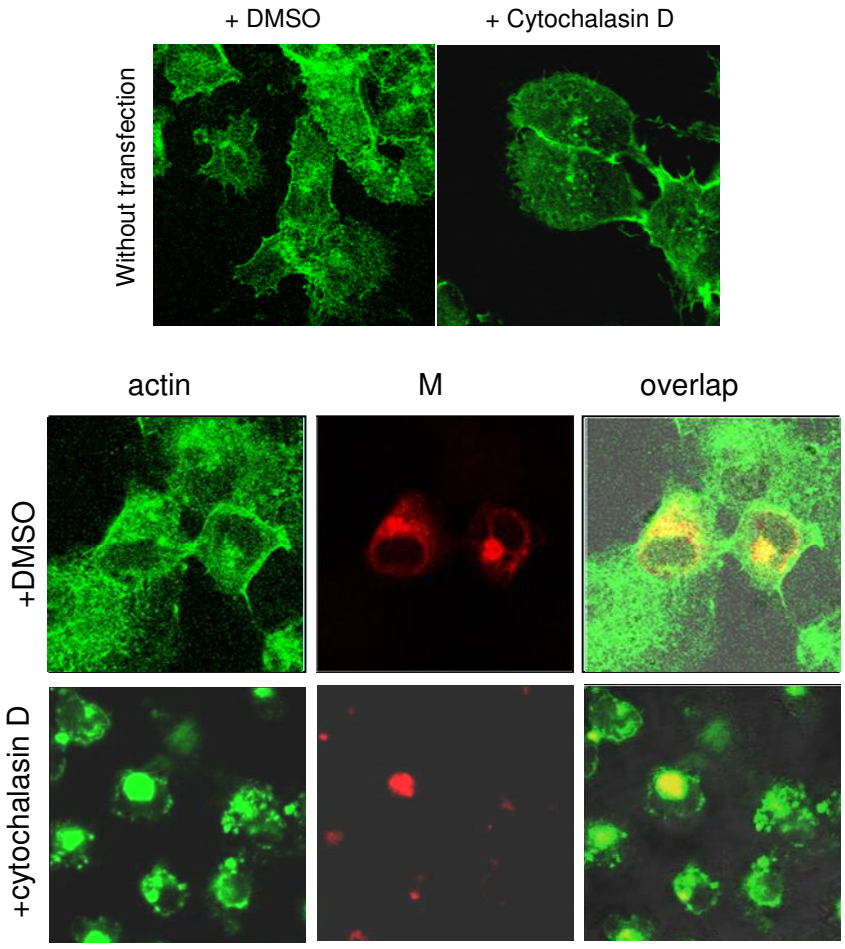

Figure 3-4

Colocalizaion of M and actin proteins in cells. The plasmids containing M gene were transfected into H1299 cells (bottom panel). After 4 hours, the cells were treated by cytochalasin D (12.5 μg/ml) and permeabilized with 0.2 % Triton X-100 and stained with anti-M antibodies at 48 hours post-transfection. The same cells were also stained with actin dye Alexa Fluor 488 Phalloidin (green). The cells only treated with DMSO/cytochalasin D server as control (upper panel).

3.2.5. Effects of deletion of amino acids A159 and K160 in the M protein on the replication, budding and release of IBV

Two approaches were used to test the effect of deletion of amino acids A159 and K160 in the M protein on the replication, budding and release of IBV. First, the A159-K160 deletion (MΔ5) and A159-P/K160-E (MAPKE) were introduced into a full-length IBV infectious clone, and the effect of the minimal mutants on the replication of viral RNA and the recovery of infectious IBV were analyzed. Introduction of full-length transcripts derived from wild type (wt), the MΔ5 deletion and the MAPKE mutation into Vero cells by electroporation showed efficient recovery of infectious IBV from cells transfected with wild type transcripts (data not shown). However, it was consistently observed that no infectious virus could be recovered from cells transfected with MΔ5 and MAPKE transcripts (data not shown).

As no infectious virus was recovered from cells transfected with MΔ5 and MAPKE transcripts, RT-PCR amplification of the negative strand RNA was performed to check if RNA replication occurred in the transfected cells. The primer pair (5'-^{14931}GCTTATCCACTAGTACATC^{14949}-3' and 5'-^{15578}CTTCTCGCACTTCTG CACTAGCA^{15600}-3') was chosen to amplify the negative strand IBV sequence spanning nucleotides 14931 to 15600 by RT-PCR. If replication of viral RNA occurred, a 670 bp PCR fragment would be expected. As shown in Fig. 3-5a, the 670 bp RT-PCR fragments were obtained from cells transfected with both wild type and mutant transcripts (lanes 2, 3, 4). The

relative amount of the fragment amplified from cells transfected with MΔ5 and MAPKE transcripts was 40 % and 54 % of that from cells transfected with wild type transcripts (Fig. 3-5a, lanes 2, 3, 4). No RT-PCR fragment was detected in control cells without transfection (Fig. 3-5a, lane 1).

RT-PCR amplification of subgenomic mRNAs was then carried out to check if subgenomic mRNA synthesis could occur in cells transfected with the mutant transcripts. The forward primer (5'-ACTTAAGATAGATATTAA-3') used in this reaction corresponded to the leader sequence spanning nucleotides 26-46 in the genomic RNA and the downstream primer (5'-CTCTGGATCCAATAACCTAC-3') spans the IBV sequence from nucleotides 24784 to 24803. If transcription of subgenomic mRNAs did occur, a 415 bp PCR product corresponding to the 5'-terminal region of the subgenomic mRNA4 would be detected. The subgenomic mRNA was detected by Southern blot. As shown in Fig. 3-5a, a dominant 415 bp was observed in cells electroporated with wild-type full-length transcripts at two days post-electroporation (lane 2). In cells transfected with MΔ5 and MAPKE transcripts, a much weaker band (3-7 % of wild type) was detected with the same primer pair (Fig. 3-5a, lanes 3 and 4). As a negative control, the amplified fragment was not detected in cells without electroporation (Fig. 3-5a, lane 1).

In the second approach, plasmids containing wild type M (pIBVM) and the A159-K160 deletion M sequence (pMΔ5) were transfected into H1299 cells

using the recombinant vaccinia/T7 virus expression system. The H1299 cell line is a continuous cell line derived from human lung carcinoma. This cell line can be efficiently infected by the Vero cell-adapted IBV and is much more resistant to the vaccinia virus-induced morphological changes and cell death. These properties make it an ideal cell line for the study. At 16 hours post-transfection, the cells were infected with IBV at a multiplicity of infection of approximately 0.5 PFU/cell to enlarge the difference of IBV infectivity, and were harvested at 24 hours post-infection. The expression of M protein and the infectivity of IBV on these cells were analyzed by Western blot with anti-M and anti-N polyclonal antibodies, respectively (Fig. 3-5b). In cells transfected with both wild type pIBVM and pMΔ5 constructs, detection of similar amounts of M protein was observed (Fig. 3-5b, top panel, lanes 1 and 2), suggesting that both constructs were expressed at similar efficiencies. However, much more N protein was detected in cells transfected with wild-type pIBVM construct than that in cells transfected with the pMΔ5 construct (Fig. 3-5b, middle panel, lanes 1 and 2). As a loading control, similar amount of actin was detected in cells transfected with both constructs (Fig. 3-5b, bottom panel). These results confirm that expression of the A159-K160 deletion M protein significantly reduces the infectivity of IBV.

a

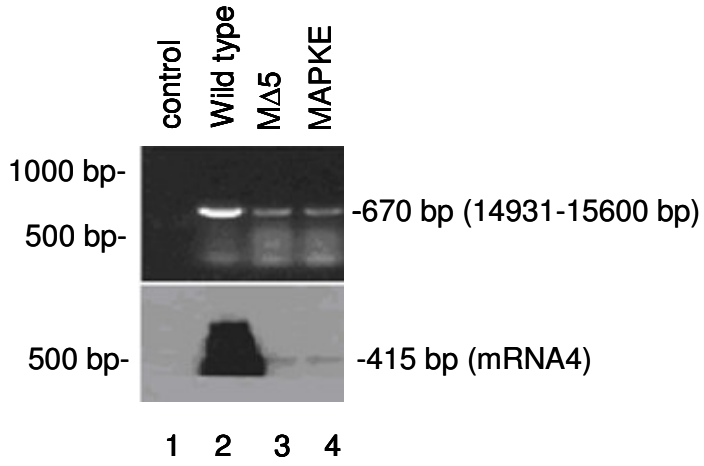

Figure 3-5

Effects of A159-K160 deletion on replication and infectivity of IBV

(a) In vitro transcripts derived from wild type, the A159-K1760 deletion and MAPKE mutation full-length IBV clones were electroporated into Vero cells. At 48 hours post-electroporation, total RNA were extracted from the cells and specific primers were used to detect the minus RNA by RT-PCR on agarose gel (upper panel) and subgenomic mRNA 4 by Southern blot (lower panel).

b

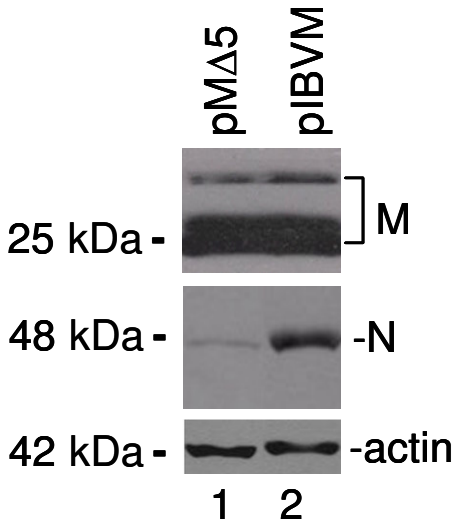

(b) H1299 cells expressing wild-type IBV M and the A159-160 deletion M (MΔ5) constructs with a vaccinia virus system were infected with IBV at a multiplicity of infection of approximately 0.5 PFU/cell. Cells were collected at 48 hours post-infection and polypeptides were analyzed by Western blot with anti-IBV M (top panel), anti-IBV N (middle panel) and anti-actin (bottom panel) antibodies.

3.2.6. Effects of disruption of actin filaments by cytochalasin D on the replication, budding and release of IBV

To define more precisely the stage of the viral replication cycle that is facilitated by the interaction between M protein and actin, the effects of disrupting actin filaments by cytochalasin D on the replication, budding and release of IBV were tested by detailed time-course experiments. Confluent monolayers of Vero cells in six-well plates were infected with IBV at a multiplicity of infection of approximately 3 PFU/cell. At 0, 4, 8, 12 and 16 hours post-infection, either 12.5 μg/ml of cytochalasin D or an equal volume of DMSO (as control) was added to the cells. The supernatants and cell pellets were separately harvested at 24 hours post-infection and the presence of IBV N protein was checked by Western blot with anti-N antibodies. Typical N protein profiles, including the full-length and posttranslational modified forms of the protein, were detected in the total cell lysates (Fig. 3-6). In cells treated with cytochalasin D, slightly less amount of the N protein was detected when cytochalasin D was added to the cells at 0, 4, 8 and 12 hours post-infection, respectively (Fig. 3-6, top panel, lanes 1-4). No obvious difference in the expression of N protein was seen when cytochalasin D was added at 16 hours post-infection (Fig. 3-6, top panel, lane 5). Western blot analysis of actin was included as a loading control (Fig. 3-6, middle panel). Analysis of the N protein in the clarified supernatants showed the detection of a single N protein species that represents the N protein incorporated into the virion particles in

cells treated with DMSO alone (Fig. 3-6, bottom panel, lanes 6-10). In the supernatants collected from cells treated with cytochalasin D, much reduced amounts of the N protein were detected in cells treated with the reagents at 12 and 16 hours post-infection (Fig. 3-6, bottom panel, lanes 4 and 5). No N protein was detected in the supernatants harvested from cells treated with cytochalasin D at 0, 4 and 8 hours post-infection, respectively (Fig. 3-6, bottom panel, lanes 1-3). The cells treated with DMSO serve as control in this experiment.

To further confirm which process in viral replication needs the interaction of actin and M proteins, plasmids pM, pMΔ5 and pMAPKE were co-transfected with three other constructs (pIBVE + pIBVN + pIBVS) into H1299 cells separately. After 16 hours, the media were collected and centrifuged at 4,000 rpm for 20 minutes. Then, each supernatant was poured on a 20 % sucrose solution, and cushioned at 38,000 rpm for 3 hours. Finally, the pellets were collected and analyzed on 15 % SDS-PAGE gel to detect the expression of structural proteins. In Fig. 3-7a, the S, N and M proteins could be detected in all cell pellets at similar levels. Furthermore, these structural proteins were also present in supernatants but not in the control (Fig. 3-7b).

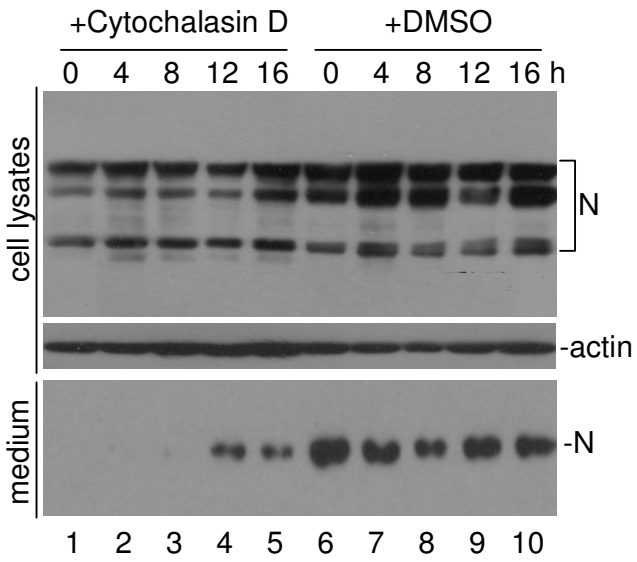

Figure 3-6

Effects of disruption of actin filaments by cytochalasin D on IBV replication. Vero cells plated in six-well plates were infected with IBV at a multiplicity of infection of approximately 0.5 PFU/cell. Cytochalasin D (12.5 μg/ml) and DMSO (as control) were added to the infected cells at the indicated times. Total cells and the culture media were separately collected at 24 hours post-infection. Cell lysates were prepared and analyzed by Western blot with anti-N (top panel) and anti-actin (middle panel) antibodies. Western blot analysis of the IBV N protein with anti-N antibodies (bottom panel) was also shown. The cells treated with DMSO serve as control.

a

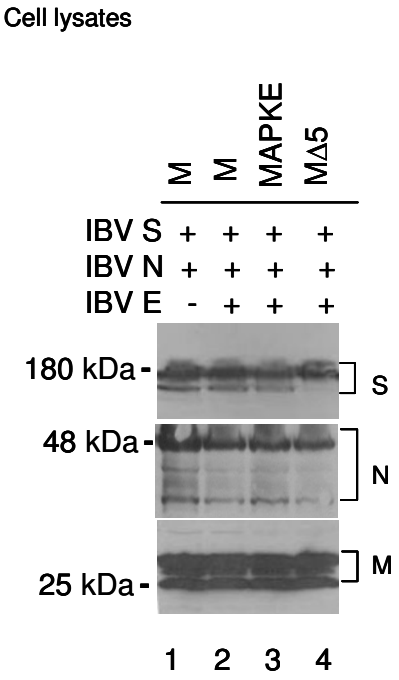

Figure 3-7

Effects of A159-K160 deletion and mutation on VLPs formation. Three IBV structural protein constructs (pIBVS + pIBVN + pIBVE) were co-transfected with pIBVM, or pIBVMΔ5, or pIBVMAPKE into H1299 cells. At 16 hours post-transfection, media and cell were collected separately. The VLPs in media were obtained by centrifugation on sucrose cushion at 38,000 rpm for 3 hours. These cell lysates and media pellets were electrophoresed on a 15 % SDS-PAGE gel to detect the expression of structural proteins.

(a) Cell lysates were analyzed on 15 % SDS-PAGE gel to detect the S, N and M proteins. The cells loaded on lane 1, served as a negative control, were transfected with pIBVS, pIBVN and pIBVM constructs, without pIBVE.

b

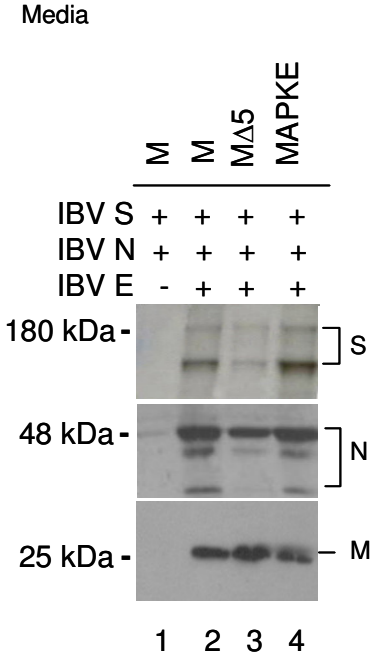

(b) The VLPs in media were obtained by centrifugation on sucrose cushion at 38,000 rpm for 3 hours. The pellets of media were separated on a 15 % SDS-PAGE gel, and the S, N and M proteins were detected.

Chapter 4

Mutational analysis of nine cleavage sites of the 3CLpro in coronavirus 1a and 1ab polyproteins shows differential effects on RNA replication and subgenomic transcription

4.1. Introduction

Replication of the IBV genome in the infected cell is likely initiated by translation of the 5' terminal region of mRNA 1 into 1a/1b fusion polyprotein of 741 kDa by a unique frame-shifting mechanism (Boursnell *et al.*, 1987). Co- and post-translational proteolytic processing of the nascent polyprotein is mediated by two virus-encoded proteases, PLP and 3CLpro (Ziebuhr *et al.*, 2000). The high substrate specificity of 3CL proteases is very important to all coronaviruses because proteolytic cleavage must be accurate to release functional proteins from the large polyprotein step by step. Otherwise, the virus replication cycle mediated by functional proteins would be disrupted. The specificity is mainly realized by the recognition between the enzyme and a wide range of positions in the substrate (Ziebuhr *et al.*, 1997, 2000).

The positions of amino acids in substrates named from the N- to C-terminal are as follows: -P4-P3-P2- P1↓-P1'-P2'-P3'-P4' (Schechter and Berger, 1967). To investigate if the Q residue in P1 position is conserved, site-directed mutagenesis at the P1 position on Flag-tag was performed. Four amino acids (A, E, N and R) were introduced to replace the Q(5) residue at the P1 position of cleavage sites by 3CLpro in pp1a and pp1ab. All of the mutant viruses could not be recovered except the Q(5)-N and Q(5)-E replacements. Meanwhile, by the in vitro cleavage assay, the Q(5)-N and Q(5)-E mutants could be cleaved by IBV 3CLpro, and their efficiency was much higher than that of Q(5)-A and Q(5)-R mutants, but less efficient than that of wild-type Q(5).

Furthermore, the N and E residues were also introduced into the P1 position of the other 3CLpro cleavage sites. Among them, the mutants of Q(1)-N, Q(1)-E, Q(2)-N, Q(2)-E, Q(4)-N, Q(6)-N, Q(9)-E and Q(11)-N can be cleaved by 3CLpro, but not for the Q(4)-E, Q(6)-E, Q(7)-N, Q(7)-E, Q(9)-N, Q(10)-N, Q(10)-E and Q(11)-E mutants. These data show that the Q residue at the P1 position is not essential in some cases, but is very important for virus replication.

4.2. Results

4.2.1. Mutational analysis of the conserved P1 residue (Q) of nine cleavage sites of 3CLpro in 1a and 1ab polyproteins

The IBV 3CLpro cleaves the 1a and 1ab polyproteins at 11 positions (Fig. 4-1). Among all the 11 sites, the Q residue at the P1 position is absolutely conserved. To analyze the functional roles of cleavage at these positions in viral replication cycles and infectivity, mutations of the Q residue to either an N or an E at nine of the 11 positions were carried out (Fig. 4-2a). Plasmids (pFlagQ(5), pFlagQ(5)-N, pFlagQ(5)-A, pFlagQ(5)-R, pFlagQ(5)-E, pFlagQ(4), pFlagQ(4)-N, pFlagQ(4)-E) were co-transfected with pIBV3C into H1299 cells respectively by Lipofectamine 2000 (Invitrogen). The proteins were expressed by a T7-vacciania system. At 16 h post-transfection, the transfected cells were collected and detected by anti-flag antibody on 12% SDS-PAGE gels. As shown in Fig. 4-2b, a 36.5 kDa protein was detected in the

cells transfected with pFlagQ(5) (lane 13). When co-expressed with pIBV3C, the 36.5 kDa protein was cleaved by IBV 3CLpro to release a 24.5 kDa protein (lane 14). The corresponding bands were also observed in the cells co-transfected with pIBV3C together with pFlagQ(5)-N, pFlagQ(5)-E pFlagQ(5)-A and pFlagQ(5)-R respectively (lanes 15-18). However, the cleaved bands in the cells expressing pFlagQ(5)-N and pFlagQ(5)-E were much stronger than the cells expressing pFlagQ(5)-A and pFlagQ(5)-R, but weaker than the cells expressing pFlagQ(5). This demonstrates that the cleavage efficiency of Q(5)-N and Q(5)-E is much higher than that of Q(5)-A and Q(5)-R, but lower than Q(5). Meanwhile, the cleavage efficiency of the Q(5)-A and Q(5)-R is about one tenth of that of wild type, and for Q(5)-N and Q(5)-E, it is about half. In Fig. 4-2b, a cleaved 10.6 kDa band was detected in the cells co-transfected with pIBV3C together with pFlagQ(4) and pFlagQ(4)-N respectively (lanes 12 and 11), but not in the cells transfected with pFlagQ(4)-E (lane 10). This shows that IBV 3CLpro favored N substitution rather than E substitution at the Q(4) position. Similarly, IBV 3CLpro can cleave Q(6)-N (Fig. 4-2c, lane 21), but not Q(6)-E (Fig. 4-2c, lane 22) mutants. Reversely, it was shown in Fig. 4-2c, 3CLpro could cleave Q(9)-E (lane 30) to release a 6.9 kDa protein, but could not cleave Q(9)-N (lane 29).

In some cases, the Q residue cannot tolerate N and E substitutions in the P1 position. For example, no cleaved band was observed in cells co-transfected pIBV3C either with pFlagQ(10)-N (Fig. 4-2c, lane 33) or with pFlagQ(10)-E

(Fig. 4-2c, lane 34), compared with the cells co-transfected with pIBV3C and pFlagQ(10) (Fig. 4-2c, lane 31). Similarly, Q(7)-N (Fig. 4-2c, lane 25), Q(11) (Fig. 4-2c, lane 37) and Q(7)-E (Fig. 4-2c, lane 26), Q(11)-E (Fig. 4-2c, lane 38) mutants could not be cleaved by IBV 3CLpro, compared to the wild types.

Furthermore, high tolerance of N and E substitutions in the P1 position of the cleavage sites of IBV 3CLpro was also observed. It was found that IBV 3CLpro can cleave Q(1)-N (Fig. 4-2b, lane 3), Q(2)-N (Fig. 4-2b, lane 7), Q(1)-E (Fig. 4-2b, lane 4) and Q(2)-E (Fig. 4-2b, lane 8) mutants to release a corresponding cleaved band as for the wild-type Q(1) and Q(2), respectively.

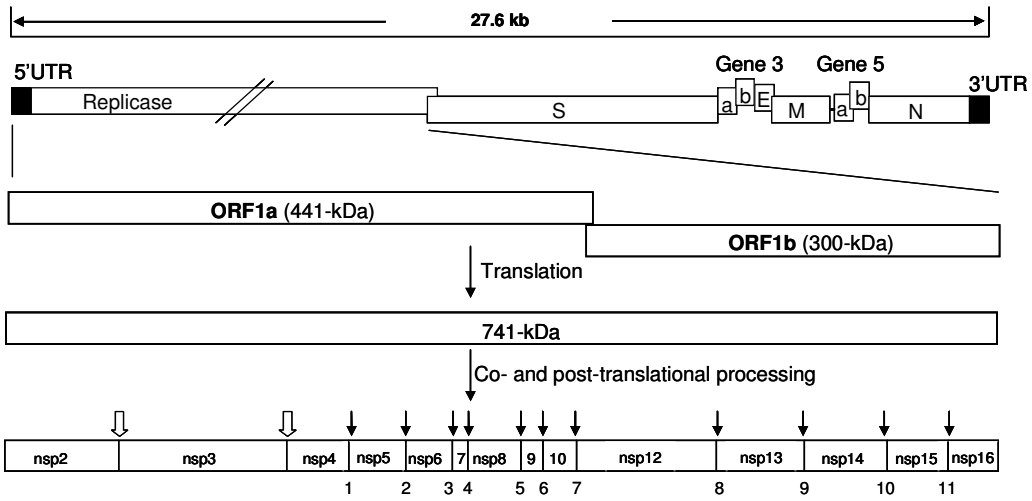

Figure 4-1

Proteolytic processing map of polyprotein 1a and 1ab by IBV 3CLpro

Diagram shows the locations of non-structural proteins in pp1a and pp1ab. ORF1a is translated to produce pp1a, a 441 kDa polyprotein. Both ORF1a and ORF1b are needed to produce pp1ab, which is about 741 kDa in length. Also shown are the positions of 11 identified Q-S (N, A) cleavage sites of the 3CLpro. The solid arrows show the cleavage sites of 3CLpro. The open arrows show the cleavage sites of PLP.

a

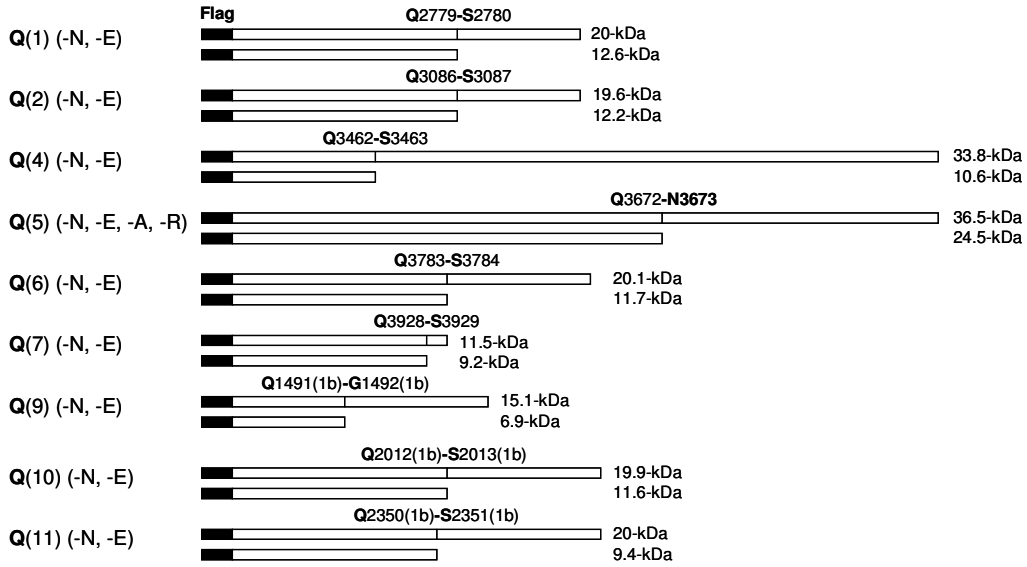

Figure 4-2

In vitro cleavage activity assay of IBV 3CLpro.

(a) The precise amino acid positions of the nine cleavage sites are indicated. Each fragment containing a cleavage site, fused with a Flag tag at the N terminus, was cloned into pKT0. The molecular masses of the expected non-cleaved and cleaved proteins are shown together.

b

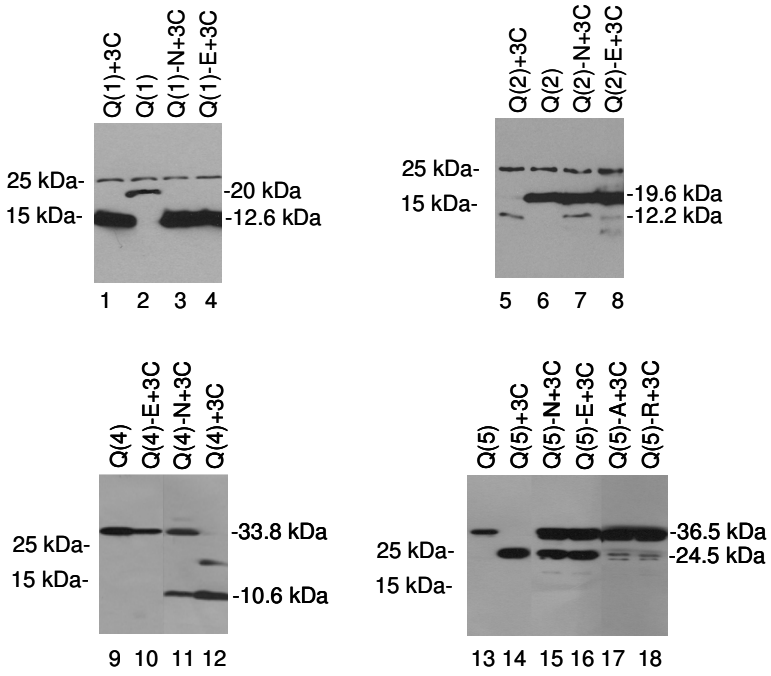

(b) Different plasmids containing site-directed mutants at the P1 position and flag tag were co-transfected with pIBV3C respectively into H1299 cells and expressed by a T7 vaccinia virus system. The transfected cells were collected at 16 h post-transfection, separated on 15% SDS-PAGE gels and detected by anti-flag antibody. Cleavage activity of IBV 3CLpro for the N and E substitutions in Q(1) (lanes 1-4); for the N and E substitutions in Q(2) (lanes 5-8); for the N and E substitutions in Q(4) (lanes 9-12); for the N, E, A and R substitutions in Q(5) (lanes 13-18).

c

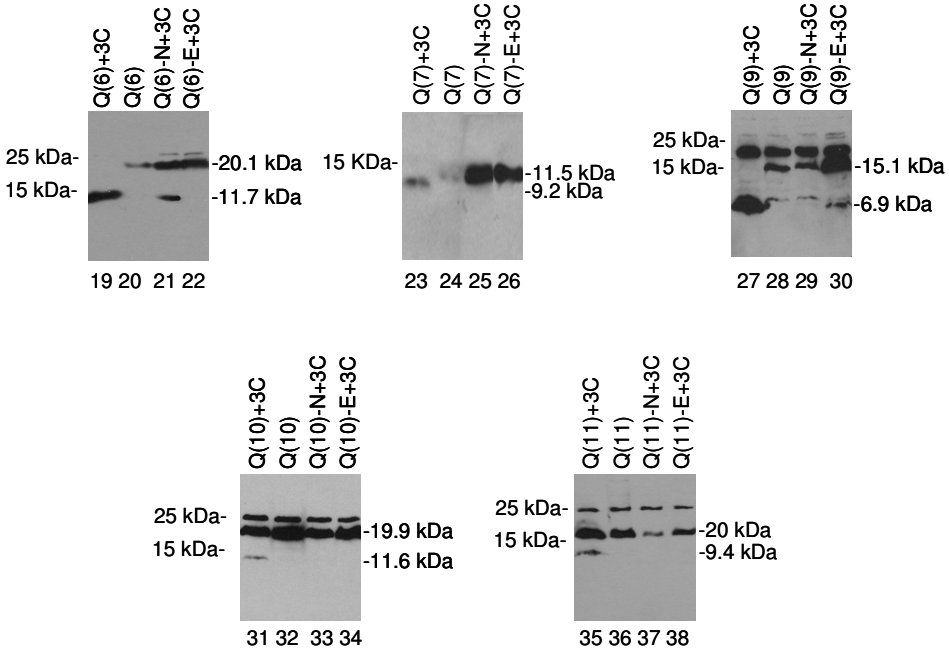

(c) Cleavage activity of IBV 3CLpro for the N and E substitutions in Q(6) (lanes 19-22); for the N and E substitutions in Q(7) (lanes 23-26); for the N and E substitutions in Q(9) (lanes 27-30); for the N and E substitutions in Q(10) (lanes 31-34); for the N and E substitutions in Q(11) (lanes 35-38).

4.2.2. Analysis of negative-strand RNA replication and subgenomic RNA transcription in cells transfected with wild-type and mutant full-length transcripts

As no infectious viruses were recovered from cells transfected with some of the mutant transcripts (Table 4-1), the Q(9)-N, Q(10)-N, Q(5)-A and Q(5)-R were chosen randomly and subjected to RT-PCR amplification of the negative strand RNA to check if RNA replication occurred in these transfected cells. Total RNA was extracted from Vero cells transfected with wild type and mutant full-length transcript at 48 h post-electroporation. RT-PCR was performed by using two primers IBV14931-F (5'-GCTT ATCCACTAGTACATC-3') and IBV15600-R (5'-CTTCTCGCACTT CTGCACTAGCA-3'). If replication of viral RNA took place, a 670 bp PCR fragment would be detected. RT-PCR fragments amplified from negative strand RNA templates were obtained from cells transfected with both wild type (Fig. 4-3a, lane 3) and the mutant transcripts (Q(9)-N, Q(10)-N, Q(5)-A and Q(5)-R (Fig. 4-3a, lanes 4-7). As a negative control (Fig. 4-3a, lane 2), the *in vitro*-synthesized transcripts were mixed with total RNA extracted from normal Vero cells and were used as a template for RT-PCR. No corresponding band was detected from the control, which confirmed that the detection of negative strand RNA from cells transfected with mutant transcripts was due to the replication of viral RNA. However, the band detected in the cells transfected with wild-type transcript was much stronger than that in the cells transfected

with mutant transcripts, indicating that transcription of the negative strand RNA occurred in cells transfected with the mutant transcripts, but their efficiency was much lower than the cells transfected with wild type transcript.

RT-PCR amplification of subgenomic mRNAs was carried out to check if subgenomic mRNA synthesis could occur in cells transfected with the mutant transcripts. Total RNA prepared from the transfected cells 2 days post-electroporation was used in RT-PCR with two primers: IBV-leader (5'-CTATTACACTAGCCTTGCGCT-3') and IBV26357-R (5'-CGGTTC AGGGGAATGAAG-3') for detection of positive-stranded subgenomic mRNAs. If transcription of subgenomic mRNAs occurred, a 617 bp PCR product corresponding to the 5'-terminal region of the subgenomic mRNA 6 and a 918 bp PCR fragment corresponding to the 5'-terminal region of the subgenomic mRNA 5 would be expected. A dominant 617 bp band and a weak 918 bp band were detected in cells electroporated with wild-type full-length transcript (Fig. 4-3b, lane 3) at 2 days post-electroporation, but not in cells electroporated with mutant transcripts (Q(9)-N, Q(10)-N, Q(5)-A and Q(5)-R) (Fig. 4-3b. lane 4-7).

a

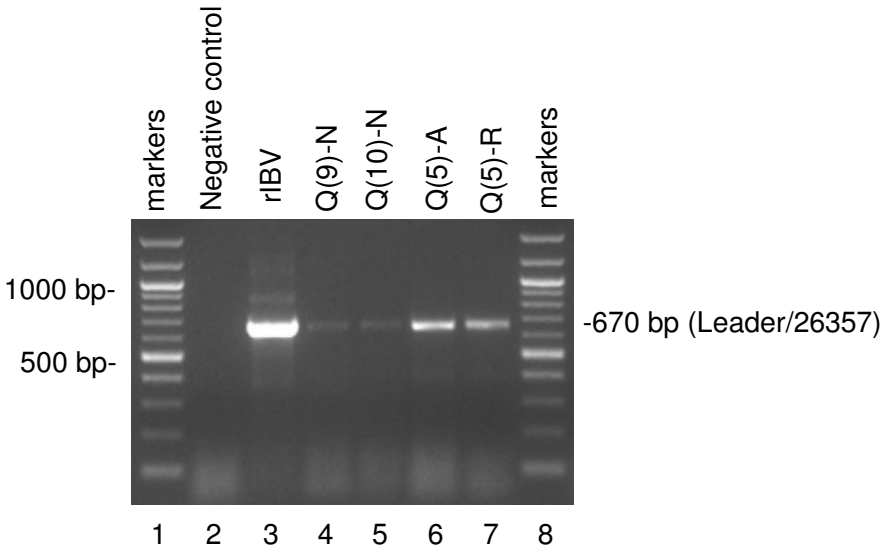

Figure 4-3

Analysis of RNA replication in cells electroporated mutant transcripts.

(a) Detection of negative strand RNA synthesis in cells electroporated with wild type (lane 3), Q(9)-N (lane 4), Q(10)-N (lane 5), Q(5)-A (lane 6), and Q(5)-R (lane 7) mutant transcripts. Total RNA was prepared from Vero cells electroporated with in vitro synthesized full-length transcripts at 48 h prost-electroporation. The region corresponding to nucleotides 14,931-15,600 of the negative sense IBV genomic RNA was amplified by RT-PCR and analyzed on 1.2% agarose gel. Numbers on the left indicate nucleotides markers in bases.

b

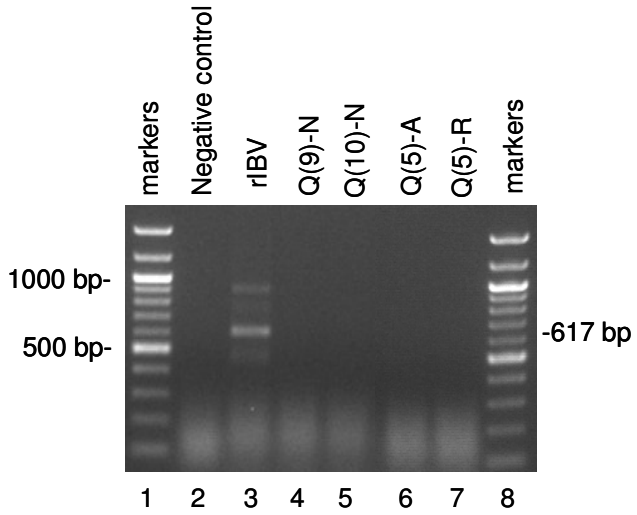

(b) Detection of subgenomic RNA synthesis in cells electroporated with wild type (lane 3), Q(9)-N (lane 4), Q(10)-N (lane 5), Q(5)-A (lane 6), and Q(5)-R (lane 7) mutant transcripts. Total RNA was prepared from Vero cells electroporated with in vitro synthesized full-length transcripts 2 days post-electroporation. Regions corresponding to the 5'-terminal of the subgenomic mRNA 6 and 5 respectively were amplified by RT-PCR and analyzed on a 1.2 % agarose gel. Numbers on the left indicated the length of DNA markers in bases.

Table 4-1. Recombinant viruses recovered from the site-directed mutant IBV clones

mutant	virus recovery
Q(1)-N	yes
Q(2)-N	yes
Q(3)-N	no
Q(4)-N	yes
Q(5)-N	yes
Q(5)-E	yes
Q(5)-A	no
Q(5)-R	no
Q(6)-N	yes
Q(7)-N	yes
Q(9)-N	no
Q(10)-N	no
Q(11)-N	no

4.2.3. Genetic stability and growth kinetics of Q(5)-N and Q(5)-E mutant viruses

Only in P1 position of Q(5), both N and E substitution recombinant viruses could be recovered. In order to study their characteristic, the recombinant wild type (rIBV), Q(5)-N and Q(5)-E mutant viruses were purified with plaque assay. The growth properties of the Q(5)-N and Q(5)-E mutant viruses on Vero cells were tested by analysis of plaque sizes and growth curves of passage 3 mutant viruses (Fig. 4-4a). Compared to cells infected with wild type recombinant virus (rIBV, average plaque size of 2.38 mm), the two mutant viruses produced much smaller plaques. For the Q(5)-N mutant virus, the average plaque size was approximately 1.48 mm, which was similar to the Q(5)-E virus (average plaque size of 1.41 mm). Meanwhile, analysis of the growth curves of wild type and mutant viruses demonstrated that the wild type virus grew faster than the two mutant viruses. At 16 hours post-infection, the wild type virus reached its highest titer, which was 102.72-fold more than its titer at 0 hour post-infection. However, the two mutant viruses reached their peak titer at 24 hours post-infection, which was 102.61-fold more than the original titer for the Q(5)-N virus, and 102.69-fold for the Q(5)-E virus.

Further characterization of the mutant viruses was carried out by analysis of the viral RNAs (Fig. 4-4c) and structural proteins (Fig. 4-4d). Northern blot analysis showed that the amount of viral RNAs in cells infected with rIBV and two mutant viruses (Q(5)-N and Q(5)-E) were different, and

exhibited an increasing order: Q(5)-N, Q(5)-E, and rIBV (Fig. 4-4c). In addition, the S, N and M proteins were detected in the infected cells at 24 h post-infection by Western blot analysis (Fig. 4-4d). The wild type virus produced much more structural protein expression than the other two mutant viruses. Notably, the Q(5)-N virus produced the least protein expression level among these three viruses.

To investigate the genetic stability of the Q(5)-N and Q(5)-E mutant viruses, these two viruses were propagated in Vero cells for 3 passages after purification. Viral RNA was isolated from the infected cells and amplified by RT-PCR. Sequencing analysis showed these two mutations were stable. No reversion to the original sequence or mutation to other nucleotides was found at this position (Fig. 4-4b).

a

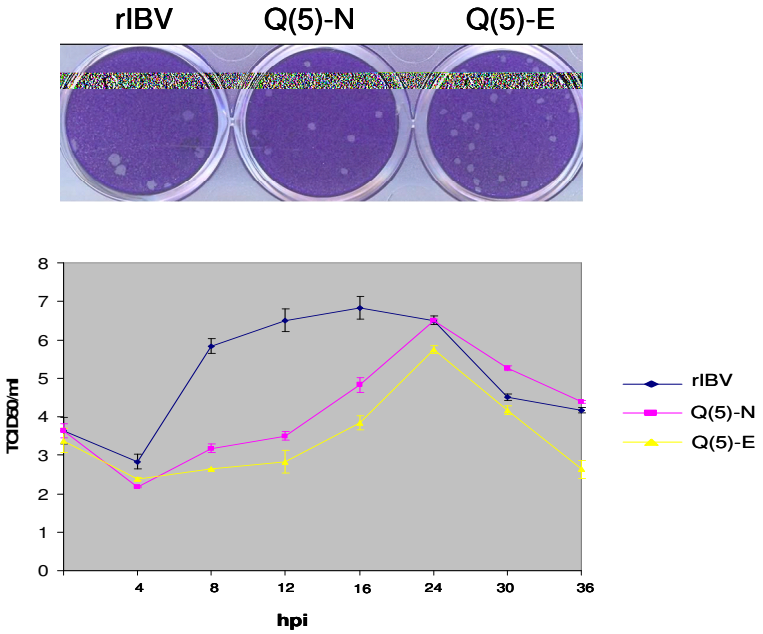

Figure 4-4

Analysis of the growth properties of rIBV, Q(5)-N, and Q(5)-E mutant viruses.

(a) Plaque sizes and one-step growth curves of rIBV, Q(5)-N, and Q(5)-E mutant viruses. Monolayers of Vero cells in a 6-well plate were infected with 100 µl of 100-fold diluted virus stock and cultured in the presence of 0.5 % carboxymethy cellulose at 37 °C for 3 days. The cells were fixed and stained with 0.1 % toluidine. To determine the one-step growth curves of rIBV, Q(5)-N, and Q(5)-E mutant viruses, Vero cells were infected with the viruses and harvested at 0, 8, 16, 24, and 32 h post-infection, respectively. TCID50 of each viral stock was determined by infecting five wells of Vero cells in 96-well plates in triplicate with 10-fold serial dilutions of each viral stock. Each error bar shows standard error of the mean.

b

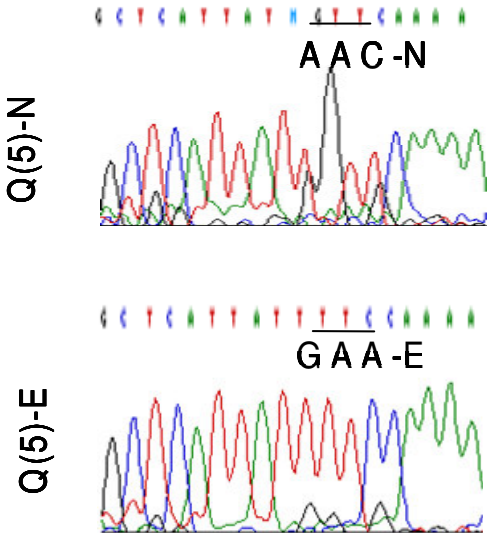

(b) Sequencing analysis of two mutations are shown. The RNAs of cells separately infected with Q(5)-N and Q(5)-E viruses were purified. RT-PCR was performed with the specific primers to verify if the mutations were still present in the mutant viruses.

c

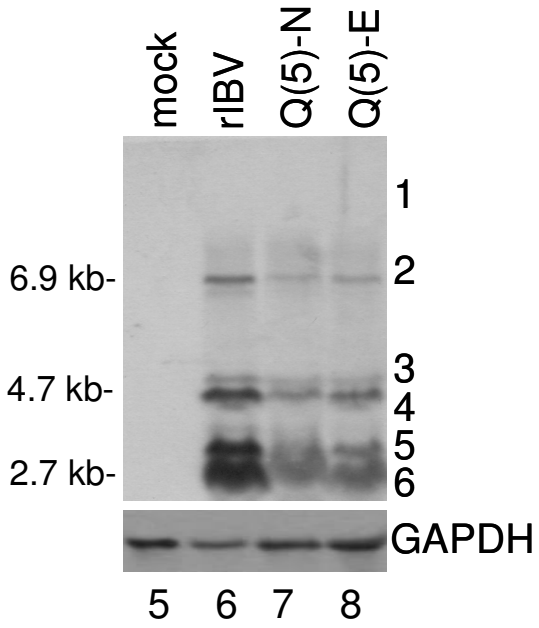

(c) Northern blot analysis of the genomic and subgenomic RNAs in cells infected with rIBV, Q(5)-N, and Q(5)-E mutant viruses. Ten micrograms of total RNA extracted from Vero cells infected with rIBV, Q(5)-N, and Q(5)-E mutant viruses, respectively, was separated on 1% agarose gel and transferred to a Hybond N+ membrane. Viral RNAs were probed with a Dig-labeled DNA probe corresponding to the 3'-terminal 208 nucleotides of the IBV genome. Numbers on the right indicate the genomic and subgenomic RNA species of IBV and numbers on the left indicate nucleotides in kilobase

d

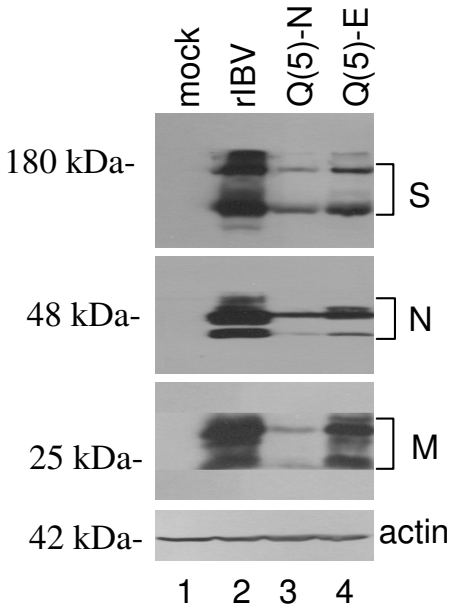

(d) Western blot analysis of viral protein expression in cells infected with wild type Q(5)-N, and Q(5)-E mutant viruses. Vero cells infected with wild type recombinant IBV (lane 2), Q(5)-N (lane 3), and Q(5)-E (lane 4) were harvested, lysates prepared, and separated on SDS-10% polyacrylamide gel. The expression of S, N, and M proteins was analyzed by Western blot with polyclonal anti-S, anti-N, and anti-M antibodies, respectively. The same membrane was also probed with anti-actin antibody as a loading control. Numbers on the left indicate molecular masses in kilodaltons.

Chapter 5

General discussion and future direction

5.1. Co-purification of actin with IBV

Actin is a ubiquitous cytoskeletal protein of eukaryotic cells and has various functional roles in the cell (Korn, 1982, Winder and Ayscough, 2005). Interaction of actin with viral components has been reported in several other viral systems. For example, the M protein of Newcastle Disease Virus interacts with actin in vitro (Garoff *et al.*, 1998; Ogino et al., 2003). Available evidence suggests that the host cytoskeleton, especially actin, is involved in the budding process of several animal viruses, such as Rous Sarcoma Virus, Mouse Mammary Tumor Virus, Sendai Virus and Measles Virus (Arthur *et al.*, 1992; Damsky *et al.,* 1977; Bohn, *et al.,* 1986). Actin is also found in paramyxovirus-infected cells, which showed that actin plays a role in the transport of synthetic viral RNA and proteins to the cytoplasmic membrane of the host cell (Stallcup *et al.*, 1983; Bohn *et al.*, 1986; Mayer *et al.*, 1990). Polymerized actin was also found in HIV preparations (Ott *et al.*, 1996; Gardet *et al.*, 2006). The functional implication for the incorporation of actin into these virus particles remains unclear. One possibility is that actin polymerization serves as an additional force for membrane bending during budding (Garoff *et al.*, 1998; Gov and Gopinathan, 2006). As an illustrative example, actin was shown to control the movement of measles virus envelope proteins on the surface of infected cells (Ehrnst and Sundquist, 1975). However, more conclusive data, such as immunogold labeling of highly purified virions, are currently lacking.

In this study, actin alone was found to be co-purified with IBV virions and the IBV M protein is associated with actin, suggesting that actin may be incorporated into IBV virions through its interaction with the M protein.

5.2. Interaction of the IBV M protein with β-actin

Enveloped viruses acquire their envelope by budding from the host cell. In this process, viral envelope proteins gather at a special membranous structure and cooperate with other viral components to induce budding (Garoff, *et al.*, 1998). For example, some viruses including human immunodeficiency virus bud from the plasma membrane and release the virion from host cells by pinching-off. Others bud at intracellular membranes (Griffiths and Rottier, 1992; Gissen and Maher, 2007). In this way, virions are wrapped within intracellular membrane-bound compartments, such as the endoplasmic reticulum (ER) and Golgi apparatus, and the newly budded viruses exit the cell by using the cellular secretory pathway (Corse and Machamer, 2003). However, the detailed mechanisms of viral assembly and budding, especially the host factors that are involved in these processes, are yet to be revealed for many viruses.

Coronavirus M protein plays essential roles in virion assembly and budding (Stern *et al.*, 1982; Sturman *et al.*, 1980; de Haan *et al.*, 2003). The protein itself cannot bud. However, with the help of E protein, VLPs may be formed at the IC membranes. As coronaviruses do not contain a matrix

protein that underlines the membrane, the M protein may serve as a matrix-like protein. The M protein appears to interact with S and hemagglutinin-esterase (HE) proteins, and the S-M-HE protein complexes can be detected in cells infected with the bovine coronavirus (Nguyen and Hogue, 1997). The M protein interacts with the mouse hepatitis virus (MHV) nucleocapsid consisting of the genomic-size mRNA 1 and N protein in a pre-Golgi compartment, probably at the ER membrane. It may interact directly with the genomic RNA through the packaging signal, initiating the M-nucleocapsid interaction. There is also a detectably direct interaction between M and N proteins in the nucleocapsid, which may further stabilize the M-genomic RNA interaction (Narayanan *et al.*, 2000). It was reported that the M and E proteins are the minimal requirements for envelope formation (Vennema *et al.*, 1996; Bosch *et al.*, 2005).

It is proposed that the formation of coronavirus envelope is dominated by lateral interactions between M molecules that form a two-dimensional lattice in intracellular membranes (Opstelten *et al.*, 1995; Zeng *et al.*, 2004). The M-M interaction is essential but not sufficient for coronavirus envelope assembly. Free energy is needed to generate and stabilize membrane curvature, suggesting that interaction of M protein with host proteins would be a requirement (de Haan *et al.*, 2000).

Actin is the most abundant protein in a typical eukaryotic cell, highly conserved, differing by no more than 5 % in species as diverse as algae and

humans. It polymerizes in a helical fashion to form actin filaments (or microfilaments) that form the cytoskeleton, a three-dimensional network inside a eukaryotic cell. Actin filaments provide mechanical support for the cell, determine the cell shape, enable cell movements (through lamellipodia, filopodia, or pseudopodia), and participate in certain cell junctions, in cytoplasmic streaming and in cell contraction during cytokinesis (Steven and Kathryn, 2005).

In this study, β-actin was shown to interact with IBV M protein through the yeast two-hybrid system. The interaction was subsequently confirmed in mammalian cells by co-immunoprecipitation. This is the first demonstration that actin interacts with coronavirus M protein, and that actin may be involved in the process of IBV replication.

5.3. Mapping of the interacting region in the M protein

Coronavirus M protein is an essential and predominant component of the virions. It plays pivotal roles in virion assembly and budding by interaction with other viral components. Firstly, the monomers of M interact with each other particularly via the transmembrane domains (de Haan *et al.* 2000). Besides, the M-N interaction region has been narrowed to the 16 residues adjacent to the carboxy terminus of TGEV M protein (Escors *et al.* 2001). However, the specific amino acids on M protein responsible for the interactions of M-S and M-E are still enigmatic.

Different mutant constructs were made and transformed into the yeast cells with actin, showing that A159 and K160 were essential for the interaction between IBV M protein and actin. Introduction of the A159-K160 deletion and the A159-P/K160-E mutation into the full-length IBV clone showed that no virus could be recovered. Mutations of amino acids A159 and K160, which are essential for the interaction of M protein with actin, are detrimental to the recovery of IBV from an infectious IBV clone due to a defect in the late stages of the IBV replication cycle. Although the mutations of amino acids A159 and K160 could also interact with other structural proteins, as demonstrated by VLPs formation, we cannot exclude the possibility that this region is essential for maintaining the integrity of the M protein and is involved in the interactions with other viral components. Nevertheless, it lends support to the conclusion that interaction of the IBV M protein with actin is essential for the completion of the IBV infection cycle.

5.4. Effects of disruption of actin filaments by cytochalasin D on the IBV replication

The actin-binding proteins are grouped into 60 distinct classes based on their primary structures (Pacholsky *et al.*, 2004). The actin-binding sites range from 10-30 residues, and show no obvious homology among different classes (Vandekerckhove and Vancompernolle, 1992). For example, Aldolase, a glycolytic enzyme, binds actin filaments to concentrate enzyme and substrate

(Grazi and Guidoboni, 1989). The sequence 32-ADESTGSIAKRLQSIGTENTE-52 of aldolase has been identified as the actin-binding motif (O'Reilly and Clark, 1993). Furthermore, Carcinoembryonic Cell Adhesion Molecule 1 (CEACAM1) was found to bind F-actin. The actin binding site is FLHFGKTGSSGPLQ, showing no similarity to other actin-binding regions (Schumann *et al.*, 2001).

It is interesting that the IBV replication cycle was disturbed in cells treated with cytochalasin D. Cytochalsin D is a useful tool for testing the participation of actin in various cell functions, because it disturbs the equilibrium between monomeric and polymeric actin by capping the barbed end of the actin filament and lowering the amount of ATP-bound actin monomer (Flanagan, 1980). When actin was disrupted, much fewer IBV virions were released from the cells into the culture medium, demonstrating that actin plays an important role in the IBV replication cycle. Two possible mechanisms were considered. First, actin may be involved in the formation of the M lattice that may promote and stabilize its curving, resulting in the enhancement of some late processes, such as virion budding and release. Second, the MHV M protein was shown to be recycled from the Golgi complex back to early compartments, such as the ER and IC (de Haan *et al*., 2000). Therefore, interaction of actin with M protein may help the retrograde transport of M protein from Golgi apparatus to certain early compartments, and provide more M protein for virion assembly and budding.

More confirmatory evidence was derived from the study using cytochalasin D. Similar amounts of viral proteins were detected in the total cell lysates, but were not detected in supernatants when cytochalasin D was added early in the viral replication cycle suggesting that actin filaments are essential for some early events, such as virion assembly and budding, during the assembly and maturation processes of IBV. As IBV proteins can be efficiently detected in the supernatants when cytochalasin D was added at 12 and 16 hours post-infection, respectively, it suggests that actin filaments are unlikely to be involved in the release of the IBV particles. Furthermore, in the VLPs formation assay, proteins of both A159-P/K160-E mutation and A159-K160 deletion constructs could interact with other structural proteins, and the VLPs could be released successfully out of the transfected cells. This result confirms that the interaction of actin and M protein is not responsible for virion release, but may be involved in virion budding.

Based on above statements, the results in this study demonstrate that the interaction of the IBV M protein with β-actin may be essential for virion assembly and budding. IBV cannot complete its life cycle without the help of actin. These findings would be helpful for developing the vaccines to inhibit the expanding of IBV in poultry industry.

5.5. Mutational analysis of the conserved P1 residue (Q) of nine cleavage sites of 3CLpro in 1a and 1ab polyproteins

The recognition between the 3CLpro and its substrates involves many positions in the substrate, at least including residues from P4 to P2'. The deletion of residue P4 or P2' in the substrate clearly has different effects on the cleavage efficiency (Shan and Xu, 2005). The positions of amino acids in substrates named from the N- to C-terminal are as follows: -P4-P3-P2-P1↓-P1'-P2'-P3'-P4' (Schechter and Berger, 1967). The P1 position of the substrates is exclusively occupied by the Q residue (Schneider and Stephens, 1990), and small, aliphatic residues (S, A, N, G and C) are found at the P1' position (Kräusslich and Wimmer, 1988; Dougherty and Semler, 1993; Bolm *et al.*, 1996).

When the S residue in position P1' is replaced by Y, I, F, W and K residues respectively, all these mutants show a cleaved band except the I mutant in the 3CL protease autocleavage assay. This implies that this position can accommodate bulky amino acids (Ng and Liu, 2000; Shan and Xu, 2005). For SARS-CoV 3SLpro, the P2 position is limited to substitution by the F residue, while the P1' position is intolerant to acidic residue substitution because of the electrostatic repulsion (Chu *et al.*, 2006). Some reports showed that substitution of the Q residue at the predicted Q-S (G) cleavage site with an E residue totally abolishes cleavage at this dipeptide bond, such as, Q(7)E, Q(3)E, Q(9)M, Q(11)E, and Q(10)E (Liu and Brown, 1995; Liu *et al.*, 1998; Ng and Liu, 2000).

The Q(1) and Q(2) residues, auto-cleavage sites of IBV 3CLpro, can tolerate both N and E substitutions, showing that 3CLpro is guaranteed to be produced even though there are different mutations present in the P1 position. It is a survival strategy used by the virus to make sure that the virus can replicate in cells successfully.

In this study, both N and E residues were introduced to substitute the Q residue at the P1 position. In most cases, the Q residue could only be functionally replaced by an N residue, but not by an E residue. These two kinds of mutants show that IBV 3CLpro favorably tolerates N substitution more than E substitution at the P1 position. It also demonstrates that the Q residue at the P1 position can be substituted by some other residues by the 3CLpro cleavage assay.

Immunofluorescence and biochemical studies demonstrated that some cleavage products are involved in viral RNA replication via their membrane association with the viral RNA replication-transcription machinery (Sims *et al.*, 2000; van der Meer *et al.*, 1999). The cleavage products of IBV 3CLpro were previously identified by their apparent molecular masses in SDS-PAGE, and the cleavage sites were mapped by site-directed mutagenesis (Liu *et al.*, 1994, 1997, 1998; Liu and Brown, 1995; Ng and Liu, 1998), which leads to a rapid verification of the cleavage sites of SARS-CoV replicases (Snijder *et al.*, 2003; Thiel *et al.*, 2003a; Harcourt *et al.*, 2004; Prentice *et al.*, 2004b).

The IBV 3CLpro is auto cleaved by itself at two Q-S dipeptide bonds:

Q(1) and Q(2). Furthermore, five cleavage sites occur in the ORF1a: two of them are Q-S dipeptide bonds (Q(4)and Q(6)), one is Q-A dipeptide bond (Q(3)), another one is Q-N dipeptide bond (Q(5)), and the last one is Q-Q dipeptide bond (Q(7)). The proteins released from the 1a ORF by 3CLpro cleavage are nsp6-10, whose molecular masses in order are 33, 34, 9, 24, 10 and 15 kDa.

There are four cleavage sites of 3CLpro in the 1b ORF product that to release nsp11-15, all of which are Q-S dipeptide bonds, i.e. Q(8), Q(9), Q(10), and Q(11). Their molecular masses of them are 100, 68, 58 39 and 35 kDa respectively. In all, the Q residue at the P1 position cleaved by IBV 3CLpro is much more conserved than the amino acids at other positions of cleavage sites.

At the very bottom of the 3CLpro S1subsite, the imidazole of H162 is suitably positioned to interact with the P1 side chain. The required neutral state of H162 over a broad pH range appears to be maintained by two important interactions: (1) stacking onto the phenyl ring of F139; (2) accepting a hydrogen bond from the hydroxyl group of the buried Y160 (Ziebuhr *et al.*, 1997; Hegyi *et al.*, 2002).

The reason why the P1 position of cleavage sites of IBV 3CLpro favors the N residue rather than the E residue is because the E residue is negatively charged, while the Q residue is neutral. The negative charge would change the neutral environment for the interaction between the substrate and the 3CLpro. Therefore, the substrate may not match exactly with the catalytic domain of 3CLpro.

5.6. Analysis of the recovered viruses from cells transfected with mutant full-length transcripts

Several mutations of cleavage sites were introduced into the full-length IBV clone. Among them, some mutant viruses could be recovered. For the N residue substitution, the mutant viruses could be recovered if the P1 position mutations could be cleaved by 3CLpro. The cleavage efficiency of mutations was about 2-4 times lower than that of wild-type. Although the cleavage was less efficient, the mutant viruses could still be recovered. However, for the Q3672A and Q3672R substitutions, no viruses could be recovered because of their much lower cleavage efficiency, i.e. about 1/10 of wild-type. This showed that the cleavage at these positions is essential for the recovery of viruses. The possibility of the recovery of mutant viruses was greater for the relatively high cleavage efficiency of mutations at the P1 position. It was further confirmed that some mutations, which could be cleaved by 3CLpro *in vitro*, still could be tolerated by the virus *in vivo*. These results demonstrate that the Q residue at the P1 position, in some cases, is not necessary for virus replication.

Plaque assay and growth curve kinetics were performed with the wild-type and two mutant viruses (Q3672N and Q3672E) to compare their growth characteristics. It turned out that lower cleavage efficiency resulted in delayed maturation of mutant viruses, because the two mutant viruses produced smaller plaques than the wild-type virus, and showed slower growth activity than the wild-type virus.

5.7. Future directions

5.7.1. Confirmation of the interaction of the A159-K160 mutant M protein with other structural proteins

A159 and K160 residues are located in the amphipathic region of the M protein. This region is responsible for the interactions of M protein with other structural proteins. In order to exclude the possibility that A159 and K160 are necessary for the interactions, coimmunoprecipitaion could be performed, although VLPs formation assay had been employed. The M protein and mutants could be co-expressed with S, M, N or E protein in mammalian cells, and co-immunoprecipitated to check if the mutants of M protein will also interact with S, N and E proteins. If the S, N and E proteins can be co-immunoprecipitated by M protein mutants, it will demonstrate that the A159 and K160 residues are not involved in the interaction of M protein with other structural proteins. On the contrary, If the structural proteins are not co-immunoprecipitated by M protein mutants, it will show that the A159 and K160 residues of M protein are also necessary for the interaction of M protein with other structural proteins. Moreover, the reason that no viruses were recovered from the mutant IBV clone transcripts may be attributed to the loss of the interaction domain.

5.7.2. Direct visualization of the interaction of M and actin in cells

In high-resolution immunocytochemistry, colloidal gold-conjugated

antibodies are used to detect and localize antigens in cellular compartments in ultrathin sections by transmission electron microscopy (TEM). Antigen detection depends on the specificity of the primary antibody and localization, and on the ability to resolve different compartments with the gold marker. Since colloidal gold particles are electron-dense, punctate and available in different sizes, this technique permits multiple labeling, colocalization and quantification (Griffiths, 1993; Lucocg, 1992; Lucocg, 1994).

In order to directly observe the interaction of actin with M protein, immunogold label could be employed to the purified IBV virions. The relevant specific antibodies can be conjugated with special colloidal gold. According to the different sizes of gold particles, the imaging of colocalization of actin and M proteins can be observed by TEM.

5.7.3. Detection of subgenomic mRNA of each mutant transcript

As shown in this study, no virus was recovered from some virus mutants at the P1 position. In order to check if RNA replication and transcription occurs in cells electroporated with these mutant transcripts, subgenomic mRNA was detected by RT-PCR. Except for the wild-type virus, there was no subgenomic mRNA detectable in the mutants, because the amount of the subgenomic mRNA was too low. Therefore, more sensitive methods, such as Southern blot of RT-PCR products and radioactive isotope labeling of probes or real-time RT-PCR could be employed.

5.7.4. Detection of cleavage bands of 3CLpro in mammalian cells

In this study, some virus mutants could be cleaved by 3CLpro *in vitro* when the Q residue at the P1 position was mutated to another residue. There was no direct evidence from the identification of cleavage bands of 3CLpro in virus-infected or plasmid DNA-transfected cells. Since certain antibodies against nonstructural proteins are not specific enough, the radioimmunoprecipitation assay can be performed. The mutant virus-infected cells or plasmids DNA-transfected cells can be labeled with [S^{35}] methionine, and lysed for immunoprecipitation with specific antibody to detect the cleavage process of different point mutants.

REFERENCES

Almeida, J. D., and Tyrrell, D. A., 1967. The morphology of three previously uncharacterized human respiratory viruses that grow in organ culture. J. Gen. Virol., 1, 175–178.

Almeida, J. D., Berry, D. M., Cunningham, C. H., Hamre, D., Hofstad, M. S., Mallucci, L., McIntosh, K., and Tyrrell, D. A. J., 1968. Coronaviruses. Nature 220, 650.

Anand, K., Palm, G.J., Mesters, J.R., Siddell, S.G., Ziebuhr, J., Hilgenfeld, R., 2002. Structure of coronavirus main proteinase reveals combination of a chymotrypsin fold with an extra alpha-helical domain. EMBO, 21, 3213–3224.

Anand, K., Ziebuhr, J., Wadhwani, P., Mesters, J. R., Hilgenfeld, R., 2003. Coronavirus main proteinase ($3CL^{pro}$) structure: Basis for design of anti-SARS drugs. Science 300, 1763–1767.

An, S., Maeda, A., Makino, S., 1998. Coronavirus Transcription Early in Infection. J. Virol. 72, 8517-8524.

An S, Chen CJ, Yu X, Leibowitz JL, Makino S., 1999. Induction of apoptosis in murine coronavirus-infected cultured cells and demonstration of E protein as an apoptosis inducer. J Virol., 73,7853-9.

Anderson, R., Wong, F., 1993. Membrane and phospholipid binding by murine coronaviral nucleocapsid N protein. Virology 194, 224-232.

Arthur, L.o., J. W. Bess, Jr., R. C. Sowder II, R. E. Benveniste, D. L. Mann, J.-C. Chermann, L. E. Henderson. 1992. Cellular proteins bound to immunodeficiency viruses: implications for pathogenesis and vaccines. Science 258, 1935-1938.

Bae, I., Jackwood, D. J., Benfield, D. A., 1991. Differentiation of transmissible gastroenteritis virus from porcine respiratory coronavirus and other antigenically related coronaviruses by using cDNA probes specific for the 5' region of the S glycoprotein gene. J. Clin. Microbiol. 29, 215-218.

Ballesteros, M. L., Sanchez, C. M., Enjuanes, L., 1997. Two amino acid changes at the N-terminus of transmissible gastroenteritis coronavirus spike protein result in the loss of enteric tropsim. Virology 227, 378-388.

Banerjee, S., An, S., Zhou, A., Silverman, R. H., Makino, S., 2000. RNase

L-Independent Specific 28S rRNA Cleavage in Murine Coronavirus-Infected Cells. J. Virol., 74,8793-8802.

Banerjee S, Narayanan K, Mizutani T, Makino S., 2002. Murine coronavirus replication-induced p38 mitogen-activated protein kinase activation promotes interleukin-6 production and virus replication in cultured cells. J Virol., 76, 5937-48.

Baric, R. S., Fu, K., Schaad, M. C., Stohlman, S. A., 1990. Establishing a genetic recombination map for murine coronavirus strain A59 complementation groups. Virology 177, 646-656.

Baric, R. S., and Sims, A. C., 2005. Development of mouse hepatitis virus and SARS-CoV infectious cDNA constructs. Curr. Top. Microbiol. Immunol. 287, 229–252.

Baric, R. S., and Yount, B., 2000. Subgenomic negative-strand RNA function during mouse hepatitis virus infection. J. Virol. 74, 4039–4046.

Barrette-Ng, I.H., Ng, K.K.S., Mark, B.L., van Aken, D., Cherney, M.M., Garen, C., Kolodenko, Y., Gorbalenya, A.E., Snijder, E.J., James, M.N.G., 2002. Structure of arterivirus nsp4—the smallest chymotrypsin-like proteinase with an alpha/beta C-terminal extension and alternate conformations of the oxyanion hole. J. Biol. Chem. 277, 39960–39966.

Baudoux, P., CARRAT, C., Besnardeau, L., Charley, B., Laude, H., 1998. Coronavirus pseudoparticles formed with recombinant M and E proteins induce Alpha synthesis by leukocytes. J. Virol. 72, 8636-8643.

Benbacer, L., Kut, E., Besnardeau, L., Laude, H., Delmas, b., 1997. Interspecies aminopeptidase-N chimeras reveal species-specific receptor recognition by canine coronavirus, feline infectious peritonitis virus, and transmissible gastroenteritis virus. J. Virol., 71, 734–737.

Bhardwaj, K., Guarino, L., and Kao, C. C., 2004. The severe acute respiratory syndrome coronavirus Nsp15 protein is an endoribonuclease that prefers manganese as a cofactor. J. Virol. 78, 12218–12224.

Bi, W., Pinon, J. D., Hughes, S., Bonilla, P. J., Holmes, K. V., Weiss, S. R., and Leibowitz, J. L., 1999. Localization of mouse hepatitis virus open reading frame 1A derived proteins. J. Neurovirol. 4, 594–605.

Bijlenga, G., Cook, J. K. A., Gelb, J. Jr. and de wit, J. J., 2004. Development and use of the H strain of avian infectious bronchitis virus from the

Netherlands as a vaccine: a review. Avian Pathology 33(6), 550-557.

Blom, N., Hansen, J., Blaas, D. & Brunak, S., 1996. Cleavage site analysis in picornaviral polyproteins: discovering cellular targets by neural networks. Protein Sci. 5, 2203-2216.

Bohn, W., Rutter, G., Hohenberg, H., Mannweiler, K., Nobis, P., 1986. Involvement of actin filaments in budding of measles virus: studies on cytoskeletons of infected cells. Virology, 149, 91-106.

Bonilla, P. J., Hughes, S. A., and Weiss, S. R., 1997. Characterization of a second cleavage site and demonstration of activity in trans by the papain-like proteinase of the murine coronavirus mouse hepatitis virus strain A59. J. Virol. 71, 900–909.

Bos, E. C.W., Heijnen, L., Luytjes,W., and Spaan,W. J. M., 1995. Mutational analysis of the murine coronavirus spike protein: Effect on cell-to-cell fusion. Virology 214, 453–463.

Bos, E. C. W., van der Meulen, H., Koerten, H. K., Spaan, W. J. M., 1996. The production of recombinant infectious DI-particles of a murine coronavirus in the absence of helper virus. Virology 218, 52-60.

Bosch, B. J., de Haan, C. A. M., Smits, S. L., and Rottier, P. J. M., 2005. Spike protein assembly into the coronavirion: Exploring the limits of its sequence requirements. Virology 334, 306–318.

Bost, A. G., Carnahan, R. H., Lu, X. T., and Denison, M. R., 2000. Four proteins processed from the replicase gene polyprotein of mouse hepatitis virus colocalize in the cell periphery and adjacent to sites of virion assembly. J. Virol. 74, 3379–3387.

Boulanfer, D., Smith, T., Skinner, M. A.,2000. Morphogenesis and release of fowlpox virus. J. Gen. Virol. 81, 675-687.

Boursnell M E G, Brown T D K, Foulds I J, 1987. Completion of the sequence of the genome of the coronavirus avian infectious bronchitis virus. J Gen Virol, 68(1),57-77.

Breslin, J. J., Smith, L. G., Fuller F.J., Guy, J.S., 1999. Sequence analysis of the matrx/nucleocapsid gene region of turkey coronavirus. Intervirology 42, 22–29.

Brierley, I., Digard, P., and Inglis, S. C., 1989. Characterization of an efficient

coronavirus ribosomal frameshifting signal: Requirement for an RNA pseudoknot. Cell 57, 537–547.

Brockway, S. M., Clay, C. T., Lu, X. T., and Denison, M. R., 2003. Characterization of the expression, intracellular localization, and replication complex association of the putative mouse hepatitis virus RNA-dependent RNA polymerase. J. Virol. 77, 10515–10527.

Bukrinskaya, A., Brichacek, B., Mann, A., Stevenson, M., 1998. Establishment of a functional human immunodeficiency virus type 1 (HIV-1) reverse transcription complex involves the cytoskeleton. J Exp. Med. 188, 2113-2125.

Callison, S. A., Hilt, D. A., Jackwood, M. W., 2005. Rapid differentiation of avian infectious bronchitis virus isolates by sample to residual ratio quantitation using real-time reverse transcriptase-polymerase chain reaction. J. Virol. Methods 124, 183-190.

Carlier M.-F., 1991. Actin: Protein structure and filament dynamics. J. Biol. Chem. 266: 1-4.

Casais, R., Dove, B., Cavanagh, D. & Britton, P., 2003. Recombinant avian infectious bronchitis virus expressing a heterologous spike gene demonstrates that the spike protein is a determinant of cell tropism. J Virol 77, 9084–9089.

Casais, R., Davies, M., Cavanagh, D., and Britton, P., 2005. Gene 5 of the avian coronavirus infectious bronchitis virus is not essential for replication. J. Virol. 79, 8065–8078.

Caul, E. O., Egglestone, S. I., 1979. Coronavirus-like particles present in simian feces. Vet. Rec., 104, 167-169.

Cavnagh, D., 1995. The coronavirus surface glycoprotein. In “the coronaviridae”, S. G. Siddell, ed., pp73-113. Plenum, New York.

Cavanagh,D., David, P. J., Pappin, D. J. C., 1986. Coronavirus IBV glycopolypeptides: locational studies using proteases and saponin, a membrane permeabilizer. Virus Res. 4, 145-156.

Cavanagh, D., and Davis, P. J., 1988. Evolution of avian coronavirus IBV: Sequence of the matrix glycoprotein gene and intergenic region of several serotypes. J. Gen. Virol. 69, 621–629.

Cavanagh, D., Davis, P. J., Pappin, D. J., Binns, M. M., Boursnell, M. E., and

Brown, T. D., 1986. Coronavirus IBV: Partial amino terminal sequencing of spike polypeptide S2 identifies the sequence Arg-Arg-Phe-Arg-Arg at the cleavage site of the spike precursor propolypeptide of IBV strains Beaudette and M41. Virus Res. 4, 133–143.

Cavanagh, D., 1992. Recent advances in avian virology. Br. Vet. J. 48, 199-222.

Chang, K. W., Sheng, Y. W., and Gombold, J. L., 2000. Coronavirus-induced membrane fusion requires the cysteine-rich domain in the spike protein. Virology 269, 212–224.

Charley, B., and Laude, H., 1988. Induction of alpha interferon by transmissible gastroenteritis coronavirus: Role of transmembrane glycoprotein E1. J. Virol. 62, 8–11.

Charlton, C. A., Volkman, L. E., 1993. Penetration of autographa californica nuclear polyhedrosis virus nucleocapsids into IPLB Sf21 cells induces actin cable formation. Virology 197, 245-254.

Chen, C.-J., and Makino, S., 2004. Murine coronavirus replication induces cell cycle arrest in G0/G1 phase. J. Virol. 78, 5658–5669.

Chen, C.-J., Sugiyama, K., Kubo, H., Huang, C., and Makino, S., 2004. Murine coronavirus nonstructural protein p28 arrests cell cycle in G0/G1 phase. J. Virol. 78, 10410–10419.

Chen, H., Gill, A., Dove, B. K., Emmett, S. R., Kemp, C. F., Ritchie, M. A., Dee, M., and Hiscox, J. A., 2005. Mass spectroscopic characterization of the coronavirus infectious bronchitis virus nucleoprotein and elucidation of the role of phosphorylation in RNA binding by using surface plasmon resonance. J. Virol. 79, 1164–1179.

Chow, K.Y., Yeung, Y. S., Hon, C. C., Zeng, F., Law, K. M., Leung, F.C., 2005. Adenovirus-mediated expression of the C-terminal domain of SARS-CoV spike protein is sufficient to induce apoptosis in Vero E6 cells. FEBS Lett. 579, 6699-704.

Christine,W., Christel, S. W., Cavanagh, D., Neumann, U., Herrler, G., 2006. Sialic acid is a receptor determinant for infection of cells by avian Infectious bronchitis virus. J Gen Virol, 87 , 1209-1216.

Chu, J.J.H., Choo, B.G.H., Lee, J.W.M.,Ng, M.L., 2003. Actin filamnets participate in West Nile (sarafend) virus mutruation process. J. Med. Virol., 71, 463-472.

Chu, L.H. M., Choy, W.Y., Tsai, S. N., Rao, Z.H., Ngai, S. M., 2006. Rapid peptide-based screening on the substrate specificity of severe acute respiratory syndrome (SARS) coronavirus 3C-like protease by matrix-assisted laser desorption/ionization time-of-flight mass spectrometry. Protein Sci. 15, 699-709.

Cinatl J Jr, Hoever G, Morgenstern B, Preiser W, Vogel JU, Hofmann WK, Bauer G, Michaelis M, Rabenau HF, Doerr HW., 2004. Infection of cultured intestinal epithelial cells with severe acute respiratory syndrome coronavirus. Cell Mol Life Sci., 61, 2100-12.

Collins, A. R., Knobler, R. L., Powell, H., and Buchmeier, M. J., 1982. Monoclonal antibodies to murine hepatitis virus-4 (strain JHM) define the viral glycoprotein responsible for attachment and cell–cell fusion. Virology 119, 358–371.

Cologna, R., Spagnolo, J. F., and Hogue, B. G., 2000. Identification of nucleocapsid binding sites within coronavirus-defective genomes. Virology 277, 235–249.

Computational Biology and Informatics Laboratory at the University of Pennsylvania, http://www.cbil.upenn.edu/MTIR/gammaActin_E-toc.html.

Compton, S. R., Rogers, D. B., Holmes, K. V., Fertsch, D., Remenick, J., McGowan, J. J., 1987. In vitro replication of mouse hepatitis virus strain A59. J. Virol. 61, 1814-1820.

Corse, E., and Machamer, C. E., 2000. Infectious bronchitis virus E protein is targeted to the Golgi complex and directs release of virus-like particles. J. Virol. 74, 4319–4326.

Corse, E., and Machamer, C. E., 2003. The cytoplasmic tails of infectious bronchitis virus E and M proteins mediate their interaction. Virology 312, 25–34.

Cowley, J. A., Dimmock, C. M., Spann, K. M., and Walker, P. J., 2000. Gill-associated virus of Penaeus monodon prawns: An invertebrate virus with ORF1a and ORF1b genes related to arteri- and coronaviruses. J. Gen. Virol. 81, 1473–1484.

Crackower, M.A., Sarao, R., Oudit, G. Y., Yagil, C., Kozieradzki, I., Scanga, S. E., 2002. Angiotensin-converting enzyme 2 is an essential regulator of heart function. Nature 417, 822-828.

Cudmore, S., Reckmann, I., Way, M., 1997. Viral manipulations of the actin cytoskeleton. Trends Microbiol. 5, 142-148.

Damsky C.H., Sheffield, J.B., Tuszynski, G.P., Warren, L., 1977. Is there a role for actin in virus budding? J. Cell Biol. 75, 593-605.

de Groot, R. T., Kuyties, W., Horzinek, M. C., 1987. Evidene for a coiled-coil structure in the spike proteins of coronaviruses. J. Mol. Biol. 196, 963-966.

de Haan, C. A. M., Kuo, L., Masters, P. S., Vennema, H., and Rottier, P. J. M.,1998. Coronavirus particle assembly: Primary structure requirements of the membrane protein. J. Virol. 72, 6838–6850.

de Haan, C. A. M.,Rottier, P. J. M., 2005. Molecular interactions in the assembly of coronaviruses, Adv. Virus Res. 64, 165-230.

de Haan, C. A. M., Masters, P. S., Shen, X., Weiss, S., and Rottier, P. J. M., 2002. The group-specific murine coronavirus genes are not essential, but their deletion, by reverse genetics, is attenuating in the natural host. Virology 296, 177–189.

de Haan, C. A. M., Vennema, H., Rottier, O. J. M., 2000. Assembly of the coronavirus envelope: homotypic interactions between the M proteins. J. Virol. 74, 4967-4978.

de Haan, C. A. M., Smeets, M., Vernooij, F., Vennema, H., and Rottier, P. J. M., 1999. Mapping of the coronavirus membrane protein domains involved in interaction with the spike protein. J. Virol. 73, 7441–7452.

de Haan, C. A. M., de Wit, M., Kuo, L., Montalto-Morrison, C., Haagmans, B. L., Weiss, S. R., Masters, P. S., and Rottier, P. J. M., 2003. The glycosylation status of the murine hepatitis coronavirus M protein affects the interferogenic capacity of the virus in vitro and its ability to replicate in the liver but not the brain. Virology 312, 395–406.

Delmas, B., and Laude, H., 1990. Assembly of coronavirus spike protein into trimers and its role in epitope expression. J. Virol. 64, 5367–5375.

Delmas, B.; Gelfi, J.; L'Haridon, R.; Vogel, L. K.; Sjostrom, H.; Noren, O.; Laude, H., 1992. Aminopeptidase N is a major receptor for the enteropathogenic coronavirus TGEV. Nature 357, 417-420.

Dhar, A. K., Cowley, J. A., Hasson, K.W., andWalker, P. J., 2004. Genomic organization, biology, and diagnosis of Taura syndrome virus and

yellowhead virus of penaeid shrimp. Adv. Virus Res. 63, 353–421.

Dohner, K., Sodeik, B., 2005. The role of the cytoskeleton during viral infection. Curr. Top Microbio. Immunol. 285, 67-108.

Dos Remedios C G, Chhabra D, eic M., 2003. The actin binding proteins:regulation of cytoseletal microfilaments. Physiol Rev, 83,433-473.

Dougherty, W. G., Semler, B. L., 1993. Expression of virus-encoded proteinases: functional and structural similarities with cellular enzymes. Microbiological Reviews 57, 781-822.

Dubois-Dalcq, M. E., Doller, E. W., Haspel, M. V., Holmes, K. V., 1982. Cell tropism and expression of mouse hepatitis viruses (MHV) in mouse spinal cord cultres. Virology 119, 317-331.

Egloff, M. P., Ferron, F., Campanacci, V., Longhi, S., Rancurel, C., Dutartre, H., Snijder, E. J., Gorbalenya, A. E., Cambillau, C., and Canard, B., 2004. The severe acute respiratory syndrome-coronavirus replicative protein nsp9 is a single-stranded RNA-binding subunit unique in the RNAvirus world. Proc. Natl. Acad. Sci. USA 101, 3792–3796.

Ehrnst, A., K. G. Sundquist. 1975. Polar appearance and nonligand induced spreading of measles virus hemagglutinin at the surface of chronically infected cells. Cell 5, 351-359.

Ehrnst, A., K. G. Sundquist. 1976. Mechanisms of appearance of viral glycoproteins at cell surface membrane. Exp. Cell Biol. 44, 198-225.

Enjuanes, L., Almazan, F., Sola, I., Zuniga, S., 2006. Biochemical aspects of coronavirus replication and virus-host interaction. Annu. Rev. Microbiol. 60, 211-230.

Escors, D., Ortego, J., Laude, H., Enjuanes, L. 2001. The membrane M protein carboxy terminus binds to transmissible gastroenteritis coronavirus core and contributes to core stability. J. Virol, 75: 1312-1324.

Fan,H., Ooi,A., Tan,Y.W., Wang,S., Fang,S., Liu,D.X. and Lescar,J. 2005. Crystal structure of the N-terminal domain from the nucleocapsid protein of coronavirus infectious bronchitis virus and spliceosomal protein complexed with an RNA hairpin. Nature, 372, 432–438.

Fang, S.G., Chen, B., Tay, F. P. L., Liu, D. X. 2006. An arginine-to-proline mutation in a domain with undefined function within the RNA helicase

protein (NSP13) is lethal to the coronavirus infectious bronchitis virus in cultured cells. Virology, 00, 1-10.

Farsang A, Ros C, Renstrom L H, 2002. Molecular epizootiology ofinfectious bronchitis virus in Sweden indicating the involvement of a vaccine strain[J].Avian Pathol, 31, 229-236.

Fazakerley, J. K., Parker, S. E., Bloom, F., Buchmeier, M. J., 1992. The V5A13.1 envelope glycoprotein deletion mutant of mouse hepatitis virus type-4 is neuroattenuated by its reduced rate of spread in the central nervous system. Virology 187, 178-188.

Flanagan, M. D., Lin, S., 1980. Cytochalasins block actin filament elongation by binding to high affinity sites associated with F-actin. J. Biol. Chem. 255, 835-838.

Fleissner, E., E. Tress. 1973. Chromatographic and electrophoretic analysis of viral proteins from hamster and chicken cells transformed by rous sarcoma virus. J. Virol. 11: 250-262.

Fosmire, J. A., Hwang, K., and Makino, S., 1992. Identification and characterization of a coronavirus packaging signal. J. Virol. 66, 3522–3530.

Fuerst, T.R., Niles, E.G., Studier, F.W., and Moss, B. 1986. Eukaryotic transient-expression system based on recombinant vaccinia virus that synthesizes bacteriophage T7 RNA polymerase. *Proc*. Natl. Acad. Sci. USA. 83**,** 8122-8126.

Gallagher, T. M., Escarmis, C., and Buchmeier, M. J., 1991. Alteration of the pH dependence of coronavirus-induced cell fusion: Effect of mutations in the spike glycoprotein. J. Virol. 65, 1916–1928.

Gardet, A., Breton, M., Fontanges, P., Trugnan, G., Chwetzoff, S., 2006. Rotavirus spike protein VP4 binds to and remodels Actin bundles of the epithelial brush border into Actin bodies J. Viol. 80, 3947-3956.

Garoff, H., Hewson, R., Opstelten, D. J., 1998. Virus maturation by budding. Mirobiol. Mol. Biol. Rev. 62, 1171-1190.

Gingras, A.C., Raught, B., and Sonenberg, N. 1999. eIF4 initiation factors: Effectors of mRNA recruitment to ribosomes and regulators of translation. Annu. Rev. Biochem**.** 68: 913–963.

Gissen, P., Maher, E. R., 2007. Cargos and genes: insights into vesicular

transport from inherited human disease. J. Med. Genet. 44, 545-555.

Godeke, G.-J., de Haan, C. A. M., Rossen, J.W., Vennema, H., and Rottier, P. J.M., 2000. Assembly of spikes into coronavirus particles is mediated by the carboxy-terminal domain of the spike protein. J. Virol. 74, 1566–1571.

Godet, M., L'haridon, R., Vautherot, J.-F., and Laude, H., 1992. TGEV corona virus ORF4 encodes a membrane protein that is incorporated into virions. Virology, 188, 666–675.

Gombold, J. K., Hingley, S. T., Weiss, S. R., 1993. Fusion-defective mutants of mouse hepatitis virus A59 contain a mutation in the spike protein cleavage signal. J. Virol. 67, 4504-4512.

Gorbalenya, A. E., Donchenko, A. P., Blinov, V. M. & Koonin, E. V., 1989. Cysteine proteases of positive strand RNA viruses and chymotrypsin-like serine proteases. A distinct protein superfamily with a common structural fold. FEBS Letters 243, 103-114.

Gosert, R., Kanjanahaluethai, A., Egger, D., Bienz, K., and Baker, S. C., 2002. RNA replication of mouse hepatitis virus takes place at double-membrane vesicles. J. Virol.76, 3697–3708.

Gov, N. S., Gopinathan, A., 2006. Dynamics of membranes driven by actin polymerization. J. Biophy. 90, 454-469

Graham, R. L., Sims, A. C., Brockway, S. M., Baric, R. S., and Denison, M. R., 2005. The nsp2 replicase proteins of murine hepatitis virus and severe acute respiratory syndrome coronavirus are dispensable for viral replication. J. Virol. 79, 13399–13411.

Grazi, E. & Guidoboni, M. 1989. Opposite effects of alfa-actinin and of fructose 1,6 -bisphosphate aldolase on the microfilament network. The role of orthophosphate revisited. Biochem. Int. 19, 1345-1353.

Greene, W. C., Peterlin, B. M., 2002. Charting HIV's remarkable voyage through the cell: basic science as a passport to future therapy. Nat. Med. 8, 673-680.

Griffiths, G., Rottier, P. J. M., 1992. Cell biology of viruses that assemble along the biosynthetic pathway. Semin. Cell Biol. 3, 367-381.

Guy, J. S., Breslin, J. J., Breuhaus, B., Vivrette, S., and Smith, L. G., 2000. Characterization of a coronavirus isolated from a diarrheic foal. J. Clin.

Microbiol. 38, 4523–4526.

Haijema, B. J., Volders, H., and Rottier, P. J. M., 2003. Switching species tropism: An effective way to manipulate the feline coronavirus genome. J. Virol. 77, 4528–4538.

Haijema, B. J., Volders, H. & Rottier, P. J. M., 2004. Live, attenuated coronavirus vaccines through the directed deletion of group-specific genes provide protection against feline infectious peritonitis. J Virol 78, 3863–3871

Halliburton, W.D., 1887. On muscle plasma. J. Physiol. 8, 133-202.

Hansen, G. H., Delmas, B., Besnardeau, L., Vogel, L. K., Laude, H., Sjostrom, H., and Noren, O., 1998. The coronavirus transmissible gastroenteritis virus causes infection after receptor-mediated endocytosis and acid-dependent fusion with an intracellular compartment. J. Virol. 72, 527–534.

Harcourt, B. H., Jukneliene, D., Kanjanahaluethai, A., Bechill, J., Severson, K. M., Smith, C. M., Rota, P. A., and Baker, S. C., 2004. Identification of severe acute respiratory syndrome coronavirus replicase products and characterization of papainlike protease activity. J. Virol. 78, 13600–13612.

He, R., Leeson, A., Andonov, A. & 8 other authors, 2003. Activation of AP-1 signal transduction pathway by SARS coronavirus nucleocapsid protein. Biochem Biophys Res Commun 311, 870-876.

Hegyi, A., Friebe, A., Gorbalenya, A. E., Ziebuhr, J., 2002. Mutational analysis of the active center of coronavirus 3C-like proteases. J. Gen. Virol. 83, 581-593.

Hiscox, J. A, Wurm, T., Wilson, L., Britton, P., Cavanagh, D., Brooks, G., 2001. The Coronavirus Infectious Bronchitis Virus Nucleoprotein Localises to the Nucleolus. J. Virol. 506-512.

Hodge, T., Cope, M. J. T. V., 2000. A myosin family tree. J. Cell Sci. 113, 3353-3354.

Hodgson, T., Casais, R., Dove, B., Britton, P. & Cavanagh, D., 2004. Recombinant infectious bronchitis coronavirus Beaudette with the spike protein gene of the pathogenic M41 strain remains attenuated but induces protective immunity. J Virol 78, 13804–13811.

Hofmann, H., Hattermann, K., Marzi, A., Gramberg, T., Geier, M., Krumbiegel, M., Kuate, S., Uberla, K., Niedrig, M., and Pohlmann, S., 2004. S protein of

severe acute respiratory syndrome-associated coronavirus mediates entry into hepatoma cell lines and is targeted by neutralizing antibodies in infected patients. J. Virol.78, 6134–6142.

Hofmann, H., G. Simmons, A. J. Rennekamp, C. Chaipan, T. Gramberg, E. Heck, M., Geier, A. Wegele, A. Marzi, P. Bates, and S. Pohlmann. 2006. Highly conserved regions within the spike proteins of human coronaviruses 229E and NL63 determine recognition of their respective cellular receptors. J. Virol. 80, 8639-8652.

Holmes, K. V., Doller, E. W., Behnke, J. N., 1981. Analysis of the functions of coronavirus glycoproteins by differential inhibition of synthesis with tunicamycin. Adv Exp Med Biol 142, 133–142.

Holmes KC, Popp D, Gebhard W, Kabsch W., 1990. Atomic model of the actin filament. Nature, 347, 21-2.

Hofmann, H., Geier, M., Marzi, A., Krumbiegel, M., Peipp, M., Fey, G. H., Gramberg, T. & Pohlmann, S., 2004. Susceptibility to SARS coronavirus S protein-driven infection correlates with expression of angiotensin converting enzyme 2 and infection can be blocked by soluble receptor. Biochem Biophys Res Commun 319, 1216–1221.

Huang, C., Ito, N., Tseng, C.-T. K., Makino, S., 2006. Severe acute respiratory syndrome coronavirus 7a accessory protein is a viral structural protein. J. Virol. 80, 7287-7294.

Hunter, T., Garrels, J. I., 1977. Characterization of the mRNAs for α-, β-, and γ-actin. Cell, 12, 767-781.

Hurst, K. R., Kuo, L., Koetzner, C. A., Ye, R., Hsue, B., and Masters, P. S., 2005. A major determinant for membrane protein interaction localizes to the carboxy- terminal domain of the mouse coronavirus nucleocapsid protein. J. Virol. 79, 13285–13297.

Ito, N., Mossel, E. C., Narayanan, K., Popov, V. L., Huang, C., Inoue, T., Peters, C. J. & Makino, S., 2005. Severe acute respiratory syndrome coronavirus 3a protein is a viral structural protein. J Virol 79, 3182–3186.

Ivanov, K. A., and Ziebuhr, J., 2004. Human coronavirus 229E nonstructural protein 13: Characterization of duplex-unwinding, nucleoside triphosphatase, and RNA 50-triphosphatase activities. J. Virol. 78, 7833–7838.

Ivanov, K. A., Hertzig, T., Rozanov, M., Bayer, S., Thiel, V., Gorbalenya, A. E.,

and Ziebuhr, J., 2004. Major genetic marker of nidoviruses encodes a replicative endoribonuclease. Proc. Natl. Acad. Sci. USA 101, 12694–12699.

Ivanov, K. A., Thiel, V., Dobbe, J. C., van der Meer, Y., Snijder, E. J., and Ziebuhr, J., 2004. Multiple enzymatic activities associated with severe acute respiratory syndrome coronavirus helicase. J. Virol. 78, 5619–5632.

Iyengar, S., Hildreth, J. E., Schwartz, D. H., 1998. Actin-dependent receptor colocalizaiton required for human immunodeficiency virus entry into host cells. J. Virol. 72, 5251-5255.

Jacobs, L., Spaan, W. J. M., Horzinek, M. C., and van der Zeijst, B. A. M., 1981. Synthesis of subgenomic mRNAs of mouse hepatitis virus is initiated independently: Evidence from UV transcription mapping. J. Virol. 39, 401–406.

Jia, W., Karaca, K., Parrish, C. R., Naqi, S. A., 1995. A novel variant of avian infectious bronchitis virus resulting from recombination among three different strains. Arch. Virol. 140, 259-271.

Jonassen, C.M., Kofstad, T., Larsen, I-L., Lovland, A., Handeland, K., Follestad, A., Lillehaug, A., 2005. Molecular identification and characterization of novel coronaviruses infecting greylag geese (Anseranser), feral pigeons (Columba livia) and mallards (Anas platyrhynchos). Journal of General Virology, 86, 1597 -1607.

Kabsch, W., Mannherz, E.G., Suck, D., Pai, E.F., and Holmes, K.C., 1990. Atomic structure of the actin:DNase I complex. Nature, 347, 37-44.

Kanjanahaluethai, A., Jukneliene, D., and Baker, S. C., 2003. Identification of the murine coronavirus MP1 cleavage site recognized by papain-like proteinase 2. J. Virol. 77, 7376–7382.

Kazi, L., Lissenberg, A., Watson, R., de Groot, R. J., Weiss, S. R., 2005. Expression of Hemagglutinin Esterase Protein from Recombinant Mouse Hepatitis Virus Enhances Neurovirulence. J. Virol. 79: 15064-15073.

Keck, J. G., Matrushima, G. K., Makino, S., 1988. In vivo RNA-RNA recombination of coronavirus in mouse brain. J. Virol. 62, 1810-1813.

Kienzle, T. E., Abraham, S., Hogue, B. G., and Brian, D. A., 1990. Structure and orientation of expressed bovine coronavirus hemagglutinin-esterase protein. J. Virol. 64, 1834–1838.

Klumperman, J., Locker, J. K., Meijer, A., Horzinek, M. C., Geuze, H. J., Rottier, P. J., 1994. Coronavirus M proteins accumulate in Golgi complex beyond the site of virion budding. J. Virol. 68, 6523-6534.

Koetzner, C. A., Parker, M. M., Ricard, C. S., Sturman, L. S., and Masters, P. S., 1992. Repair and mutagenesis of the genome of a deletion mutant of the coronavirus mouse hepatitis virus by targeted RNA recombination. J. Virol. 66, 1841–1848.

Koolen M J, Borst M A, Horzinek M C, 1990. Immunogenic peptide comprising a mouse hepatitis virus A59 B-cell epitope and an influenza virus T-cell epitope protects against lethal infection. J Virol, 64 (12), 6270～6273.

Korn, E. D., 1982. Actin polymerization and its regulation by proteins from nonmuscle cells. Physiol. Rev. 62, 672-737.

Kottier, S. A., Cavanagh, D., Britton, P., 1995. Experimental evidence of recombination in coronavirus infectious bronchitis virus. Virology 213, 569-580.

Kuo, L., Godeke, G.-J., Raamsman, M. J. B., Masters, P. S., and Rottier, P. J. M., 2000. Retargeting of coronavirus by substitution of the spike glycoprotein ectodomain: Crossing the host cell species barrier. J. Virol. 74, 1393–1406.

Kuo, L., Masters, P. S., 2003. The Small Envelope Protein E Is Not Essential for Murine Coronavirus Replication. J. Virol. 77: 4597-4608.

Kräusslich, H. G., Wimmer, E., 1988. Viral proteinases. Annual Review of Biochemistry 57, 701-754.

Krijnse Locker, J., Griffiths, G., Horzinek, M. C., Rottier, P. J. M., 1992. O-glycosylation of the coronavirus M protein. Differential localization of sialyltransferases in N- and O-linked glycosylation. J. Biol. Chem. 267, 14094-14101.

Kyuwa, S., Cohen, M., Nelson, G., Tahara, S. M., Stohlman, S. A.,1994. Modulation of Cellular Macromolecular Synthesis by Coronavirus: Implication for Pathogenesis. J. .Virol.,68, 6815-6819.

Lachance, C., Arbour, N., Cashman, N. R., Talbot, P. J., 1998. Involvement of Aminopeptidase N (CD13) in Infection of Human Neural Cells by Human Coronavirus 229E. J Virol, 72, 6511-6519.

Lai, M. M. C., and Cavanagh, D., 1997. The molecular biology of coronaviruses. Adv.Virus Res. 48, 1–100.

Lai, M. M. C. & Holmes, K. V., 2001. Fields Virology, edited by D. M. Knipe & P. M. Howley, pp. 1163-1179. Philadelphia: Lippincott Williams & Wilkins.

Lai, M. M. C., Holmes, K. V. H. Coronaviridae: The Viruses and Their Replication**.** Field's Virology.

Lai, M. M. C., and Holmes, K. V., 2001. Coronaviridae: The viruses and their replication. In “Fields Virology” (D. M. Knipe and P. M. Howley, eds.), 4th edn. pp. 1163–1185. Lippincott, Williams & Wilkins, Philadelphia.

Lai, M. M. C., and Stohlman, S. A., 1981. Comparative analysis of RNA genomes of mouse hepatitis viruses. J. Virol. 38, 661–670.

Lamb, R. A., B. W. J. Mahy, P. W. Choppin. 1976, The synthesis of sendai virus polypeptides in infected cells. Virology 69,116-131.

Landecker, H. 2000. Immortality, In Vitro: A history of the HeLa cell line. Indiana. Uni. Press. 53-74.

Lanier, J.M., Volkman, L.E., 1998. Actin binding and nucleation by autographa california M nucleopolyhedrovirus. Virolog 243,167-177.

Lau, S. K. P., Woo, P. C. Y., Li, K. S. M., Huang, Y., Tsoi, H.-W., Wong, B. H. L., Wong, S. S. Y., Leung, S.-Y., Chan, K.-H., and Yuen, K.-Y., 2005. Severe acute respiratory syndrome coronavirus-like virus in Chinese horseshoe bats. Proc. Natl. Acad. Sci. USA 102, 14040–14045.

Laude, H., Rasschaert, D., Huet, J. C., 1987. Sequence and N-terminal processing of the transmembrane protein E1 of the coronavirus transmissible gastroenteritis virus. J. Gen. Virol. 68, 1687-1693.

Laude, H. 1993. Porcine respiratory coronavirus: molecular features and virus-host interactions. Vet. Res. 68, 1687-1693.

Laude, H., and Masters, P. S., 1995. In “The Coronaviridae” (S. G. Siddell, ed.), pp.141–163. Plenum, New York.

Laude, H., Gelfi, J., Lavenant, L., and Charley, B., 1992. Single amino acid changes in the viral glycoprotein M affect induction of alpha interferon by the coronavirus transmissible gastroenteritis virus. J. Virol. 66, 743–749.

Laude, H., Rasschaert D., Huet, J.-C., 1987. Sequence and N-terminal processing of the transmembrane protein El of the coronavirus transmissible gastroenteritis virus. Journal of General Virology 68, 1687-1693.

Lavi, E., Wang, Q., Weiss, S. R., Gonatas, N. K., 1996. Syncytia formation induced by coronavirus infection is associated with fragnentation and fearrangement of the Golgi apparatus. Virology 221, 325-334.

Leibowitz. J. L., DeVries, J. R., Haspel, M. V., 1982. Genetic analysis of murine hepatitis virus strain JHM. J. Virol. 42, 1080-1087.

Leung WK,To KF,Chan PK,et al., 2005. Enteric involvement of severe acute respiratory syndrome-associated coronavirus infection. Gastroenterology, 125,1011-1017.

Liao, Y., J. Lescar, J. P. Tam, and D. X. Liu. 2004. Expression of SARS-coronavirus envelope protein in *Escherichia coli* cells alters membrane permeability. Biochem. Biophys. Res. Commun. 325:374–380.

Li, W., Shi, Z., Yu, M., Ren, W., Smith, C., Epstein, J. H., Wang, H., Crameri, G., Hu, Z., Zhang, H., Zhang, J., McEachern, J. et al., 2005. Bats are natural reservoirs of SARSlike coronaviruses. Science 310, 676–679.

Li, W.; Moore, M. J.; Vasilieva, N.; Sui, J.; Wong, S. K.; Berne, M. A.; Somasundaran, M.; Sullivan, J. L.; Luzuriaga, K.; Greenough, T. C.; Choe, H.; Farzan, M., 2003. Angiotensin-converting enzyme 2 is a functional receptor for the SARS coronavirus. Nature 426: 450-454.

Li, F., Li, W., Farzan, M., Harrison, S. C., 2005. Structure of SARS Coronavirus Spike Receptor-Binding Domain Complexed with Receptor. Science, 309,1864-1868.

Li FQ, Xiao H, Tam JP, Liu DX., 2005. Sumoylation of the nucleocapsid protein of severe acute respiratory syndrome coronavirus. FEBS Lett. 579, 2387-2396.

Lim, K. P., and Liu, D. X., 1998. Characterization of the two overlapping papain-like proteinase domains encoded in gene 1 of the coronavirus infectious bronchitis virus and determination of the C-terminal cleavage site of an 87-kDa protein. Virology, 245, 303–312.

Lim, K. P., Liu, D.X., 2001. The Missing Link in Coronavirus Assembly J. Biol. Chem., 276, 17515-17523.

Lim K. P, Lisa Fong-Poh NG, D. X. Liu, 2000. Identification of a novel cleavage activity of the first papain-like proteinase domain encoded by ORF1a of the coronavirus avian IBV and characterization of the cleavage products. J. Virol, 74, 1674-1685.

Lisa Fong-Poh NG, Liu D. X., 2000. Further characterization of the coronavirus infectious bronchitis virus 3C-like proteinase and determination of a new cleavage site. Virology, 272, 27-39.

Lissenberg, A., Vrolijk, M. M., van Vliet, A. L. W., Langereis, M. A., de Groot-Mijnes, J. D. F., Rottier, P. J. M., de Groot, R. J, 2005. Luxury at a Cost? Recombinant Mouse Hepatitis Viruses Expressing the Accessory Hemagglutinin Esterase Protein Display Reduced Fitness In Vitro. J. Virol. 79: 15054-15063.

Liu C, Kokuho T, Onodera T, 2001. DNA Mediated Immunization with Encoding the Nucleoprotein Gene of Porcine Transmi-sible Gastroenteritis virus. Virus Res, 2001,80, 75-82.

Liu, D. X., and Inglis, S. C., 1991. Association of the infectious bronchitis virus 3c protein with the virion envelope. Virology 185, 911–917.

Liu, D. X., Shen, S., Xu, H. Y., and Wang, S. F., 1998. Proteolytic mapping of the coronavirus infectious bronchitis virus 1b polyprotein: Evidence for the presence of four cleavage sites of the 3C-like proteinase and identification of two novel cleavage products. Virology 246, 288–297.

Liu, D. X., Brown, T. D., 1995**.** Characterisation and mutational analysis of an ORF 1a-encoding proteinase domain responsible for proteolytic processing of the infectious bronchitis virus 1a/1b polyprotein. Virology 209, 420-427.

Liu, D. X., Brierley, I., Tibbles, K. W., Brown, T. D., 1994. A 100-kilodalton polypeptide encoded by open reading frame (ORF) 1b of the coronavirus infectious bronchitis virus is processed by ORF 1a products. J. Virol. 68, 5772-5780.

Liu, D. X., Tibbles, K. W., Cavanagh, D., Brown, T. D., Brierley, I., 1995. Identification, expression, and processing of an 87 kDa polypeptide encoded by ORF1a of the coronavirus infectious bronchitis virus. Virology 208, 48-57.

Liu, D. X., Xu, H. Y., Brown, T. D. K., 1997. Proteolytic processing of the coronavirus infectious bronchitis virus 1a polyprotein: identification of a 10-kilodalton polypeptide and determination of its cleavage sites. J Virol 71,

1814–1820.

Locker, J. K., Rose, J. K., Horzinek, M. C. & Rottier, P. J., 1992. Membrane assembly of the triple-spanning coronavirus M protein. Individual transmembrane domains show preferred orientation. J Biol Chem 267, 21911–21918.

Lu, W., Zheng, b. J., and 8 other authors, 2006. Severe acute respiratory syndrome-associated coronavirus 3a protein forms an ion channel and modulates virus release. 103(33), 12540–12545.

Lu, Y., and Denison, M. R, 1997. Determinants of mouse hepatitis virus 3C-like proteinase activity. Virology 230, 335–342.

Lu, Y., Lu, X., and Denison, M. R., 1995. Identification and characterization of a serinelike proteinase of the murine coronavirus MHV-A59. J. Virol. 69, 3554–3559.

Locker, J. K., Rose, J. K., Horzinek, M. C., Rottier, P. J. M., 1992. Membrane assembly of the triple-spanning coronavirus M protein. Individual transmembrane domains show preferred orientation. J. Biol. Chem. 267, 21911-21918.

Luo, Z., Weiss, S., 1998. Roles in cell-to-cell fusion of two conserved hydrophobic regions in the murine coronavirus spike protein. Virology 244, 483-494.

Luo, H. B.,H, Chen, J., Chen, K. X., Shen, X., Jiang, H.L., 2006. Carboxyl Terminus of Severe Acute Respiratory Syndrome Coronavirus Nucleocapsid Protein: Self-Association Analysis and Nucleic Acid Binding Characterization. Biochem. 45, 11827 -11835, 2006

Luo C, Luo H, Zheng S, Gui C, Yue L,Yu C, Sun T, He P, Chen J, Shen J, Luo X, Li Y, LiuH, Bai D, Shen J, Yang Y, Li F, Zuo J, Hilgenfeld R, PeiG, ChenK, ShenX, Jiang H. 2004. Nucleocapsid protein of SARS coronavirus tightly binds to human cyclophilin A. Biochem Biophys Res Commun 321:557–565.

Luo H, Chen Q, Chen J, Chen K, Shen X, Jiang H. 2005. The nucleocapsid protein of SARS coronavirus has a high binding affinity to the human cellular heterogeneous nuclear ribonucleoprotein A1. FEBS Lett 579:2623–2628.

Luytjes, W., Bredenbeek, P. J., Noten F. F. H., 1988. Sequence of mouse hepatitis virus A59 mRNA 2: indications for RNA-recombination between

coronavirus and influenza C virus. Virology 166, 415-422.

Luytjes, W. D., Sturman, L. S., Bredenbeek, P. J., Charite, J., Van der Zeijst, B. A. M., Horzinek, M. C. & Spaan, W. J. M., 1987. Primary structure of the glycoprotein E2 of coronavirus MHV-A59 and identification of the trypsin cleavage site.Virology, 161, 479-487.

Machesky, L. M., Insall, R. H., Volkman, L. E., 2001. WASP homology sequences in baculoviruses. Mol. Biol. Cell 11, 286-287.

Maciver, S. K., 2004. http://www.bms.ed.ac.uk/reaserach/others/smaciver/Encyclop/encycloABP.htm.

Madu, I. G., Chu, V. C., Lee, H, Regan, A. D., Bauman, B. E., Whittaker, G. R., 2007. Heparan sulfate is a selective attachment factor for the avian aoronavirus infectious bronchitis virus beaudette. Avian Diseases. 51, 45-51.

Maeda, J., J. F. Repass, A. Maeda, and S. Makino. 2001. Membrane topology of coronavirus E protein. Virology. 281:163–169.

Machamer, C. E., Mentone, S. A., Rose, J. K., Farquhar, M. G., 1990. The E1 blycoprotein of an avian coronavirus is targeted to the cis Golgi complex. Proc. Natl. Acad. Sci. U. S. A. 87, 6944-6948.

Machamer, C. E., Rose, J. K., 1987. A specific transmembrane domain of a coronavirus E1 glycoprotein is required for its retention in the Golgi region. J. Cell Biol. 105, 1205-1214.

Makino, S., Taguchi, F., Fujiwara, K., 1984. Defective interfering particles of mouse hepatitis virus. Virology 133, 9-17.

Makino, S., Shieh, C-K., Soe, L. H., 1988. Primary structure and translation of a defective-interfering RNA of murine coronavirus. Virology 166, 550-560.

Makino, S., Yokomori, K., Lai, M. M. C., 1990. Analysis of efficiently packaged defective-interfering RNAs of murine coronavirus: localization of a possible RNA-packaging signal. J. Virol. 64, 604-6053.

Masters, P. S., 2006. The molecular biology of coronavirus. Advances in Virus Research. 66, 193-292.

Masters, P. S., 1992. Localization of an RNA-binding domain in the nucleocapsid protein of the coronavirus mouse hepatitis virus. Arch. Virol. 125, 141–160.

Masters, P. S., Koetzner, C. A., Kerr, C. A., Heo, Y., 1994. Optimization of targeted RNA recombination and mapping of a novel nucleocapsid gene mutation in the coronavirus mouse hepatitis. J. Virol. 68, 328-337.

Masters, J. R. 2002. HeLa cells 50 years on: the good, the bad and the ugly. Nature Rev. Cancer. 2, 315-319.

McIntosh, K., 1974. Coronaviruses. A comparative review. Curr. Top. Microbiol. Imunol. 63, 85–129.

Molenkamp, R., and Spaan, W. J. M., 1997. Identification of a specific interaction between the coronavirus mouse hepatitis virus A59 nucleocapsid protein and packaging signal. Virology 239, 78–86.

Moyer, S. A., Baker, S. C., Horikami, S. M., 1990. Host cell proteins required for measles virus reproduction. J. Gen. Virol. 71, 775-783.

Murti, K.G., Chen, M., Goorha, R., 1985. Interaction of frog virus 3 with the cytomatrix. III. Role of microfilaments in virus release. Virology, 142, 317-325.

Nal, B., Chan, C., Kien, F., Siu, L., Tse, J., Chu, K., et al., 2005. Differential maturation and subcellular localization of severe acute respiratory syndrome coronavirus surface proteins S, M and E. J Gen Virol 86: 1423–1434.

Narayanan, K., Maeda, A., Maeda, J., Makino. S., 2000, Characterization of the coronavirus M protein and nucleocapsid interaction in infected cells. J. Virol 74, 8127-8134.

Nash, T. C., and Buchmeier, M. J., 1997. Entry of mouse hepatitis virus into cells by endosomal and nonendosomal pathways. Virology 233, 1–8.

Nedellec P., Dveksler G. S., Daniels E., Turbide C., Chow B., Basile A. A., Holmes K. V. and Beauchemin N., 1994. Bgp2, a new member of the carcinoembryonic antigen-related gene family, encodes an alternative receptor for mouse hepatitis viruses. J Virol, 68, 4525–4537.

Nelson, G. W., and Stohlman, S. A., 1993. Localization of the RNA-binding domain of mouse hepatitis virus nucleocapsid protein. J. Gen. Virol. 74, 1975–1979.

Nelson, G. W., Stohlman, S. A., and Tahara, S. M., 2000. High affinity interaction between nucleocapsid protein and leader/intergenic sequence of mouse hepatitis virus RNA. J. Gen. Virol. 81, 181–188.

Ng, L.F., Liu, D.X., 1998. Identification of a 24-kDa polypeptide processed from the coronavirus infectious bronchitis virus 1a polyprotein by the 3C-like proteinase and determination of its cleavage sites, Virology, 243, 388–395.

Ng, L.F., Liu, D.X., 2000. Further characterization of the coronavirus infectious bronchitis virus 3C-like proteinase and determination of a new cleavage site, Virology 272, 27–39.

Nguyen, V.-P., Hogue, B. G., 1997. Protein interactions during coronavirus assembly J. Virol. 71, 9278-9284.

Nomura, R., Kiyota, A., Suzaki, E., Kataoka, K., Ohe, Y., Miyamoto, K., Senda, T., and Fujimoto, T., 2004. Human coronavirus 229E binds to CD13 in rafts and enters the cell through caveolae. J. Virol. 78, 8701–8708.

Nomura, R., A. Kiyota, E. Suzaki, K. Kataoka, Y. Ohe, K. Miyamoto, T. Senda and T. Fujimoto, 2004. Human coronavirus 229E binds to CD 13 in rafts and enters the cell through caveolae, J. Virol., 78, 8701–8708.

Ogino, T., Iwama, M., Ohsawa, Y., Mizumoto, K., 2003. Interaction of cellular tubulin with Sendai virus M protein regulates transcription of viral genome. Biochem. Biophy. Res. Commun. 311, 283-293.

Ontiveros, E., Kuo, L., Masters, P. S., and Perlman, S., 2001. Inactivation of expression of gene 4 of mouse hepatitis virus strain JHM does not affect virulence in the murine CNS. Virology 289, 230–238.

Opstelten, D.-J. E., M. J. B. Raamsman, K. Wolfs, M. C. horzinek, P. J. M. Rottier. 1995. Envelope glycoprotein interactions in coronavirus assembly. J. Cell Biol. 131:339-349.

Opstelten, D. J. E., de Groote, P., Horzinek, M. C., Vennema, H., Rottier, P. J. M., 1995. Disulfide bonds in folding and transport of mouse hepatitis coronavirus glycoproteins. J. Virol. 67, 7394-7401.

O'Reilly, G. & Clarke, F. 1993. Identification of an actin binding region in aldolase. FEBS Letters. 1, 69-72.

Ortego, J., Sola, I., Almazan, F., Ceriani, J. E., Riquelme, C., Balasch, M., Plana, J., and Enjuanes, L., 2003. Transmissible gastroenteritis coronavirus gene 7 is not essential but influences in vivo virus replication and virulence. Virology 308, 13–22.

Orvell, C.1978. Structural polypeptides of mumps virus. J. Gen. Virol. 41:527-539.

Ott, D. E., L.V. Coren, B. P. Kane, L. K. Busch, D. G. Johnson, R. C. Sowder II, E. N. Chertova, L. O. Arthur, L. E. Henderson. 1996. Cytoskeletal proteins inside human immunodeficiency virus type 1 virions. J. Virol. 70, 7734-7743.

Owens, R., Gilbert, R., Davidson, A., Siddell, S., Poon, L. L. et al., 2004. The nsp9 replicase protein of SARS-coronavirus, structure and functional insights. Structure 12, 341–353.

Paavilaninen, V. O., Bertling, E., Falck, S., Lappalainen, P., 2004. Regulation of cytoskeletal dynamics by actin-monomer-binding proteins. Trends Cell Biol. 14, 386-394.

Pacholsky, D., Vakeel, P., Himmel. M., Löwe, T., Stradal, T., Rottner, K., Fűrst, D. O., van der Ven, P. F. M., 2004. Xin repeats define a novel actin-binding motif. J. Cell Sci.117, 5257-5268.

Pantaloni, D., Clainche, C. L., Carlier, M.-F., 2001. Mechanism of actin-based motility. Science, 292, 1502-1506.

Parker, M. M., and Masters, P. S., 1990. Sequence comparison of the N genes of five strains of the coronavirus mouse hepatitis virus suggests a three domain structure for the nucleocapsid protein. Virology 179, 463–468.

Pasternak, A. O., Spaan, W. J. M., Snijder, E. J., 2006. Nidovirus transcription: how to make sense...?. J. Gen. Virol. 87, 1403-1421.

Pederson, T., Aebi, U., 2002. Actin in nucleus: what form and what for? J. Struct. Biol. 140, 3-9.

Peng, D., Koetzner, C. A., Masters, P. S., 1995. Analysis of second-site revertants of a murine coronavirus nucleocapsid protein deletion mutant and construction of nucleocapsid protein mutants by targeted RNA recombination. J. Virol. 69, 3449-3457.

Perotti, M. E., Tan,X., Phillips, D.M., 1996. Directional budding of human immunodeficiency virus from monocytes. J. Virol., 70, 5916-5921.

Peti, W., Johnson, M. A., Herrmann, T., Neuman, B. W., Buchmeier, M. J., Nelson, M., Joseph, J., Page, R., Stevens, R. C., Kuhn, P., and Wuthrich, K., 2005. Structural genomics of the severe acute respiratory syndrome coronavirus: Nuclear magnetic resonance structure of the protein nsP7. J.

Virol. 79, 12905–12913.

Pewe, L., Zhou, H., Netland, J., Tangudu, C., Olivares, H., Shi, L., Look, D., Gallagher, T., and Perlman, S., 2005. A severe acute respiratory syndrome-associated coronavirus-specific protein enhances virulence of an attenuated murine coronavirus. J. Virol. 79, 11335–11342.

Pfleiderer, M., E. Routledge, G. Herrler, and S. G. Siddell. 1991. High-level expression of the murine coronavirus hemagglutinin-esterase. J. Gen. Virol. 72, 1309–1315.

Pinon, J. D., Mayreddy, R. R., Turner, J. D., Khan, F. S., Bonilla, P. J., and Weiss, S. R., 1997. Efficient autoproteolytic processing of the MHV-A59 3C-like proteinase from the flanking hydrophobic domains requires membranes. Virology 230, 309–322.

Pollard T. D., Earnshaw W. D., 2004. Cell Biology, First Edition, SAUNDERS.

Poon, L. L. M., Chu, D. K.W., Chan, K. H.,Wong, O. K., Ellis, T. M., Leung, Y. H. C., Lau, S. K. P., Woo, P. C. Y., Suen, K. Y., Yuen, K. Y., Guan, Y., and Peiris, J. S. M., 2005. Identification of a novel coronavirus in bats. J. Virol. 79, 2001–2009.

Pratelli A, Martella V, Decaro N, 2003. Genetic diversity of a canine coronavirus detected in pups with diarrhoea in Italy. J Virol Methods,110,9-17.

Prentice, E., Jerome, W. G., Yoshimori, T., Mizushima, N., and Denison, M. R. 2004. Coronavirus replication complex formation utilizes components of cellular autophagy. J. Biol. Chem. 279, 10136–10141.

Prentice, E., McAuliffe, J., Lu, X., Subbarao, K., and Denison, M. R., 2004. Identificationand characterization of severe acute respiratory syndrome coronavirus replicase proteins. J. Virol. 78, 9977–9986.

Putics, A., Filipowicz,W., Hall, J., Gorbalenya, A. E., and Ziebuhr, J., 2005. ADP-ribose-10-monophosphatase: A conserved coronavirus enzyme that is dispensable for viral replication in tissue culture. J. Virol. 79, 12721–12731.

Raamsman, M. J. B., Krijnse Locker, J., de Hooge, A., de Vries, A. A. F., Griffiths, G., Vennema, H., and Rottier, P. J. M., 2000. Characterization of the coronavirus mouse hepatitis virus strain A59 small membrane protein E. J. Virol. 74, 2333–2342.

Racaniello, V. R., and Baltimore, D., 1981. Cloned poliovirus cDNA is infectious in mammalian cells. Science 214, 916–919.

Rando, O. J., Zhao, K., Crabtree, G. R., 2000. Searching for a function for nuclear actin. Trends Cell Biol. 10, 92-97.

Ravkov, E.V., Nichol, S.T., Peters, C.J., Compans, R. W., 1998. Role of actin microfilamnets in Black creek canal virus morphogenesis. J. Virol., 72,2865-2870.

Riordan, J.F. 2003. Angiotensin I – converting enzyme and its relatives. Genome Biol., 4, 225 – 235.

Risco, C., Anton, I. M., Enjuanes, L., Carrascosa, J. L., 1996. The Transmissible Gastroenteritis Coronavirus Contains a Spherical Core Shell Consisting of M and N Proteins. J. Virol. 70, 4773 – 4777.

Risco, C., Anton, I. M., Sune, C., Pedregosa, A. M., Martin-Alonso, J. M., Parra, F., Carrascosa, J. L., Enjuanes, L., 1995. Membrane protein molecules of transmissible gastroenteritis coronavirus also expose the carboxy-terminal region on ht external surface of the viron. J. Virol. 69, 5269-5277.

Risco, C., Muntion, M., Enjuanes, L., Carrascosa, J. L., 1998. Two Types of Virus-Related Particles Are Found during Transmissible Gastroenteritis Virus Morphogenesis. J.Virol. 72, 4022-4031.

Robbins, S. G., Frana, M. F., McGowan, J. J., Boyle, J. F., and Holmes, K. V., 1986. RNAbinding proteins of coronavirus MHV: Detection of monomeric and multimeric N protein with an RNA overlay-protein blot assay. Virology 150, 402–410.

Rottier, P., Branderberg, D., Armstrong, J., van der Zeijst, B., Warren, G., 1984. Assembly in vitro of a spanning membrane protein of the endoplasmic reticulum: the E1 glycoprotein of coronavirus mouse hepatitis virus A59. Proc. Natl. Acad. Sci. U. S. A. 81, 1421-1425.

Rottier, P. J. M. 1995. The coronavirus membrane glycoprotein, p.115-139. In S. G. Siddell (ed.), The Coronaviridae. Plnum Press, New York, N.Y.

Salanueva, I. J., Carrascosa, J.L., Risco, C., 1999. Structural maturation of the transmissible gastroenteritis coronavirus.J. Virol. 73, 7952-7964.

Sawicki, S. G., Sawicki, D. L., 1990. Coronavirus transcription: subgenomic mouse hepatitis virus replicative intermediates function in RNA synthesis. J. Virol. 64, 1050-1056.

Sawicki, S. G., and D. L. Sawicki. 1986. Coronavirus minus-strand RNA synthesis and effect of cycloheximide on coronavirus RNA synthesis. J. Virol. 57:328-334.

Sawicki, S. G., D. L. Sawicki, D. Younker, Y. Meyer, V. Thiel, H. Stokes, and S. G. Siddell. 2005. Functional and genetic analysis of coronavirus replicase-transcriptase proteins. PLoS Pathogens 1:e39.

Schechter I, Berger A., 1967. On the size of the active site in proteases. I. Papain. Biochem Biophys Res Commun, 27, 157–162.

Schiller, J. J., Kanjanahaluethai, A., and Baker, S. C., 1998. Processing of the coronavirus MHV-JHM polymerase polyprotein: Identification of precursors and proteolytic products spanning 400 kilodaltons of ORF1a. Virology 242, 288–302.

Schneider, T. D., Stephens, R. M., 1990. Sequence logos: a new way to display consensus sequences. Nucleic Acids Res. 18, 6097-6100.

Schumann, D., Chen, C.-J., Kaplan, B. & Shively, J. E. 2001. Carcinoembryonic antigen cell adhesion molecule 1 directly associates with cytoskeleton proteins actin and tropomyosin. J.Biol.Chem. 276, 47421-47433.

Schwarz, B., Routledge, E., and Siddell, S. G., 1990. Murine coronavirus nonstructural protein ns2 is not essential for virus replication in transformed cells. J. Virol. 64, 4784–4791.

Sethna P. B, Brian D. A., 1997. Coronavirus Genomic and Subgenomic Minus-Strand RNAs Copartition in Membrane-Protected Replication Complexes. J.Virol. 71, 7744-7749.

Sethna, P. B., Hofmann, M. A., and Brian, D. A., 1991. Minus-strand copies of replicating coronavirus mRNAs contain antileaders. J. Virol. 65, 320–325.

Sethna, P. B., Hung, S. L., Brian, D. A., 1989. Coronavirus subgenomic minus-strand RNAs and the potential for mRNA replicons. Proc. Natl. Acad. Sci. USA 86, 5626-5630.

Seybert, A., Hegyi, A., Siddell, S. G., and Ziebuhr, J., 2000. The human coronavirus 229E superfamily 1 helicase has RNA and DNA duplex-unwinding activities with 50-to-30 polarity. RNA 6, 1056–1068.

Shan YF, Xu GJ., 2005. Study on substrate specificity at subsites for severe acute respiratory syndrome coronavirus 3CL protease. Acta Biochim Biophys Sin, 37, 807-813.

Siddell, S. G., 1995. The small membrane protein. In "The Coronaviridae", S. G. Siddell, ed. Pp1-10. Plenum, New York.

Simmons, G., Reeves, J. D., Rennekamp, A. J., Amberg, S. M., Piefer, A. J., and Bates, P., 2004. Characterization of severe acute respiratory syndrome-associated coronavirus (SARS-CoV) spike glycoprotein-mediated viral entry. Proc. Natl. Acad. Sci. USA 101, 4240–4245.

Snijder, E. J., and Meulenberg, J. J., 1998. The molecular biology of arteriviruses. J. Gen. Virol. 79, 961–979.

Snijder, E. J., Bredenbeek, P. J., Dobbe, J. C., Thiel, V., Ziebuhr, J., Poon, L. L. M., Guan, Y., Rozanov, M., Spaan, W. J. M., and Gorbalenya., A. E., 2003. Unique and conserved features of genome and proteome of SARS coronavirus, an early split-off from the coronavirus group 2 lineage. J. Mol. Biol. 331, 991–1004.

Song, H. C., Seo, M. Y., Stadler, K., Yoo, B. J., Choo, Q. L., Coates, S. R., Uematsu, Y., Harada, T., Greer, C. E., Polo, J. M., Pileri, P., Eickmann, M. et al., 2004. Synthesis and characterization of a native, oligomeric form of recombinant severe acute respiratory syndrome coronavirus spike glycoprotein. J. Virol. 78, 10328–10335.

Stallcup, K. C., C. S. Raine, and B. N. Fields, 1983. Cytochalasin B inhibits the maturation of measles virus. Virology 124:59-74.

Steinhauser, D. A., Holland , J. J., 1986. Direct method for quantitation of extreme polymerase error frequencies at selected single base sites in viral RNA. J. Virol. 57, 219-228.

Stern, D.F., Burgess, L., Sefton, B. M., 1982. Structural analysis of virion proteins of the avian coronavirus infectious bronchitis virus. J. Virol. 42:208-219.

Stern, D. F., Sefton, B. M., 1982. Synthesis of coronavirus mRNAs: kinetics of inactivation of infectious bronchitic virus RNA synthesis by UV light. J. Virol. 42, 755-759.

Steven J. W., and Kathryn R. A, 2005. Actin-binding proteins. J Cell Sci, 118, 651-654.

Stohlman, S. A., Fleming, J. O., Patton, C. D., and Lai, M. M. C., 1983. Synthesis and subcellular localization of the murine coronavirus nucleocapsid protein. Virology 130, 527–532.

Stohlman, S. A., Baric, R. S., Nelson, G. N., Soe, L. H., Welter, L. M., and Deans, R. J., 1988. Specific interaction between coronavirus leader RNA and nucleocapsid protein. J. Virol. 62, 4288–4295.

Straub, F.B. and Feuer, G.., 1950. Adenosinetriphosphate the functional group of actin. Biochim. Biophys. Acta. 4, 455-470.

Sturman, L. S., 1977. Characterization of a coronavirus: I. Structural proteins: Effect of preparative conditions on the migration of protein in polyacrylamide gels. Virology 77, 637–649.

Sturman, L. S., and Holmes, K. V., 1983. The molecular biology of coronaviruses. Adv. Virus Res. 28, 35–111.

Sturman, L.S., Holmes, K.V., Behnke, J., 1980. Isolation of coronavirus envelope glycoproteins and interaction with the viral nucleocapsid. J. Virol. 33:449-462.

Sturman, L. S., Ricard, C. S., and Holmes, K. V., 1990. Conformational change of the coronavirus peplomer glycoprotein at pH 8.0 and 37 degrees C correlates with virus aggregation and virus-induced cell fusion. J. Virol. 64, 3042–3050.

Surjit, M., Liu, B., Kumar, P., Chow, V. T. K. & Lal, S. K., 2004. The nucleocapsid protein of the SARS coronavirus is capable of self-association through a C-terminal 209 amino acid interaction domain. Biochem Biophys Res Commun 317, 1030–1036.

Surjit, M., Liu, B., Jameel, S., Chow, V. T. K., Lal, S. K., 2004. The SARS coronavirus nucleocapsid protein induces actin reorganization and apoptosis in COS-1 cells in the absence of growth factors. Biochem J. 383, 13–18.

Surjit, M., Liu, B., Chow, V. T. K., Lal, S. K., 2006. The Nucleocapsid Protein of Severe Acute Respiratory Syndrome-Coronavirus Inhibits the Activity of Cyclin-Cyclin-dependent Kinase Complex and Blocks S Phase Progression in Mammalian Cells. J. Biol. Chem. 281,10669-10681.

Sutton, G., Fry, E., Carter, L., Sainsbury, S., Walter, T., Nettleship, J., Berrow, N., Swift, A. M., Machamer, C. E., 1991. A Golgi retention signal in a

membrane-spannig domain of coronavirus E1 protein. J. Cell Biol. 115, 19-30.

Lavi, E., Wang , Q., Weiss, S. R., Gonatas, N. K., 1996. Syncytia Formation Induced by Coronavirus Infection Is Associated with Fragmentation and Rearrangement of the Golgi Apparatus. Virology, 221(2), 325-334.

Tan, Y. W., Fang, S.G., Fan, H., Lescar, J., Liu, D. X., 2006. Amino acid residues critical for RNA-binding in the N-terminal domain of the nucleocapsid protein are essential determinants for the infectivity of coronavirus in cultured cells. Nucleic Acids Research, 34, 4816-4825.

Tan YJ, Fielding BC, Goh PY, Shen S, Tan TH, Lim SG, Hong W., 2004. Overexpression of 7a, a protein specifically encoded by the severe acute respiratory syndrome coronavirus, induces apoptosis via a caspase-dependent pathway. J Virol., 78,14043-7.

Tang NL, Chan PK, Wong CK, To KF, Wu AK, Sung YM, Hui DS, Sung JJ, Lam CW., 2005. Early enhanced expression of interferon-inducible protein-10 (CXCL-10) and other chemokines predicts adverse outcome in severe acute respiratory syndrome. Clin Chem., 51,2333-40.

Tetsuya Mizutani, T., Fukushi, S., Saijo, M., Kurane, I., Morikawa, S., 2004. Importance of Akt signaling pathway for apoptosis in SARS-CoV-infected Vero E6 cells. Virology, 32, 169-174.

Thiel, V., and Siddell, S. G., 2005. Reverse genetics of coronaviruses using vaccinia virus vectors. Curr. Top. Microbiol. Immunol. 287, 199–227.

Thiel, V., Ivanov, K. A., Putics, A., Hertzig, T., Schelle, B., Bayer, S., Weissbrich, B., Snijder, E. J., Rabenau, H., Doerr, H. W., Gorbalenya, A. E., and Ziebuhr, J., 2003. Mechanisms and enzymes involved in SARS coronavirus genome expression. J. Gen. Virol. 84, 2305–2315.

Thiel, V., Rashtchian, A., Herold, J., Schuster, D. M., Guan, N. & Siddell, S. G., 1997. Effective amplification of 20-kb DNA by reverse transcription PCR. Anal Biochem 252, 62–70.

Tooze, J., Tooze, S. A., 1985. Infection of AtT20 murine pituitary tumour cells by mouse hepatitis virus strain A59: virus budding is restricted to the Golgi region. Eur. J. Cell Biol. 37, 203-212.

Tooze, J., Tooze, S. A., Warren, G., 1984. Replication of coronavirus MHV-A59 in sac-cells: determination of the first site of budding of progeny virions. Eur. J. Cell Biol. 33, 281-293.

Tresnan, D. B., Levis, R. & Holmes, K. V., 1996. Feline aminopeptidase Nserves as a receptor for feline, canine, porcine, and human coronaviruses in serogroup I. Journal of Virology 70, 8669-8674.

Tyrrell, D. L. J., E. Norrby. 1978. Structural polypeptides of measles virus. J. Gen. Virol. 39, 219-229.

Vandekerckhove, J., Vancompernolle, K., 1992. Structural relationships of actin-binding proteins. Curr. Opin. Cell Biol. 4, 36-42.

van der Hoek, L., Pyrc, K., Jebbink, M. F., Vermeulen-Oost, W., Berkhout, R. J., Wolthers, K. C., Wertheim-van Dillen, P. M., Kaandorp, J., Spaargaren, J., Berkhout, B., 2004. Identification of a new human coronavirus. Nat Med., 10(4):368-73.

van der Most, R. G., Bredenbeek, P. J., Spaan, W. J. M., 1991. A domain at the 3'-end of the polymerase gene is essential for encapsidation of coronavirus defective interfering RNAs. J. Virol. 65, 3219-3226.

van der Most, R. G., Luytjes, W., Rutjes, S., and Spaan, W. J. M., 1995. Translation but not the encoded sequence is essential for the efficient propogation of defective interfering RNAs of the coronavirus mouse hepatitis virus. J. Virol. 69, 3744–3751.

van Loo, N. D., Fortunati, E., Ehlert, E., Rabelink, M., Grosveld, F., Scholte, B. J., 2001. Baculovirus infection of nondividing mammalian cells: mechanisms of entry and nuclear transport of capsids. J. Virol. 75, 961-970.

van Valen., Leigh, M., and Maiorana, V. C. 1991. HeLa, a new microbial species. Evolutionary Theory. 10, 71-74.

Vennema, H., Poland, A., Foley, J., Pedersen, N. C., 1998. Feline infectious peritonitis viruses arise by mutation from endemic feline enteric coronaviruses. Virology 243, 150-157.

Vennema, H., Godeke, G.-J., Rossen, J. W. A., Voorhout, W. F. , Horzinek, M. C., Opstelten, D.-J. E., Rottier, P. J M., 1996. Nucleocapsid-independent assembly of coronavirus-like particles by coexpression of viral envelope protein genes. EMBO J. 15, 2020-2028.

von Grotthuss, M., Wyrwicz, L. S., and Rychlewski, L., 2003. mRNA cap-1 methyltransferase in the SARS genome. Cell 113, 701–702.

Wang, F.-I., Fleming, J. O., Lai, M. M. C., 1992. Sequence analysis of the spike protein gene of murine coronavirus variants: study of genetic sites affecting neuropathogenicity. Virology 186, 742-749.

Wang, L., Junker, D., Collison, E. W., 1993. Evidence of natural recombination within the S1 gene of the infectious bronchitis virus. Virology 192, 710-716.

Wege, H., Muller, A., and ter Meulen, V., 1978. Genomic RNA of the murine coronavirus JHM. J. Gen. Virol. 41, 217–227.

Wang X, M I Khan., 2000. Molecular Characterixation of an Infectious Bronchitis virus strain isolated from an outbreak in vaccinated layers[J].Avi Dis, 44,1000-1006.

Weiss, S. R. and Navas-Martin, S., 2005. Coronavirus Pathogenesis and the Emerging Pathogen Severe Acute Respiratory Syndrome Coronavirus. Microbiology and Molecular Biology Reviews, Vol. 69 (4), 635-664.

Weismiller, D. G., Sturman, L. S., Buchmeier, M. J., Fleming, J. O., and Holmes, K. V., 1990. Monoclonal antibodies to the peplomer glycoprotein of coronavirus mouse hepatitis virus identify two subunits and detect a conformational change in the subunit released under mild alkaline conditions. J. Virol. 64, 3051–3055.

Welch, M. D., Mullins, R. D., 2002. Cellular control of actin nucleation. Annu. Rev. Cell Dev. Biol. 18, 247-288.

Wen-Xin Zheng, Ling-Ling Chen, Hong-Yu Ou, Feng Gao, Chun-Ting Zhang, 2005. Coronavirus phylogeny based on a geometric approach. Molecular Phylogenetics and Evolution 36, 224-232.

WHO: http://www.who.int/csr/sars/ country/tale2003_09_23/en.

Wilk, T., Fowen, B.M., Fuller, S. D., 1999. Actin associates with the nucleocapsid domain of the human immunodeficiency virus Gag polyprotein. J. Virol. 73, 1931-1940.

Williams, A. K., Wang , L., Sneed, L. W., Collisson, E. W., 1992. Comparative analysis of the nucleocapsid genes of several strains of infectious bronchitis virus and other coronavirus. Virus Res. 25, 213-222.

Winder, S. J, Ayscough, K. R., 2005. Actin-binding proteins. J. Cell Sci. 118, 651-654.

Winter, C., Schwegmann-Webels, C., Cavanagh, D., Neumann, U., Herrler, G., 2006. Sialic acid is a recptor determinant for infetion of cells by avian infectious bronchitis virus. J. Gen. Virol. 87, 1209-1216.

Woo, P. C. Y., Lau, S. K. P., Chu, C.-M., Chan, K.-H., Tsoi, H.-W., Huang, Y., Wong, B. H. L., Poon, R.W. S., Cai, J. J., Luk,W.-K., Poon, L. L. M.,Wong, S. S. Y. et al., 2005. Characterization and complete genome sequence of a novel coronavirus, coronavirus HKU1, from patients with pneumonia. J. Virol. 79, 884–895.

Wurm T, Chen H, Hodgson T, Britton P, Brooks G, Hiscox JA., 2001. Localization to the Nucleolus is a Common Feature of Coronavirus Nucleoprotein, and the Protein May Disrupt Host Cell Division. J. Virol. 75, 9345-9356.

Xu, H. Y., Lim, K. P., Shen, S., and Liu, D. X., 2001. Further identification and characterization of novel intermediate and mature cleavage products released from the ORF 1b region of the avian coronavirus infectious bronchitis virus 1a/1b polyprotein. Virology 288, 212–222.

Yamada, Y. K., Yabe, M., Ohtsuki, T., and Taguchi, F., 2000. Unique N-linked glycosylation of murine coronavirus MHV-2 membrane protein at the conserved O-linked glycosylation site. Virus Res. 66, 149–154.

Yang, Z.-Y., Huang, Y., Ganesh, L., Leung, K., Kong, W.-P., Schwartz, O., Subbarao, K., and Nabel, G. J., 2004. pH-dependent entry of severe acute respiratory syndrome coronavirus is mediated by the spike glycoprotein and enhanced by dendritic cell transfer through DC-SIGN. J. Virol. 78, 5642–5650.

Yang, H., Yang, M., Ding, Y. & 12 other authors, 2003. The crystal structures of severe acute respiratory syndrome virus main protease and its complex with an inhibitor. Proc Natl Acad Sci U S A 100, 13190–13195.

Yang Y, Xiong Z, Zhang S, Yan Y, Nguyen J, Ng B, Lu H, Brendese J, Yang F, Wang H, Yang XF., 2005. Bcl-xL inhibits T-cell apoptosis induced by expression of SARS coronavirus E protein in the absence of growth factors. Biochem J., 392,135-43.

Yeager, C. L.; Ashmun, R. A.; Williams, R. K.; Cardellichio, C. B.; Shapiro, L. H.; Look, A. T.; Holmes, K. V., 1992. Human aminopeptidase N is a receptor for human coronavirus 229E. Nature 357: 420-422.

Youn, S., Leibowitz, J. L., and Collisson, E. W., 2005. In vitro assembled, recombinant infectious bronchitis viruses demonstrate that the 5a open reading frame is not essential for replication. Virology 332, 206–215.

Yount, B., Curtis, K. M., and Baric, R. S., 2000. Strategy for systematic assembly of large RNA and DNA genomes: Transmissible gastroenteritis virus model. J. Virol. 74, 10600–10611.

Yount, B., Denison, M. R., Weiss, S. R., and Baric, R. S., 2002. Systematic assembly of a full-length infectious cDNA of mouse hepatitis virus strain A59. J. Virol.76, 11065–11078.

Yount, B., Curtis, K. M., Fritz, E. A., Hensley, L. E., Jahrling, P. B., Prentice, E., Denison, M. R., Geisbert, T. W., and Baric, R. S., 2003. Reverse genetics with a full-lengthinfectious cDNA of severe acute respiratory syndrome coronavirus. Proc. Natl. Acad. Sci. USA 100, 12995–13000.

Yu, X., Bi, W., Weiss, S. R., and Leibowitz, J. L., 1994. Mouse hepatitis virus gene 5b protein is a new virion envelope protein. Virology 202, 1018–1023.

Yuan-Pin Huang, Ching-Ho Wang, 2006. Development of attenuated vaccines from Taiwanses infectious bronchitis virus strains. Vaccine 24, 785-791.

Yang, H., Yang, M., Ding, Y., Liu, Y., Lou, Z., Zhou, Z., Sun, L., Mo, L., Ye, S., Pang, H., Gao, G.F., Anand, K., Bartlam, M., Hilgenfeld, R., Rao, Z., 2003. The crystal structures of severe acute respiratory syndrome virus main protease and its complex with an inhibitor. Proc. Natl. Acad. Sci. USA. 100, 13190–13195.

Youn, S., Leibowitz, J. L., Collisson, E. W., 2005. In vitro assembled, recombinant infectious bronchitis viruses demonstrate that the 5a open reading frame is not essential for replication. Virology 332, 206-215.

Yuan X, Li J, Shan Y, Yang Z, Zhao Z, Chen B, Yao Z, Dong B, Wang S, Chen J, Cong Y., 2005. Subcellular localization and membrane association of SARS-CoV 3a protein. Virus Res., 109,191-202.

Zeng, W., Thomas, G. L., Glazier, J. A., 2004. Non-Turing stripes and spots: a novel mechanism for biological cell clustering. Physica A: Statistical mechanics and its applications. 341, 482-494.

Zhai, Y., Sun, F., Li, X., Pang, H., Xu, X., Bartlam, M., and Rao, Z., 2005. Insights into SARS-CoV transcription and replication from the structure of the nsp7–nsp8 hexadecamer. Nat. Struct. Mol. Biol. 12, 980–986.

Zheng, W. X., Chen, L. L., Ou, H. Y., Gao, F., Zhang, C. T., 2005. Coronavirus phylogeny based on a geometric approach. Mol Phylogenet Evol, 36, 224-132.

Zhou, M., and Collisson, E. W., 2000. The amino and carboxyl domains of the infectious bronchitis virus nucleocapsid protein interact with 3' genomic RNA. Virus Res. 67, 31–39.

Zhou, M., Williams, A. K., Chung, S., Wang , L., Collisson, E. W., 1996. The infectious bronchitis virus nucleocapsid protein binds RNA sequences in the 3; terminus of the genome. Virology 217, 191-199.

Ziebuhr, J., 2005. The coronavirus replicase. Curr. Top. Microbiol. Immunol. 287, 57–94.

Ziebuhr, J., Herold, J., Siddell, S. G.,1995. Characterization of a human coronavirus (strain 229E) 3C-like proteinase activity. J. Virol. 69, 4331-4338.

Ziebuhr J, Heusipp G, Siddell SG., 1997. Biosynthesis, purification, and characterization of the human coronavirus 229E 3C-like proteinase. J Virol, 71, 3992–3997.

Ziebuhr, J, Snijder, EJ, Gorbalenya, AE., 2000. Virus-encoded proteinases and proteolytic processing in the Nidovirales. J Gen Virol, 81, 853–879.

Ziebuhr, J., Thiel, V., and Gorbalenya, A. E., 2001. The autocatalytic release of a putative RNA virus transcription factor from its polyprotein precursor involves two paralogous papain-like proteases that cleave the same peptide bond. J. Biol. Chem., 276, 33220–33232.

Zigmond, S. H., 1993. Recent quantitative studies of actin filamnet turnover during cell locomotion. Cell Motil. Cytoskeleton 25, 309-316.